

**Stem Cell Signaling and RNA Regulation
in Regenerating Skeletal Muscle**

by

Thomas Orion Vogler

B.S., Bucknell University, 2010

A thesis submitted to the
Faculty of the Graduate School of the
University of Colorado in partial fulfillment
of the requirement for the degree of
Doctor of Philosophy
Department of Molecular, Cellular, and Developmental Biology
2019

This thesis entitled:
Stem Cell Signaling and RNA Regulation in Regenerating Skeletal Muscle
written by Thomas Orion Vogler
has been approved for the Department of Molecular, Cellular and Developmental
Biology

Dr. Leslie Leinwand (Committee Chair)

Dr. Bradley B. Olwin (Thesis Advisor)

Date: _____

The final copy of this thesis has been examined by the signatories, and we find that both the content and the form meet acceptable presentation standards of scholarly work in the above-mentioned discipline.

IACUC protocol# 2516

Vogler, Thomas Orion (Ph.D., Molecular, Cellular, and Developmental Biology)

Stem Cell Signaling and RNA Regulation in Regenerating Skeletal Muscle

Thesis directed by Professor Bradley B. Olwin

Abstract

Skeletal muscle can regenerate to replace damaged tissue. By continuously replacing damaged tissue, muscle regeneration endows near lifelong strength and function to skeletal muscle. If skeletal muscle regeneration is impaired or ineffective, muscle function declines, which significantly increases morbidity and mortality. In fact, loss of skeletal muscle regeneration is common in many degenerative diseases, such as muscular dystrophies, myopathies and age-related muscle degeneration. It is imperative that we understand the mechanisms of skeletal muscle regeneration so that we can effectively design and develop therapies that will revitalize degenerating muscle.

My work on the mechanisms of skeletal muscle regeneration focuses on two intimately linked cell types: (1) rare, mononuclear cells with tremendous regenerative potential called muscle stem cells (MuSCs) and (2) large, multinucleated cells without regenerative potential called myofibers. When myofiber are damaged and muscle regeneration is needed, MuSCs activate and expand to form a pool of myoblast cells that then fuse to existing myofibers or fuse together to form new myofibers. How MuSC regulate the balance between making new myofibers (differentiation) and making more stem cells (self-renewal) is not fully understood. Here, we show that constitutive FGF receptor 1 signaling in MuSC during skeletal muscle regeneration increases MuSCs numbers by promoting self-renewal and impairs regeneration by blocking differentiation.

We further demonstrate that constitutive FGF receptor 1 signaling in MuSC from aged muscle increases MuSC numbers and, surprisingly, restores skeletal muscle to a youthful state.

During skeletal muscle regeneration, MuSCs differentiate and fuse together to make myofibers. Myofibers are the workhorses of skeletal muscle – capable of contracting and generating force – but composed of hundreds of post-mitotic myonuclei without the ability to divide and make new myofibers. The contraction of myofibers is dependent on the sarcomere, a complex, interdigitating network of proteins. Sarcomeric proteins are translated from large mRNAs during skeletal muscle regeneration. How these large RNAs are regulated during skeletal muscle regeneration is unknown. Here we show the RNA-binding protein, TDP-43, binds mRNAs encoding sarcomeric proteins and forms cytoplasmic, amyloid-like oligomeric assemblies, termed myo-granules, during skeletal muscle regeneration in mice and humans. In healthy muscle, myo-granules are cleared as myofibers mature. Although myo-granules occur during normal muscle regeneration, myo-granules can seed TDP-43 amyloid fibrils *in vitro*, and are increased in a mouse model of inclusion body myopathy. Therefore, heightened assembly or decreased clearance of functionally normal myo-granules could be the source of cytoplasmic TDP-43 aggregates common to neuromuscular disease.

Dedication

To my wife, for your unwavering love and support, especially considering my odd fascination with mouse muscles.

And

To my family, for passing down a well-sourced guidebook to the adventures of life in academics.

“To have a great adventure, and survive, requires good judgment. Good judgment comes from experience. Experience, of course, is the result of poor judgment.”

-Geoff Tabin

Acknowledgements

Throughout my time in graduate school I have been fortunate to work with many people who share my enthusiasm for scientific discovery. This community begins with my thesis advisor, Dr. Brad Olwin. Brad taught me how to be bold in the pursuit of the unknown and how to challenge accepted ideas (as diplomatically as possible). He also gave me enough freedom in the lab to feel free but enough advice to feel secure. Brad's prolific creativity is a source of inspiration, and I will continue to draw upon it for years to come. Brad, thank you for a wonderful 5 years.

For most of graduate school, I was the least experienced member of the Olwin Lab. I benefited greatly from this by learning from the talented scientists around me. So, to every past and present member of the Olwin Lab, thank you for your kindness, advice and time. Specifically, I would like to thank Dr. Brad Pawlikowski and Dr. Jason Doles for your insights and candor on science, graduate school and life. I will also thank The Connection for facilitating these discussions. For the past two years, I have also had the pleasure of mentoring Oscar Whitney. Thank you for your enthusiasm about science, bulk foods, and interesting facts. Hopefully I didn't teach you too many bad habits.

To my MSTP classmates, thank you for your encouragement and support over our long journey in this program. But most importantly, thank you for your friendship. You've made a daunting dual-degree program feel like a home. I've shared some of the most important moments of my life with many of you, and I look forward to sharing many more. Specifically, I'd like to thank the soon to be double-doctor, Dr. Joshua Wheeler, it's been such a blast, my friend. You've been a colleague, a beach-stormer, a climbing

partner and a friend. Your talent for science is only superseded by your legendary work ethic, and I was lucky enough to benefit from the combination of the two. Cheers!

Finally, I would like to thank my wife. You support me while working harder than me, you celebrate with me when I succeed, and you love me when I'm a mess. I consider myself lucky, but as the years pass with you, I only feel luckier. You once told me that you'd always be my fiercest champion and kindest critic. You've shown me every day, what that means. And for that, I thank you and I love you.

CONTENTS

CHAPTER

I.	Introduction	1
II.	Effects of FGFR1 signaling in MuSCs on muscle regeneration ..	21
	Introduction.....	23
	Results.....	26
	Discussion	41
	Methods.....	46
III.	TDP-43 and RNA form amyloid-like myo-granules in skeletal muscle regeneration	53
	Introduction.....	55
	Results.....	56
	Discussion	92
	Methods.....	95
IV.	hnRNPA2B1 in normal skeletal muscle formation and regeneration.....	113
	Introduction.....	115
	Results.....	116
	Discussion	128
	Methods.....	131
V.	Discussion.....	137
	References.....	147

TABLES

Table

3.1. Myo-granule protein composition	81
3.2. Myo-granule properties identified by mass spectrometry	82
4.1. GO term analysis of RNAs that interact with hnRNPA2B1 in myotubes.....	121

FIGURES

Chapter 1 Figures

- 1.1. MuSCs during the regeneration of skeletal muscle6
- 1.2. Basic components of the skeletal muscle sarcomere 15

Chapter 2 Figures

- 2.1. Ectopic activation of caFGFR1 in MuSCs from young mice27
- 2.2. caFGFR1 expands MuSCs and blocks differentiation *in vitro*.....29
- 2.3. caFGFR expression in MuSCs from uninjured young mice does not increase MuSC numbers *in vivo*31
- 2.4. caFGFR1 expression in MuSCs impairs regeneration in young mice32
- 2.5. caFGFR1 expression in MuSCs delays muscle regeneration in young mice33
- 2.6. caFGFR expression promotes MuSC asymmetry and drives continued expansion of MuSCs *in vivo*.....35
- 2.7. MuSC-specific expression of caFGFR1 in aged muscle increases MuSC numbers38
- 2.8. MuSC-specific expression of caFGFR1 in aged muscle Increases myofiber size.....39
- 2.9. MuSC-specific expression of caFGFR1 restores aged muscle to youthful state40
- 2.10 Model for *in vivo* expansion of MuSCs driven by asymmetric FGFR1 signaling43

Chapter 3 Figures

- 3.1. Increased cytosolic TDP-43 during normal skeletal muscle formation57

3.2. TDP-43 adopts higher-ordered state during normal skeletal muscle formation	60
3.3. During muscle formation TDP-43 adopts a higher-ordered state distinct from stress granules.....	62
3.4. Myo-granules containing TDP-43 are amyloid like RNP oligomers	65
3.5. Myo-granules isolated from cells and mice contain TDP-43 and are amyloid-like oligomers.....	66
3.6. Myo-granules in skeletal muscle contain TDP-43 and are amyloid-like oligomers.....	68
3.7. TDP-43 eCLIP on skeletal muscle myoblasts and myotubes	71
3.8. TDP-43 binds to mRNAs that encode sarcomeric proteins during muscle formation	74
3.9. TDP-43 binds to select sarcomeric mRNA transcripts during muscle formation	76
3.10. Myo-granule protein composition	79
3.11. TDP-43 is an essential protein for skeletal muscle formation	84
3.12. Myo-granules form during human muscle regeneration	87
3.13. Myo-granules that seed amyloid-like fibers are increased in human muscle regeneration and in multisystem proteinopathy.....	88
3.14. Myo-granules are increased in VCP disease and are capable of seeding amyloid-like fibers	90
3.15. Myo-granules in normal skeletal muscle regeneration and in disease	94

Chapter 4 Figures

4.1. Localization of hnRNPA2B1 during skeletal muscle regeneration..	118
4.2. Enhanced CLIP reveals hnRNPA2B1 interacts primarily with	

the 3' UTR of RNA in skeletal muscle.....	119
4.3. Enhanced CLIP reveals hnRNPA2B1 and TDP-43 mainly interact with distinct RNAs in muscle	122
4.4. Knockout of hnRNPA2B1 in C2C12 myoblasts	123
4.5. Knockout of hnRNPA2B1 in C2C12 myoblasts does not affect proliferation.....	125
4.6. Knockout of hnRNPA2B1 in C2C12 inhibits myogenic differentiation.....	126

Chapter 1: Introduction

Skeletal Muscle Regeneration: From Muscle Stem Cells to Myofibers

A Brief History of Skeletal Muscle Regeneration

Skeletal muscle, the most abundant tissue in humans, powers our ability to eat, breath, move and talk. To maintain the strength needed for these tasks and to revitalize damaged tissue, skeletal muscle can regenerate. Historical descriptions of muscle regeneration in humans were first reported over 150 years ago (Carlson, 1973; Zenker, 1864). However, in the mid-20th century, modern histology and microscopy revealed that myofibers – the contractile units of skeletal muscle – are terminally differentiated cells, with multiple mitotically inactive nuclei that are unable to participate in regeneration. The paradox that skeletal muscle can regenerate yet myofibers cannot make new myofibers eventually lead to a milestone in our understanding of muscle regeneration in the 1960's, the discovery of muscle stem cells (MuSCs)(Church et al., 1966; Mauro, 1961; Reznik, 1969; Shafiq et al., 1967). MuSCs are rare stem cells located between the myofiber and the basal lamina. Upon injury, MuSCs activate and expand to form a pool of myoblast cells that then fuse to existing myofibers or form new myofibers by fusing together. The new myofibers made from MuSCs restore skeletal muscle strength and function after damage.

By the early 1970s, the basic framework for muscle regeneration was established where (1) skeletal muscle myofibers degenerate after an injury (2) MuSCs activate, expand and differentiate (3) myoblasts fuse to make new myofibers and (4) new myofibers grow and mature to functional contractile cells (Allbrook et al., 1971; Carlson, 1973; Moss and Leblond, 1970a, 1970b). Then from the late 1970s to the 1980s, this basic framework was expanded to show muscle regeneration included complex

interactions between MuSCs, inflammatory cells, nerves, blood vessels, fibroblasts and the extracellular matrix (Reviewed by: (Bodine-Fowler, 1994; Tedesco et al., 2010)). How each of these cell types contribute to the creation of myofibers and how newly formed myofibers rebuilt the contractile unit (a.k.a. the sarcomere), still remained a mystery.

Over the next 30 years, genetic, molecular and cellular mechanisms that regulate the highly orchestrated process of muscle regeneration were discovered (Collins et al., 2005; Karalaki et al., 2009; Yin et al., 2013). However, with this new knowledge came an unsettling appreciation that many untreated diseases and syndromes including muscular dystrophies, neuromuscular diseases and age-related muscle degeneration have impaired muscle regeneration (Cohn and Campbell, 2000; Shi and Garry, 2006). The dearth of effective treatments for these degenerative diseases plagues our society and strains our healthcare system (Beaudart et al., 2014; Evans and Campbell, 1993; Ryall et al., 2008; Tedesco et al., 2010). We must now apply the 150 years knowledge we have accumulated to manipulate the mechanisms of muscle regeneration to improve 21st century medicines.

Skeletal Muscle Injury and Degeneration

Skeletal muscle is injured or damaged in humans by trauma, disease or aging. Following any muscle injury, rapid necrosis of the damaged myofibers occurs. During necrosis, the cell membrane of myofibers, called the sarcolemma, breaks down (Karalaki et al., 2009). The breakdown of the sarcolemma releases cytosolic muscle

proteins of the myofiber, such as creatine kinase, into the serum. In fact, measuring serum creatine kinase is a common, non-specific test for skeletal muscle damage. Creatine kinase levels are increased by mechanical stress, running marathons, and by diseases like muscular dystrophies (Sorichter et al., 1997; Zatz et al., 1991). Thus, the release of cytosolic muscle proteins is an early signal of a muscle injury and an initial step in muscle regeneration.

The release of cytosolic muscle proteins from necrotic myofibers causes a sequential invasion of inflammatory cells to the site of injury (Tidball, 2017). Neutrophils respond first to the damaged tissue and invade injured muscles within an hour of damage (Fielding et al., 1993). Neutrophils are the predominate inflammatory cells to initially infiltrate an injury but peak after only 24-48 hours and then quickly decrease in number (Lu et al., 2011). During this initial phase, neutrophils mediate the post-injury muscle tissue as they: (1) phagocytose necrotic debris (2) release proteases that degrade the remaining cellular components too large for phagocytosis and (3) secrete pro-inflammatory cytokines that magnify the inflammatory response (Smith et al., 2008; Tidball, 2005). Together the neutrophil response acts to degrade and eliminate the damaged myofibers so the injury site can be prepared for muscle regeneration.

Macrophages invade injured muscle after neutrophils continue to phagocytose degraded cellular debris left by neutrophils. Macrophage numbers peak between 5-7 days post-injury (Smith et al., 2008). The phagocytic macrophages clear necrotic tissue but leave the extracellular matrix intact. The empty extracellular matrix, or ghost fiber, acts as a scaffold for MuSCs to regenerate myofibers (Webster et al., 2016).

Macrophages also activate and regulate myogenic stem cells during the early stages of regeneration by secreting cytokines and growth factors; however, the mechanisms regulating macrophage-induced myogenic activation are not fully elucidated (Tidball, 2017).

The initial phase of muscle regeneration removes necrotic tissue by neutrophils and macrophages. This sequential inflammatory process prepares the extracellular space and myogenic cells for muscle regeneration. Impairments in the inflammatory process delays and impairs muscle regeneration and is an active area of research.

Muscle Stem Cell Activation and Proliferation

Following the degeneration of damaged muscle, the next phase of muscle regeneration requires extensive MuSC and myoblast cell proliferation (Figure 1.1). Inhibiting this cell proliferation by irradiation impairs regeneration (Quinlan et al., 1995). Labeling proliferating cells with [H^3]thymidine clearly show MuSCs expand dramatically during the first five days post-injury and are the source for new nuclei in regenerating myofibers (Snow, 1978). Although there are other cells in muscle with myogenic potential that respond to injuries (Asakura et al., 2002; Mitchell et al., 2010), I will focus on the activation, proliferation and differentiation of MuSC.

In uninjured muscle, MuSCs reside on the surface of individual myofibers and are surrounded by the basal lamina, comprising ~1% of the total nuclei in skeletal muscle (Yin et al., 2013). Most MuSCs in uninjured muscle are quiescent and non-dividing, while a minority (2-5%) are active and maintain adult skeletal musculature (Keefe et al.,

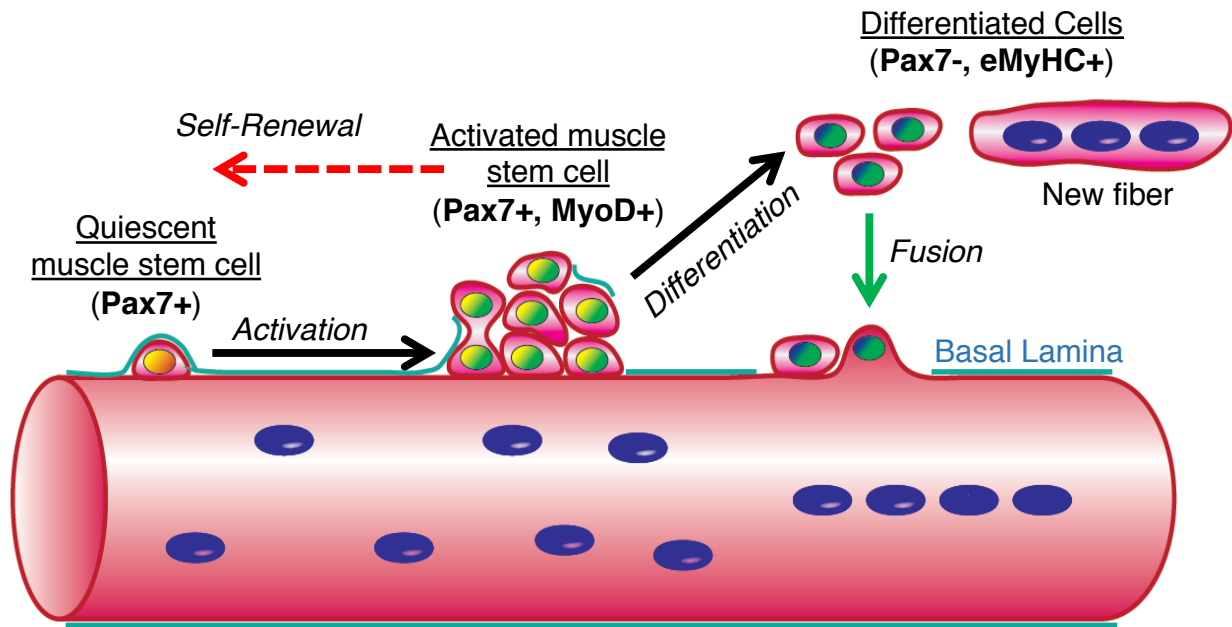


Figure 1.1 – MuSCs during the regeneration of skeletal muscle

Schematic of MuSC activation, proliferation and fusion during skeletal muscle regeneration and repair. Upon receiving the appropriate signals, quiescent Pax7+ MuSCs activate by turning on MyoD. These activated cells are termed myoblasts and can either self-renew by turning off MyoD or differentiate by turning off Pax7 and turning on mature muscle transcripts like embryonic myosin heavy chain (eMyHC). Differentiated cells can either fuse to a damaged myofiber (and cause centrally located nuclei) or fuse together and form *de novo* fibers.

2015; Pawlikowski et al., 2015). Quiescent MuSC express the transcription factor Pax7 but not the myogenic transcription factors MyoD or myogenin (Cornelison and Wold, 1997). Following a muscle injury and exposure to pro-myogenic stimuli, MuSCs activate, which increases myogenic transcripts, such as MyoD, and leads to a global epigenetic and gene expression program that promote MuSC proliferation (Figure 1.1) (Almada and Wagers, 2016; Cooper et al., 1999).

MuSC activation is governed by multiple niche factors and signaling pathways (Yin et al., 2013). Together these factors and pathways converge to initiate the myogenic program, which allows MuSC to become proliferating myoblasts. Wnt and sphingolipid signaling both increase significantly during MuSC activation (Reviewed by (Yin et al., 2013)). The growth factors IGF-1, IGF-2, HGF, PDGF, EGF and FGF are located in the MuSC niche and activate signaling pathways in MuSC following an injury (Shi and Garry, 2006; Yin et al., 2013). Although it is unclear how these signals are coordinated, many of these myogenic signals converge on the the p38 α/β MAPK pathway to awaken MuSC into the proliferative state (Bernet et al., 2014; Troy et al., 2012). The p38 α/β MAPK pathway induces MyoD protein production by regulating MyoD mRNA levels by inhibiting the RNA-destabilizing protein tristetraprolin (TTP) (Hausburg et al., 2015). Activated MuSCs expressing MyoD re-enter the cell cycle approximately 24-36 hours post-injury (Webster et al., 2016). Together these niche factors and subsequent signaling pathways activate quiescent MuSCs and transform them into proliferating myoblasts. In mice, activated MuSCs expand for approximately five days following an induced injury, increasing their numbers more than 10-fold

(Murphy et al., 2011; Webster et al., 2016). However, understanding how all of these signals converge to maintain MuSC proliferation *in vivo*, represents an understudied area of muscle regeneration.

Muscle Stem Cell Self-Renewal

During the first five days after a muscle injury the majority of the MuSC population will proliferate, differentiate and then fuse together to make new myofibers. However, at roughly five days post injury, MuSC self-renewal increases to replenish the quiescent MuSC population (Figure 1.1) (Pawlikowski et al., Submitted). Self-renewal ensures a small proportion of activated MuSCs avoids terminal differentiation and repopulates the stem cell pool for future rounds of regeneration (Dumont et al., 2015). During self-renewal, MuSCs decrease MyoD expression, increase cell cycle inhibitors and maintain Pax7 expression to exit the cell cycle and return to quiescence (Pawlikowski et al., Submitted). Many cell-intrinsic and extrinsic regulators of MuSC self-renewal have been identified such as cell cycle inhibitors (Chakkalakal et al., 2014), receptor tyrosine kinase signaling (Bernet et al., 2014; Chakkalakal et al., 2012), Wnt7a signaling (Le Grand et al., 2009) and Myf5 expression (Kuang et al., 2007). Understanding how MuSCs decide between proliferation versus self-renewal is an area of active research.

Actively dividing MuSCs can undergo two types of cell divisions: (1) symmetric cell division, where both daughter cells acquire identical fates and (2) asymmetric cell divisions, where each daughter cell adopts a different cell fate. Adult stem cells typically

self-renew via asymmetric division (Knoblich, 2008). In MuSCs, polarization of Pard3 asymmetrically activates p38 α/β MAPK signaling, stabilizing MyoD in one daughter cell, while the other daughter re-acquires quiescence and self-renews (Troy et al., 2012). The upstream regulators of this asymmetric signaling pathway is still an active area of research (Cosgrove et al., 2014; Rozo et al., 2016; Wang et al., 2019) but FGF signaling was found to be a critical regulator of asymmetric p38 α/β MAPK signaling and MuSC self-renewal (Bernet et al., 2014).

FGF signaling in MuSC during skeletal muscle regeneration

Since the first publications linking FGF to myogenesis and MuSC behavior over 30 years ago (Clegg et al., 1987; Lim and Hauschka, 1984; Olwin and Hauschka, 1986; Seed et al., 1988), complex and incompletely understood roles for FGF regulation of skeletal muscle regeneration have been identified. Of the 18 paracrine FGFs, mRNA of four are detected in MuSCs (FGF1, FGF2 and FGF4, and FGF6) that stimulate expansion of cultured MuSCs (Hannon et al., 1996; Kastner et al., 2000; Sheehan and Allen, 1999). Only FGF2 and FGF6 are found embedded within the extracellular matrix and basal lamina of uninjured adult skeletal muscle tissue (J. DiMario et al., 1989) and function in skeletal muscle regeneration. During muscle regeneration FGF2 and FGF6 increase (Anderson et al., 1995; Floss et al., 1997) and influences MuSC behavior by acting through FGF receptors (FGFRs) expressed on MuSCs.

Among the four FGFRs, MuSCs predominately express FGFR1 and FGFR4, with FGFR2 and FGFR3 expressed at low levels (Cornelison et al., 2001; Yablonka-Reuveni

et al., 2015). Each FGFR possesses an extracellular domain containing three immunoglobulin-like domains, a trans-membrane domain, and an intracellular split tyrosine kinase domain (Eswarakumar et al., 2005). FGF binding to an FGFR and subsequent receptor activation to transduce intracellular signals in MuSCs, requires a ternary interaction between an FGF, either heparan sulfate or Klotho and the appropriate FGFR, which stabilizes the complex and promotes receptor activation by autophosphorylation of the FGFR activation domain (Ornitz and Itoh, 2015). In addition to heparan sulfate proteoglycans, integrins and Fibronectin modulate FGF signaling in MuSCs (Lukjanenko et al., 2016; Rozo et al., 2016). Determining the relative contribution of individual FGFRs to MuSC function, and how these change over time, has proven difficult due to expression of multiple FGFRs that redundantly activate multiple intracellular signaling pathways. Thus, it is not surprising that conditional deletion of only one FGFR from MuSCs produces only subtle phenotypes (Weinstein et al., 1998; Yablonka-Reuveni et al., 2015; Zhao et al., 2006). Elimination of FGFR signaling either by adding an FGFR inhibitor (Bernet et al., 2014) or by expression of a dominant negative FGFR mutant (Flanagan-Steet et al., 2000) promotes terminal differentiation of MuSCs and reduces muscle mass, respectively. Thus, FGF signaling appears to play a critical role in MuSC function but the contributions of the individual FGFRs are not yet resolved.

A number of distinct intracellular signaling pathways are activated upon engagement of an FGFR with an FGF, including p38 α / β MAPK, ERK MAPK, PI3 kinase, Akt, activation of STAT, and stimulation of Phospholipase C gamma/Protein

Kinase C signaling (Brewer et al., 2016; Ornitz and Itoh, 2015). FGFR activation of p38 α / β MAPK in MuSCs (Bernet et al., 2014; Jones et al., 2005) occurs via a yet unidentified signaling pathway. Asymmetric activation of FGFR1 in MuSCs drives asymmetric activation of p38 α / β MAPK, which inhibits Tristetraprolin (TTP) in one presumptive daughter cell, permitting MyoD induction, where the other daughter reacquires quiescence, self-renewing the satellite stem cell (Hausburg et al., 2015; Troy et al., 2012). Delineating the mechanisms involved in FGFR stimulation of asymmetric p38 α / β MAPK phosphorylation will provide an understanding of p38 α / β MAPK functions and the signals that regulate p38 α / β MAPK subcellular localization. Further, how FGFR1 signaling becomes asymmetrically localized in MuSCs, and the consequences of asymmetric signaling, are open questions.

Muscle Stem Cell Differentiation and Fusion

MuSC self-renewal is critical for repopulating the MuSC pool for future rounds of muscle regeneration, yet the vast majority of activated MuSCs (myoblasts) differentiate and fuse together to rebuild myofibers (Figure 1.1). Rebuilding even a single new myofiber is a heroic effort, requiring hundreds of proliferating myoblasts to exit the cell cycle, undergo global transcriptional changes and then fuse together to create a multinucleated cell. During regeneration, myoblasts fusion takes place within ghost fibers, which are extracellular matrix remnants left after damaged myofibers are cleared by phagocytic cells (Webster et al., 2016). Ghost fibers provide a scaffold to direct the location and orientation of multinucleated cells as myoblasts differentiate and fuse. This

highly complex process is unlike any other in the human body and requires the coordination of many cell interactions for successful regeneration.

As proliferating myoblasts expand in a ghost fiber they must first differentiate before fusion and muscle myofiber regeneration occurs. Myoblast differentiation is driven by the Pax7-MyoD-Myogenin axis. These three transcription factors are expressed in MuSCs at different stages after muscle injury and drive cell fates by controlling global transcription profiles in cells. Pax7 is solely expressed in quiescent MuSC while activated MuSCs and proliferating myoblasts express both Pax7 and MyoD. To differentiate, proliferating myoblasts must withdraw from the cell cycle and then down-regulate Pax7 expression and express myogenin (Olguin and Olwin, 2004). Myogenin promotes this process by negatively regulating Pax7 expression to drive myoblast differentiation (Olguin et al., 2007). Knocking out myogenin in mice causes a buildup of undifferentiated myoblasts and poor myofiber formation (Hasty et al., 1993). Myogenin drives the expression of mature myogenic transcripts like myosin heavy chain, which is necessary to build sarcomeres, and myomaker, which is critical for myoblast fusion (Ganassi et al., 2018; Hasty et al., 1993; Millay et al., 2013, 2014). Thus, withdrawal from the cell cycle and myogenin expression are the markers of myoblast terminal differentiation and immediately precede myoblast fusion.

Primary myoblast fusion involves the fusion of cell membranes from two differentiated myoblasts to create a single, syncytial, multinucleated cell, called a myotube (Abmayr and Pavlath, 2012). Secondary fusion occurs when a myoblast fuses with an existing myotube, which results in the growth of the myotube (Hindi et al., 2013).

A muscle-specific fusogenic protein, myomaker, discovered in 2013 (Millay et al., 2013), is required for fusion and for skeletal muscle formation. A second fusion protein was discovered in 2017 simultaneously by three groups and subsequently named three different ways, myomixer, myomerger and minion (Bi et al., 2017; Quinn et al., 2017; Zhang et al., 2017). How myomaker and myomixer-myomerger-minion function together to coalesce two membranes is still debated but it is clear these proteins are critical for fusion.

Fusion generates a multinucleated myotube, but this cell needs to increase in size considerably to become a functional myofiber with hundreds of nuclei. Myofibers grow in size by the fusion of additional myoblast, and without fusion, myofibers cannot grow or hypertrophy (Goh and Millay, 2017). During the initial stages of fusion and myotube growth, the myonuclei line up in the center of the cell. The reason for this particular organization is still unknown. However, once this initial myotube is made, subsequent fusion events occur on the periphery of the myofiber and the centrally-located nuclei are pushed toward the periphery (Roman et al., 2017)(Pawlikowski et al., Submitted). Each fusion event provides new myonuclei which enhance transcription of genes that encode contractile and mature muscle proteins. Fusion may also provide factors that enhance myofiber growth such as ribosomes for protein translation, mitochondria for energy and signaling molecules for hypertrophy (Goh and Millay, 2017). Together, these factors contribute to the assembly and growth of myofibers during muscle regeneration.

Myoblast differentiation and fusion represents a turning point in skeletal muscle regeneration. During differentiation, the predominant cell type switches from a highly proliferative myoblast to a terminally differentiated, multinucleated myotube. In the next phase of regeneration, myotubes grow to become mature myofibers that contract and generate force. In mice, these two phases occur simultaneously between days 5 and 28 post injury. Although this covers the largest percentage of time during the regeneration process, our cellular and molecular understanding of this phase is weak.

Myotube Growth and Sarcomere Formation

As muscles grow, they must assemble an interdigitating network of proteins called the sarcomere. Although sarcomeres are composed of hundreds of large structural and regulatory proteins, the two primary structures are the thin filaments, composed of actin, and the thick filaments, composed of myosin. The Z-line is the anchoring point for thin filaments and is parallel to the M-line, which is the anchoring point for the thick filaments (Figure 1.2). Sarcomeres contract when thick filament myosin proteins bind to thin filament actins, and hydrolyze ATP to generate a power stroke (Quiat et al., 2011; Spudich and Watt, 1971). The power stroke shortens the distance between two Z-lines by sliding them towards the M-line, which shortens the length of the sarcomere. Myofibril units are composed of hundreds of repeating sarcomeres and the coordinated contractions of sarcomeres and myofibril units generates force.

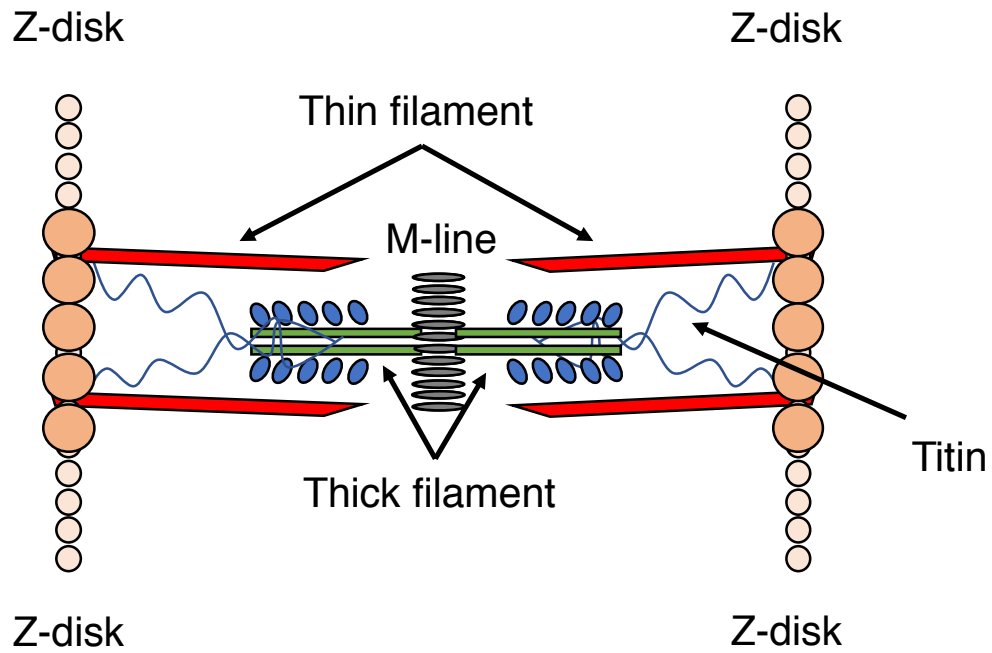


Figure 1.2 – Basic components of the skeletal muscle sarcomere

Schematic of skeletal muscle sarcomere. The two primary structures of sarcomeres in skeletal muscle are the thin filaments, composed of actin, and the thick filaments, composed of myosin. The Z-disk is the anchoring point for thin filaments and is parallel to the M-line, which is the anchoring point for the thick filaments. Spanning the distance between the Z-disk and the M-line is the giant structural protein, Titin.

Many structural and regulatory proteins in the sarcomere, such as myosin heavy chain, troponin, and nebulin, are some of the largest proteins in the human body, and in fact the sarcomeric protein, titin, is the largest. Although the components of sarcomeres and how they generate force has been known for many years, it is still debated how these proteins assemble to form the sarcomere during regeneration (Holtzer et al., 1997; Rhee et al., 1994; Rui et al., 2010; Sparrow and Schöck, 2009). Electron microscopy studies reveal the formation of small filamentous structures held together by Z-line during early regeneration. These structures then develop into sarcomeres and myofibril units as sarcomeric proteins are added. The cytoplasm of regenerating muscle contains large numbers of ribosomes that translate the enormous sarcomeric proteins needed to build these structures (Carlson, 1973). The mechanisms controlling how, when and where sarcomeric proteins are being made and organized is both controversial and understudied.

The genes that encode proteins needed to regenerate sarcomeres after injury are expressed as RNA in the nuclei of differentiated myoblasts and myotubes. These RNAs are spliced and processed to make mRNA, which is then packaged and transported into the cytoplasm where they are translated into proteins that assemble the sarcomere. RNA-binding proteins help regulate the processing, packaging and transport of RNA, but the role of RNA-binding proteins in regulating sarcomeric and myogenic RNAs is lacking. Furthermore, many sarcomeric RNA transcripts are very long. The average human mRNA is 3.3 kilobases (kb) long (Piovesan et al., 2016), the myosin heavy chain 3 mRNA is twice the average length (Karsch-Mizrachi et al., 1989), while other sarcomeric transcripts are far larger: nebulin (Lehtokari et al., 2006) and obscurin

(Fukuzawa et al., 2005) transcripts are approximately 25kb and the massive titin mRNA is more than 100 kb (Labeit et al., 2006). Many of these RNAs have multiple binding sites for RNA-binding proteins, presumably to help regulate packaging and transport (Vogler et al., 2018). The misregulation these large RNAs could cause the formation of aberrant intermolecular RNA-RNA interactions, which are thought to be toxic to cells and may drive degenerative diseases (Van Treeck and Parker, 2018). Therefore, preventing RNA-RNA interactions in RNAs that encode sarcomere proteins may be essential for sarcomere building and muscle regeneration (Vogler et al., 2018).

Completed Muscle Regeneration

The length of time to complete skeletal muscle regeneration depends largely on the type and severity of muscle injury as well as the health of the injured organism. In healthy mice, the process of regenerating muscle takes approximately 30 days after a BaCl₂-induced injury (Hardy et al., 2016). By 30 days, the inflammatory cells return to pre-injury levels (Tidball, 2017). The MuSCs return to pre-injury numbers and reenter quiescence. Most myofibers have peripheral nuclei, are filled with sarcomeres and have a similar size compared to before the injury. Most importantly, the strength and function of the muscle returns to pre-injury levels (Sato et al., 2003). Complete recovery from muscle injury also requires the growth of new blood vessels into the damaged tissue and the reinnervation of new myofibers by motor neurons (Bodine-Fowler, 1994; Liu et al., 2017c; Sanes et al., 1978). Together, these events culminate in a regenerated skeletal muscle; however, if any stage of the aforementioned regeneration process is disrupted or altered, muscle regeneration will fail to revitalize muscle function after an

injury. Understanding and treating conditions that delay or impair muscle from fully regenerating is a broad and active area of research.

Muscle regeneration in aging and disease

Impaired muscle regeneration occurs in many diseases and syndromes including cachexia, muscular dystrophies, neuromuscular diseases and age-related muscle degeneration (Bernet et al., 2014; Cosgrove et al., 2014; Dumont et al., 2015; He et al., 2013; Sacco et al., 2010). Both cell intrinsic and extrinsic factors contribute to aged-induced and disease-induced deficiencies (for reviews see: (Blau et al., 2015; Feige et al., 2018; Hwang and Brack, 2018; Shi and Garry, 2006)). While many pathways that affect muscle regeneration have been identified, there remains a paucity of effective therapeutic interventions for impaired regeneration. As recently as 2015, Novartis researchers identified skeletal muscle as the last undrugged organ system (Garber, 2016; Meriggioli and Roubenoff, 2015). Understanding how to manipulate the events of muscle regeneration is critical for the development of beneficial skeletal muscle therapies.

Skeletal muscle atrophy, reductions in regenerative capacity and increases in adipose and fibrotic tissue are consequences aging (Blau et al., 2015; Brack et al., 2007; Feige et al., 2018; Hwang and Brack, 2018). This age-related muscle degeneration, also called sarcopenia, increases morbidity and mortality of older individuals. The mechanisms driving sarcopenia are unclear but involve MuSC-extrinsic changes in inflammation, growth factor regulation and fibrosis, which produce an

environment refractive to muscle regeneration. Additionally, intrinsic changes in MuSC signaling pathways can reduce MuSC numbers, blunting the regenerative response to muscle injury. Cell-intrinsic and cell-extrinsic factors combine to drive sarcopenia. For example, both MuSC-intrinsic and MuSC-extrinsic defects in FGF regulation have been identified in aged mice muscle (Bernet et al., 2014; Chakkalakal et al., 2012).

Understanding the effects of targeting both cellular and environmental changes in aged muscles are needed to develop effective therapies for sarcopenia.

Skeletal muscle diseases are a heterogeneous group of over 50 conditions with distinct pathophysiology. The two largest sub-categories of skeletal muscle diseases are the dystrophies and the myopathies, which include one of the most common genetic childhood diseases, Duchenne's Muscular Dystrophy (DMD), and the most common muscle disease of the elderly, inclusion body myopathy (IBM). A hallmark of both DMD and IBM – as well as many other muscle diseases – is the presence of continuous skeletal muscle regeneration (Sacco et al., 2010). In DMD, mutations in the dystrophin gene produce a dysfunctional dystrophin protein, which reduces the integrity of myofibers, leading to myofiber necrosis and continuous cycles of degeneration and regeneration (Hoffman et al., 1987). Continuous regeneration leads to exhaustion of MuSCs and of the regenerative capacity, which eventually leads to impaired muscle function, loss of movement and death in patients (Birnkrant et al., 2018). In IBM, the mechanism that causes degeneration is unknown but is thought to involve impairments in protein homeostasis. A buildup of proteins in myofibers becomes toxic and the myofibers undergo continuous degeneration and regeneration. Similar to DMD, the

continuous regeneration in IBM eventually reduces muscle strength and confines patients to wheelchairs. Genetic mouse models for both diseases exist and recapitulate many aspects of the human conditions, which has increased our understanding of the pathophysiology of these diseases tremendously (Custer et al., 2010; Grahame Bulfield et al., 1984; Yucel et al., 2018). However, effective treatments for either condition remain elusive.

Linking muscle regeneration physiology to pathophysiology

In the following chapters, I examined two separate mechanisms that help control muscle regeneration; one in MuSCs and one in myofibers. In both cases I asked how these mechanisms influence normal muscle regeneration and then applied that knowledge to understand a degenerative condition. In Chapter 2, I examined how FGF signaling controls MuSCs numbers during normal muscle regeneration. I then examine how increasing FGF signaling in MuSCs in aged mice affects age-related muscle degeneration. In Chapters 3 & 4, I examine how the RNA-binding proteins TDP-43 and hnRNPA2B1 help regulate RNAs during muscle regeneration. These two RNA-binding proteins are implicated or mutated in IBM and their role in normal regeneration suggests how they contribute to disease. Together, this work underscores the importance of studying the mechanisms of normal physiology to understand disease pathophysiology. Future work will be aimed at pharmacologically or genetically manipulating pathophysiology to restore normal physiology.

Chapter 2:

Effects of FGFR1 signaling in MuSCs on muscle regeneration

Summary

Lifelong maintenance and function of skeletal muscle stem cells (MuSCs) is regulated by the interaction of the MuSC and the components of the MuSC environment, such as growth factors, immune cells, signaling receptors and the extracellular matrix. Defects in how MuSC respond to the environment drives a loss in MuSC numbers and regenerative capacity in aged muscle. Since MuSC from aged muscle have an impaired response to fibroblast growth factor (FGF), which causes precocious differentiation and subsequent loss of MuSC numbers, restoring FGF signaling in MuSC represents a potential therapeutic approach to rescue the age-related decline in MuSC numbers and function. Here, we show that constitutive FGF receptor 1 signaling in MuSC during skeletal muscle regeneration increases MuSCs numbers by promoting self-renewal and impairs regeneration by blocking differentiation. We further demonstrate that constitutive FGF receptor 1 signaling in MuSC from aged muscle increases MuSC numbers and restores skeletal muscle to a youthful state. Thus, our data highlight the potential therapeutic benefit of activating FGF signaling in MuSC in aged muscle to increase MuSC numbers and restore muscle function in aging.

Introduction

Reduction of skeletal muscle mass, function, and regenerative capacity occurs during normal aging, which can lead to an intractable muscle wasting condition called sarcopenia in elderly individuals (Narici and Maffulli, 2010). The development of sarcopenia results in frailty, decreased ambulation and increased morbidity (Beaudart et al., 2014). The mechanisms that lead to sarcopenia include changes in skeletal muscle metabolism, changes in protein homeostasis, compromised regeneration and a loss in muscle stem cell (MuSC) numbers and function (Bernet et al., 2014; Chakkalakal et al., 2012; Collins et al., 2007; Price et al., 2014; Shefer et al., 2006; Tierney et al., 2014). MuSCs – a rare population of cells that reside between the myofiber plasma membrane and the basal lamina – are critical to muscle regeneration as loss of MuSCs by genetic ablation abrogates regeneration (Fry et al., 2014; Lepper et al., 2011; Murphy et al., 2011; Piccirillo et al., 2014; Relaix et al., 2006; Sambasivan et al., 2011; Seale et al., 2000). In aged skeletal muscle, there is a decline in MuSC numbers and function, which impairs regeneration (Chakkalakal et al., 2012). The mechanisms that control the decline in MuSC numbers and function are not well understood.

MuSCs activation, proliferation and differentiation are influenced by components of the MuSC niche, such as growth factors, immune cells, signaling receptors and the extracellular matrix (Bernet et al., 2014; He et al., 2013; Rozo et al., 2016; Sacco et al., 2010; Yin et al., 2013). Age-related changes to the MuSC niche compromises MuSC function. For example, loss of fibronectin and β 1-integrin during aging drives a loss of MuSC homeostasis by impairing the interaction between the MuSC and the MuSC

niche (Lukjanenko et al., 2016; Rozo et al., 2016). Although exposing aged muscle to a young environment improves regeneration (Conboy et al., 2003, 2005), transplantation of MuSC from aged muscle into a young environment does not fully rescue MuSC function. Cell-intrinsic defect in the response to fibroblast growth factor ligands were discovered in MuSCs from aged muscle (Bernet et al., 2014). Changes in niche factors such as β 1-integrin, which cooperates with FGF ligands, may drive loss of FGF2 responsiveness in MuSCs as muscles age (Rozo et al., 2016).

The loss of FGF2 responsiveness in MuSCs as muscles age (Bernet et al., 2014; Shefer et al., 2006; Yablonka-Reuveni et al., 1999), correlates with reduced self-renewal and a concomitant increase in MuSC differentiation (Bernet et al., 2014; Chakkalakal et al., 2012). In aged mice FGF2 production by skeletal muscle myofibers is elevated, perhaps compensating for reduced FGF2 responsiveness of MuSCs observed *in vivo* (Chakkalakal et al., 2012; Li et al., 2015) and *in vitro* (Bernet et al., 2014; Shefer et al., 2006; Yablonka-Reuveni et al., 1999). Elevated p38 α / β MAPK signaling accompanies the loss of FGF responsiveness in MuSCs from aged mice, which promotes terminal differentiation and reduces self-renewal by increasing MyoD in both daughter cells (Bernet et al., 2014; Cosgrove et al., 2014). Reducing MuSC self-renewal and promoting terminal differentiation of both daughter cells may drive the gradual loss in MuSC numbers in aged mice.

Ectopic activation of FGFR1 partially rescues self-renewal in MuSCs from aged mice and is accompanied by asymmetric localization of phospho-p38 α / β MAPK (Bernet et al., 2014). The asymmetric localization of phospho-p38 α / β MAPK appears to be

driven by the asymmetric localization of FGFR1. The loss of FGFR1 asymmetric localization in MuSC from aged mice may be due to a breakdown in the interaction between the MuSC and the MuSC niche. The altered activity of the niche molecule, β 1-integrin, reduces FGF2 sensitivity of MuSCs from aged mice and reduces MuSC self-renewal (Rozo et al., 2016). MuSCs from aged mice and β 1-integrin conditional mutant mice have similar phenotypes where precocious MuSC differentiation is accompanied by decreased proliferation, and impaired self-renewal (Bernet et al., 2014; Rozo et al., 2016). Treating MuSCs from aged mice with a β 1-integrin activating antibody enhances proliferation, while reducing differentiation and activating FGFR1 promotes asymmetric localization of phospho-p38 α / β MAPK (Bernet et al., 2014). Together, this suggests rescuing FGF signaling in MuSCs is an attractive therapeutic approach to improve muscle regeneration in aged muscle.

Although much is understood about FGFR signaling in MuSC, it is still unknown what effect *in vivo* activation of FGFR signaling will have on MuSCs numbers in young and aged mice. To activate FGFR signaling, MuSCs predominately signal through FGFR1 and FGFR4, with FGFR2 and FGFR3 expressed at low levels (Cornelison et al., 2001). However, the downstream activation of FGFR signaling by FGFR4 is reduced compared to FGFR1 (Kwiatkowski et al., 2008; Wang et al., 1994). Therefore, we examined the *in vivo* effects of FGFR1 activation in MuSC from young mice and then attempted to rescue the FGF signaling defects of MuSC in aged mice.

Results

Constitutive FGFR1 signaling expands cultured MuSCs

To test whether ectopic activation of FGFR1 in MuSCs will increase MuSC numbers and alter muscle regeneration we bred mice for temporal and spatial control of a constitutively active FGFR1 (caFGFR1) (Cilvik et al., 2013) (Figure 2.1a). A transgenic mouse expressing caFGFR1, a chimeric receptor consisting of the FGFR3c(R248C) mutant extracellular and transmembrane domains (Naski et al., 1996) fused to the intracellular FGFR1 tyrosine kinase domain, driven by a tetracycline operator sequence, was bred to *Lox Stop Lox rtTA* mice and *Pax7^{CreERT2}* mice. In mice with all three alleles, tamoxifen injection recombines the ROSA26 locus only in MuSCs resulting in MuSC-specific rtTA expression. Treatment of mice with doxycycline allows rtTA binding to the tetracycline response element (TRE) and subsequent expression of caFGFR1 only in MuSCs (Figure 2.1a). Detection of caFGFR1 expression in MuSCs by qPCR shows doxycycline addition in mouse chow induces expression of caFGFR1 (Figure 2.1b). Upon doxycycline removal caFGFR1 expression is lost (Figure 2.1b). Using an antibody that recognizes the myc-tag fused to the C-terminal end of caFGFR1, we find caFGFR1 protein is present in doxycycline treated Pax7+ MuSCs but not MuSCs treated with a DMSO control (Figure 2.1c). Thus, by treating MuSC or mice with doxycycline, we have temporal control of a constitutively active FGFR1 in MuSC.

If FGFR1 signaling permits MuSC proliferation, then caFGFR1 expression in MuSC should maintain the proliferative state of MuSCs. In cultured MuSCs, addition of

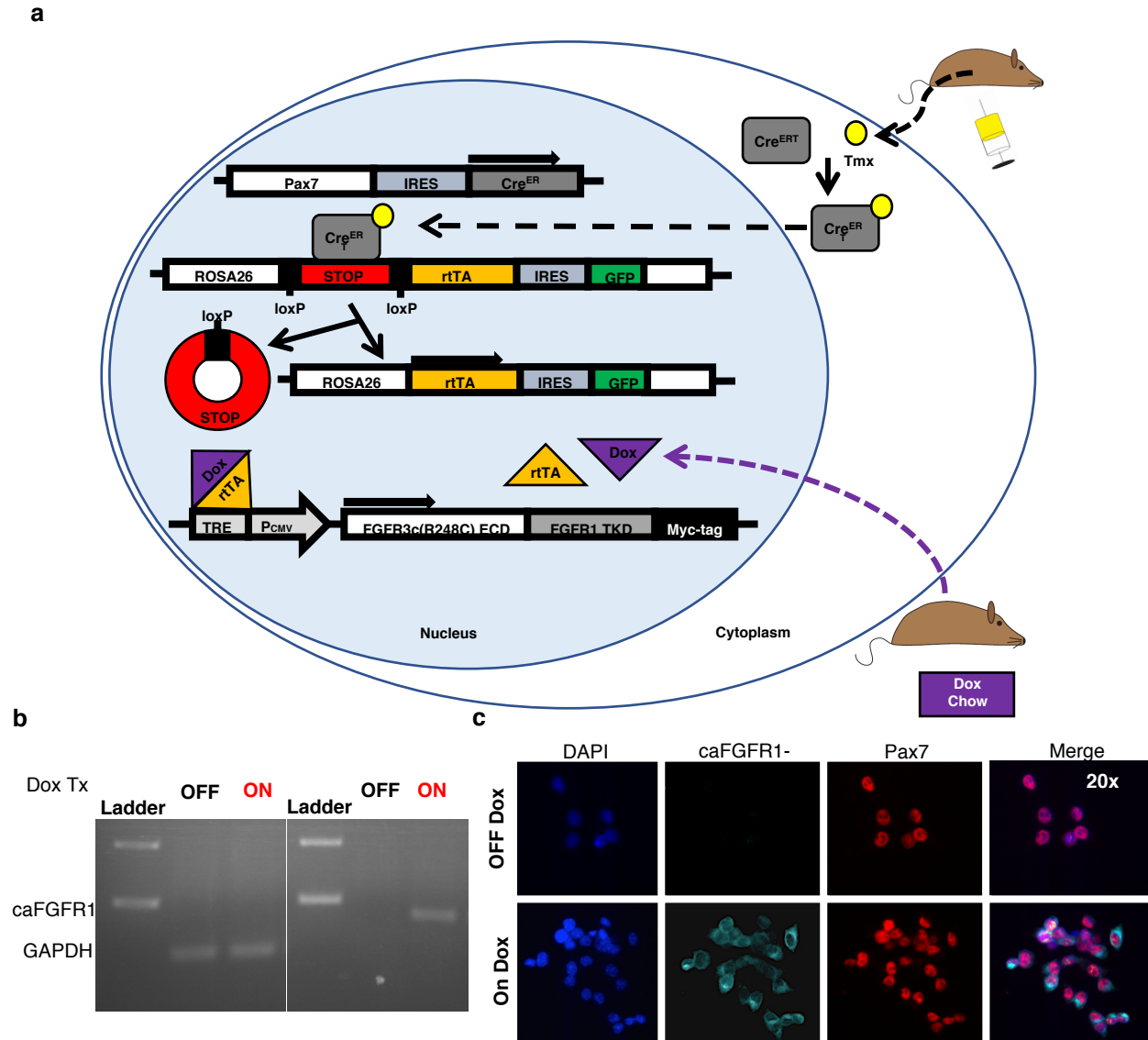


Figure 2.1 – Ectopic activation of caFGFR1 in MuSCs from young mice

(a) Schematic of a transgenic mouse containing a constitutively active FGFR1 (caFGFR1) transgene. caFGFR1 is a chimeric receptor consisting of the FGFR3c(R248C) mutant extracellular and transmembrane domains fused to the intracellular FGFR1 tyrosine kinase domain, driven by a tetracycline operator sequence. **(b)** Mice treated with tamoxifen (Tmx) for 5 days were either switched to Doxycycline (Dox) chow or maintained on regular chow for 7 days. MuSCs were isolated and cultured for 72hr with or without in the absence of FGF2. mRNA was isolated and amplified for caFGFR1. **(c)** Representative images of cultured MuSCs from (b) were stained for caFGFR1 (using the myc-tag), and Pax7. Nuclei were counterstained with DAPI. n = 3 mice per condition.

exogenous FGF-2 is used to activate FGFR1 signaling and permits proliferation by preventing terminal differentiation, which increases MuSCs numbers in culture (Bernet et al., 2014; Yin et al., 2013). Therefore, we expressed caFGFR1 in isolated MuSCs and assayed for cell cycle progression by pulsing with EdU. MuSCs given exogenous FGF-2 incorporated EdU in approximately 70% of MuSCs, regardless of caFGFR1 expression (Figure 2.2a-b). Without exogenous FGF-2, MuSCs expressing caFGFR1 incorporated EdU in 50% of the cells, which was significantly less than with FGF-2, suggesting FGF-2 is a more potent signal for cell-cycle progression than caFGFR1. However, MuSCs without caFGFR1 expression and without FGF-2 incorporated EdU in only 25% of the cells (Figure 2.2a-b). Thus, expression of caFGFR1 significantly increases actively cycling MuSC numbers in culture (Figure 2.2a-b).

Constitutive FGFR1 signaling acts on activated MuSCs from young mice

Since caFGFR1 expression increased the number of actively cycling MuSC in culture, we asked if caFGFR1 expression would increase MuSCs numbers *in vivo*. We thus examined the effect of caFGFR1 expression on MuSC numbers in uninjured skeletal muscle from 4-6-month-old mice. We found no significant difference in MuSC numbers between MuSCs expressing caFGFR1 for 10 days and MuSCs not expressing caFGFR1 (Figure 2.3a-b). Additionally, caFGFR1 expression for 90 days, or pulsed on and off for three, two-week intervals, revealed no significant changes to MuSC numbers compared to control mice (Figure 2.3c-d). However, in uninjured adult skeletal muscle, most MuSCs are quiescent and therefore not actively cycling like MuSCs in culture. In

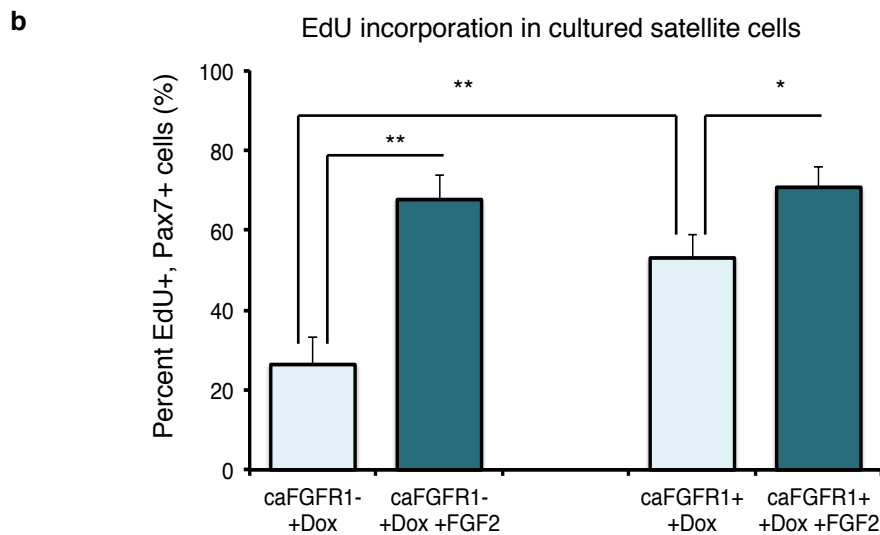
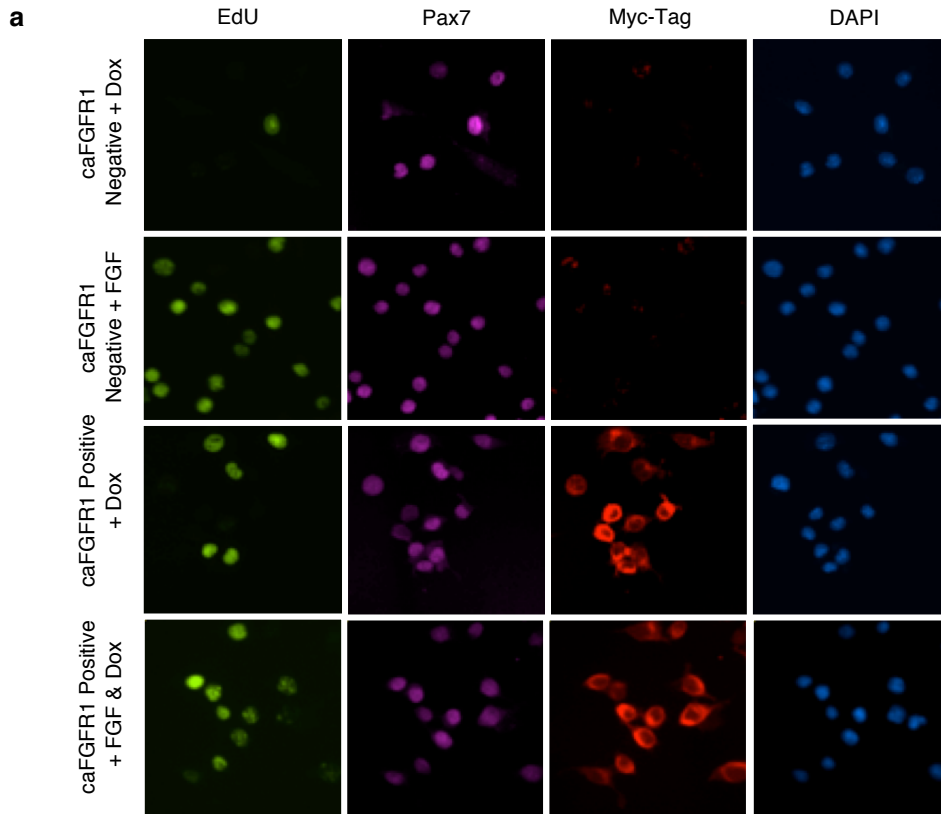


Figure 2.2 – caFGFR1 expands MuSCs and blocks differentiation *in vitro*

(a) Representative images of MuSCs isolated from a caFGFR1⁻ and a caFGFR1⁺ mice. MuSC were cultured with or without FGF2 in the presence of Dox for 72hrs. MuSCs were pulsed with 10 μ M EdU for two hours before fixation. MuSCs were stained for EdU, Pax7 and caFGFR1 (using the Myc-Tag). n = 3 mice per condition. Nuclei counterstained with DAPI. **(b)** Quantification of experiment described in (a); n=3 per condition; >100 cells quantified per n; **=p-value < 0.01; *=p-value < 0.05

these quiescent MuSCs, FGFR1 appears unable to activate MuSCs, which is consistent with evidence that FGF-signaling does not act as a mitogenic signal in MuSCs (Clegg et al., 1987; Yablonka-Reuveni et al., 2015).

Although FGFR1 signaling does not activate quiescent MuSCs in an uninjured, young adult mouse, FGFR1 signaling may influence the behavior of activated MuSCs *in vivo*. To test the effect of constitutive FGFR1 signaling on activated MuSCs *in vivo*, we injured the tibialis anterior (TA) muscle of 4-6-month-old young mice expressing caFGFR1 and examined the number of Pax7+ MuSCs. Seven days post BaCl₂-induced muscle injury MuSC numbers were significantly increased in mice that expressed caFGFR1 compared to controls (Figure 2.4a-b). At 30 days post injury, MuSC numbers were not significantly different between mice expressing caFGFR1 and controls (Figure 2.5d). Thus, ectopic caFGFR1 expression increases the number of MuSCs specifically during the first week of regeneration after an BaCl₂-induced muscle injury.

During the regeneration of skeletal muscle, MuSCs must maintain a balance between two pools of cells: (1) self-renewing MuSCs that will make more stem cells and (2) differentiating myoblasts that will rebuild the myofibers. Increasing MuSCs numbers after injury, through caFGFR1 expression, could thus impair muscle regeneration by decreasing myoblasts capable of differentiating and rebuilding myofibers. To test this possibility, we examined the myofiber size distribution in regenerating skeletal muscle of caFGFR1-expressing mice. At seven days post BaCl₂-induced muscle injury, the mice expressing caFGFR1 in MuSCs had smaller myofiber Feret diameters (Figure 2.4c).

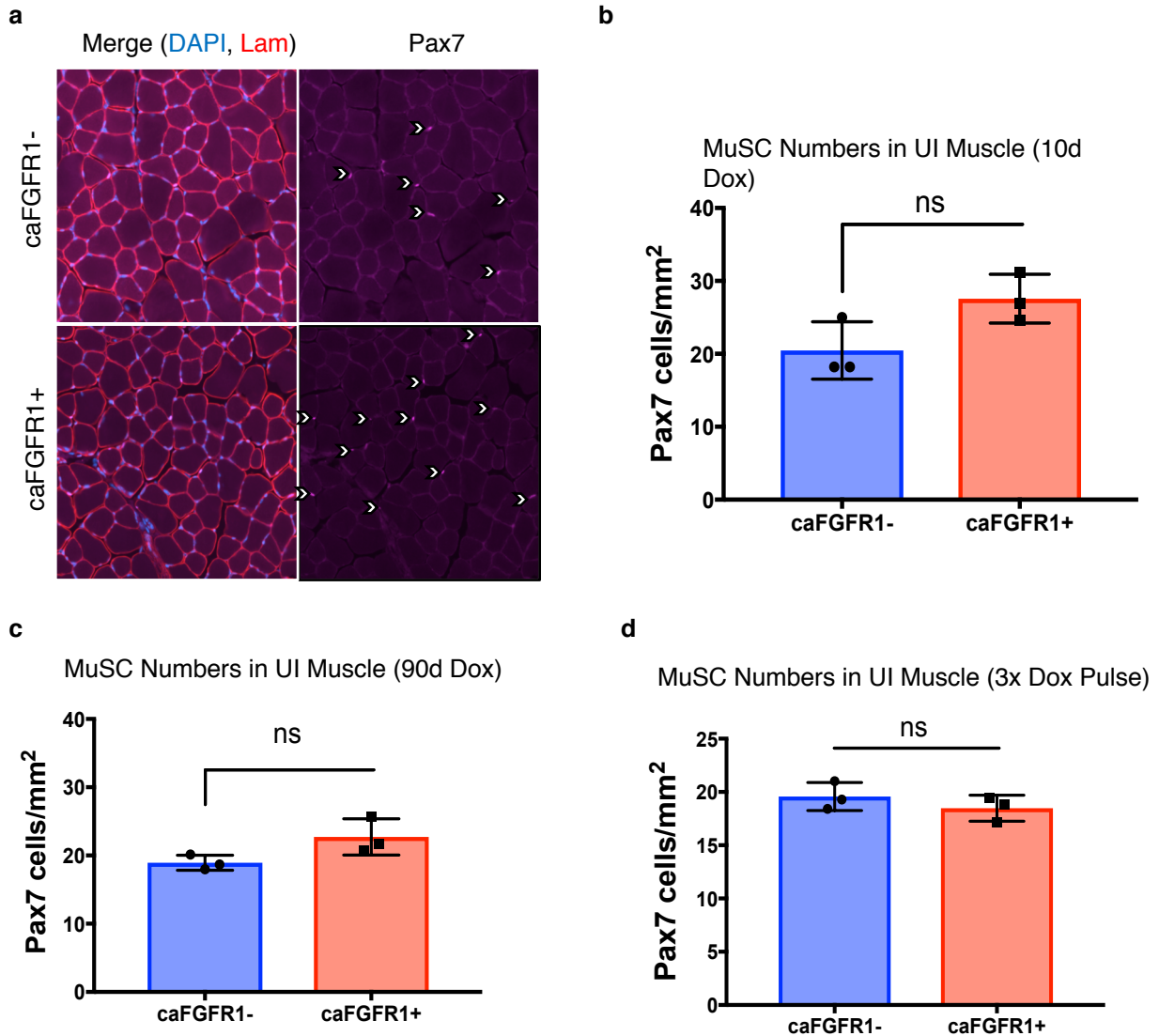


Figure 2.3 – caFGFR expression in MuSCs from uninjured young mice does not increase MuSC numbers *in vivo*

(a) Representative images of the tibialis anterior (TA) muscles of caFGFR1⁻ and caFGFR1⁺ mice induced with tmx for 5 days and treated with Dox chow for 10 days. Immunoreactivity for laminin and Pax7 was assessed. Nuclei were counterstained with DAPI. (b) Quantification of Pax7⁺ MuSC in (a) (c) Quantification of Pax7⁺ MuSCs per mm² from TA muscles of caFGFR1⁻ and caFGFR1⁺ mice induced with tmx for 5 days and treated with Dox chow for 90 days. Nuclei were counterstained with DAPI. (d) Quantification of Pax7⁺ MuSCs per mm² from TA muscles of caFGFR1⁻ and caFGFR1⁺ mice induced with tmx for 5 days and treated with three, 2 week pulses of Dox treatments. Nuclei were counterstained with DAPI. For b-d, n.s. = not significant; p-value > 0.05. n = 3 mice per condition; >250 Pax7⁺ cells counted per condition.

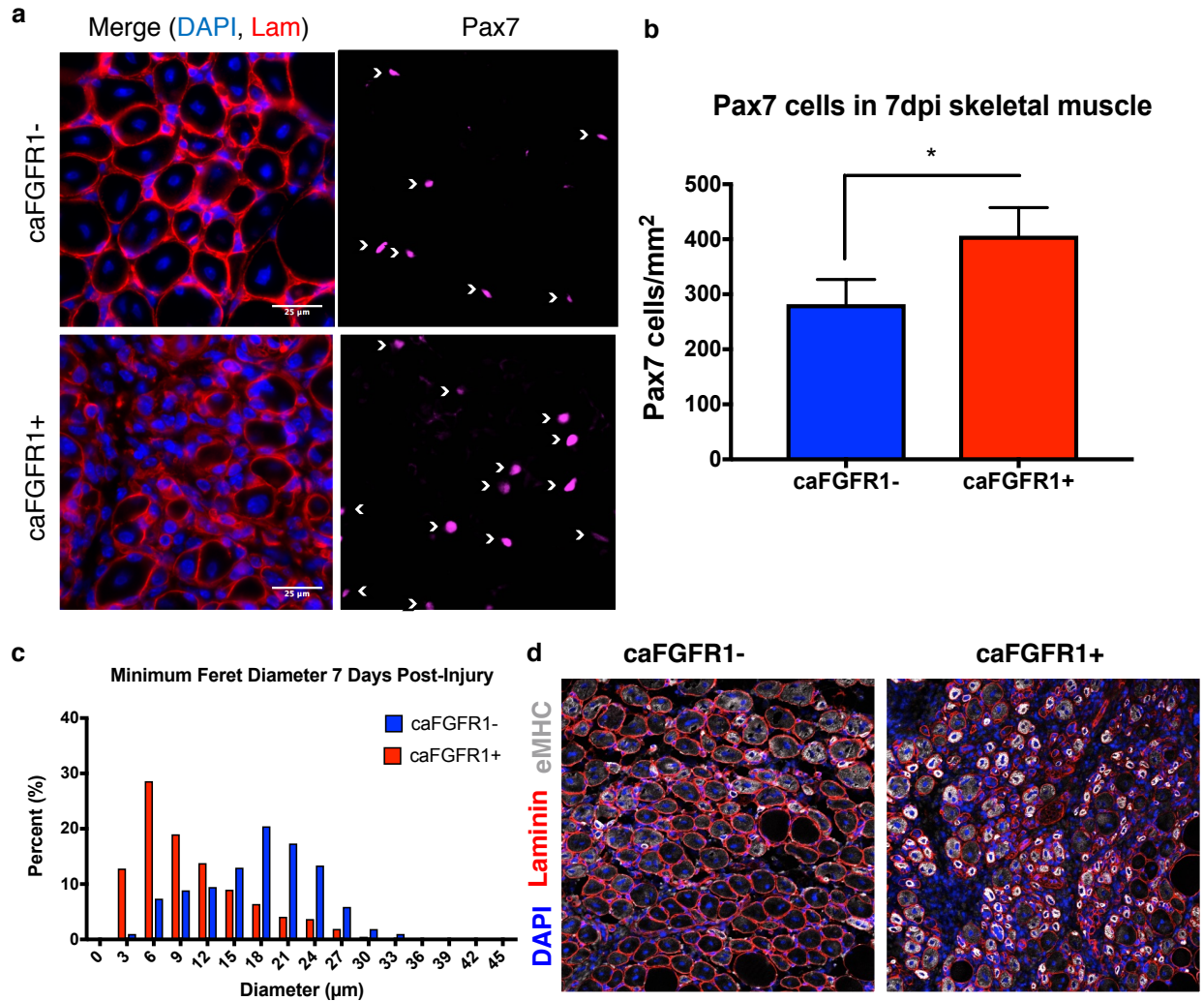


Figure 2.4 – caFGFR1 expression in MuSC impairs regeneration in young mice

(a) Representative images of the TA muscles of caFGFR1⁻ and caFGFR1⁺ mice injured with BaCl₂, and allowed to regenerate for 7 days. Sections were immunostained for laminin (red) and Pax7 (magenta). Nuclei were counterstained for DAPI. (b) Quantification of MuSCs per mm² from tissue in (a). n = 4; * = P-value < 0.05 in two-tailed paired t-test. (c) Myofibers from (a) quantified for minimum Feret's Diameter; >500 myofibers per condition; n = 3 mice per condition. (d) Representative images of the TA muscles of caFGFR1⁻ and caFGFR1⁺ mice injured with BaCl₂, and allowed to regenerate for 7 days. Sections were immunostained for laminin (red) and embryonic myosin heavy chain (eMHC)(white). Nuclei were counterstained for DAPI.

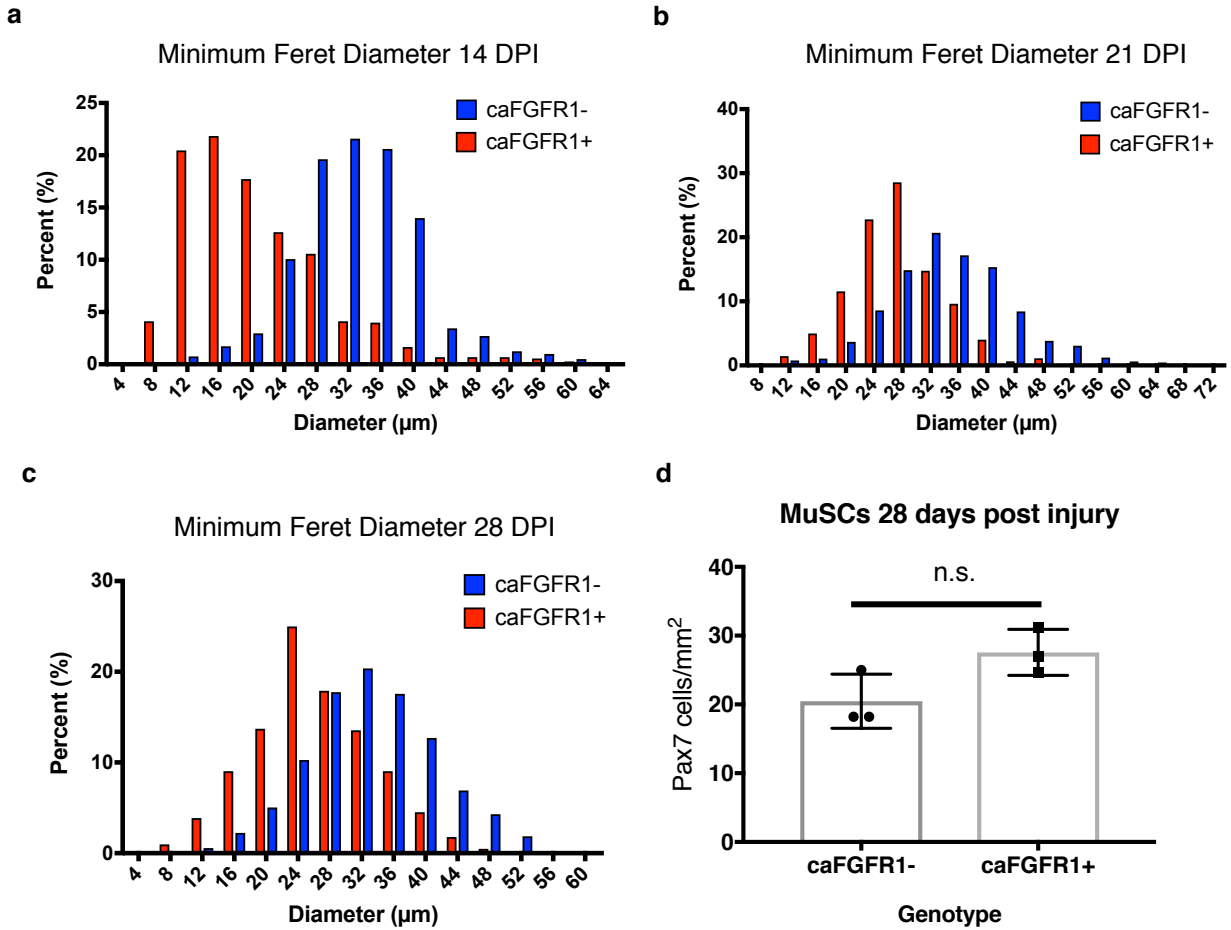


Figure 2.5 – caFGFR1 expression in MuSC delays muscle regeneration in young mice

(a-c) TA muscles of caFGFR1⁻ and caFGFR1⁺ mice were injured with BaCl₂, and allowed to regenerate for (a) 14 days (b) 21 days and (c) 28 days. Sections were fixed and immunostained for laminin. Myofibers were quantified for minimum Feret's Diameter; >500 myofibers per condition; n = 1 for a & b; n = 3 mice per condition for c. (d) Quantification of Pax7⁺ MuSCs per mm² from tissue in (c). n = 3 mice per condition. n.s = not significant p-value = >0.05.

Embryonic myosin heavy chain (eMHC) expression – a marker for early muscle regeneration that decreases at 5 days post-injury in control muscle – was increased in mice expressing caFGFR1 in MuSCs at seven days post-injury (Figure 2.4d). Thus, muscle regeneration in mice expressing caFGFR1 in MuSCs was significantly delayed compared to controls. Delayed muscle regeneration persisted in mice expressing caFGFR1 in MuSCs compared to controls, as myofiber diameters were smaller at 14, 21 and 28 days post-injury (Figure 2.5a-c). Therefore, expression of caFGFR1 in MuSCs increases MuSC numbers during regeneration by impairing MuSC differentiation potential in young muscle (Clegg et al., 1987; Yablonka-Reuveni et al., 2015).

Constitutive FGFR1 signaling drives asymmetric expansion in MuSCs from young mice

Ectopic FGFR1 signaling in cultured MuSCs from aged mice partially rescues self-renewal by driving asymmetric localization of phospho-p38 α / β MAPK (Bernet et al., 2014). However, it is unknown if caFGFR1 expression in MuSC from young muscle will drive asymmetric FGFR1 signaling. In isolated MuSCs we observed asymmetric localization of the caFGFR1 protein (Figure 2.6a). Additionally, phosphorylated FGFR1 was asymmetric and colocalized with caFGFR1 protein in cells expressing caFGFR1, but in MuSCs without caFGFR1 the phosphorylated FGFR1 is not asymmetric (Figure

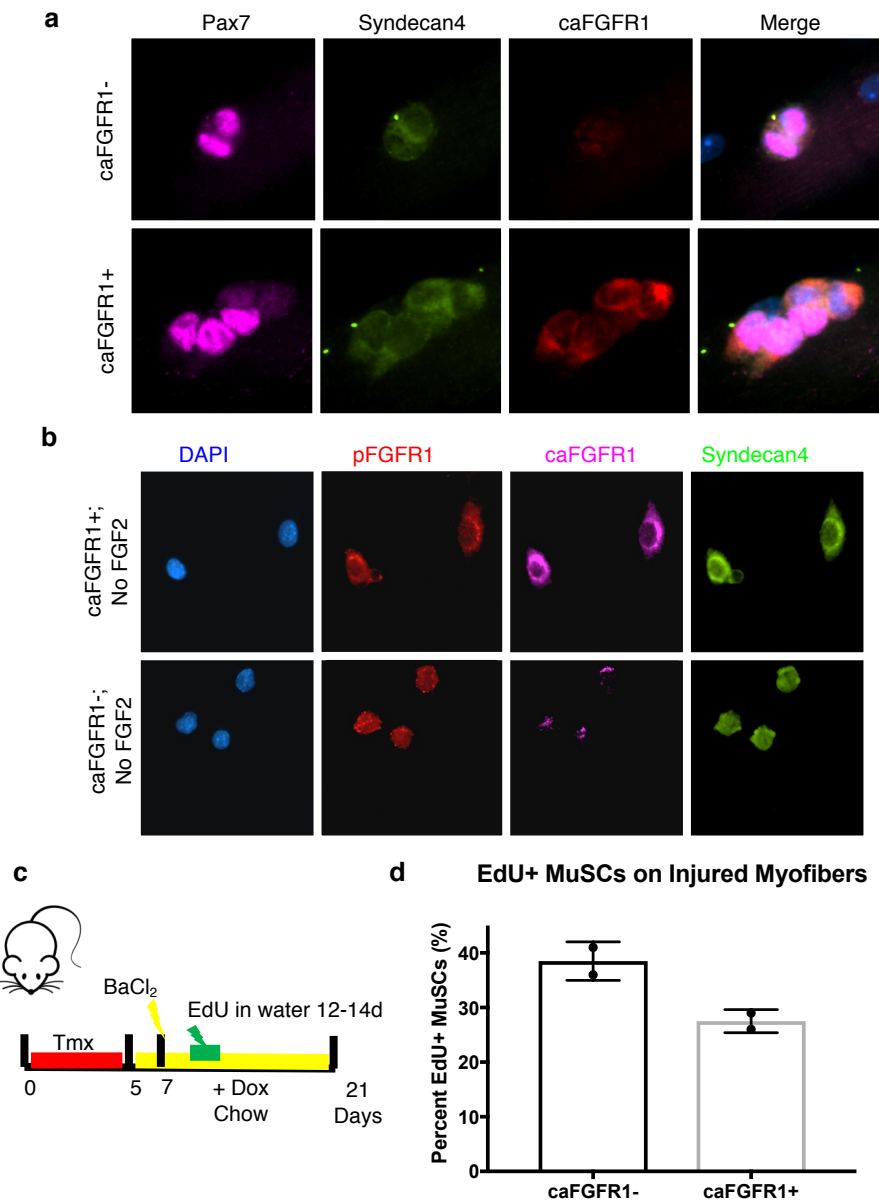


Figure 2.6 – caFGFR1 expression promotes MuSC asymmetry and drives continued expansion of MuSC *in vivo*

(a) Representative images of EDL-associated MuSC from caFGFR1⁻ and caFGFR1⁺ mice fed Dox chow for 10d. EDL muscles were removed, myofibers isolated and cultured with Dox for 72h without FGF2. MuSCs were immunostained for Pax7, Syndecan4 and caFGFR1 (myc-tag). Nuclei were counterstained with DAPI. **(b)** Representative images cultured MuSC from caFGFR1⁻ and caFGFR1⁺ mice fed Dox chow for 10d. MuSCs were cultured with Dox for 72h without FGF2. MuSCs were immunostained for Syndecan4, caFGFR1 (myc-tag) and phosphoFGFR1. Nuclei were counterstained with DAPI. **(c)** Schematic EdU pulse assay. caFGFR1⁻ and caFGFR1⁺ mice were induced with Tmx for 5 days then placed on Dox chow. Mice were then injured with BaCl₂, pulsed with EdU from 5-7 days post inju. EDL myofibers were collected 14 DPI. **(d)** Quantification of Pax7⁺; EdU⁺ MuSCs on myofibers from (c). n = 2 mice per condition.

2.6b). This suggests that caFGFR1 expression drives asymmetric localization of FGFR1 signaling in MuSCs and may influence asymmetric cell divisions in young mice.

Asymmetric cell divisions are thought to produce two distinct daughter cells after a muscle injury, a quiescent MuSCs and a myoblast. It is hypothesized that the daughter cell lacking the FGFR1 signaling self-renews and becomes quiescent while the cell with FGFR1 signal continues to expand. If caFGFR1 is expressed in both daughter cells, there may be a decrease in quiescent MuSC number with a concomitant increase in dividing Pax7+ myoblasts. To test this, we examined the timing of self-renewal in caFGFR1-expressing and control MuSCs. In control mice not expressing caFGFR1, 39% of quiescent MuSC were established between five and seven days post-injury, which is consistent with previous reports (Pawlikowski et al., Submitted). However, constitutive FGFR1 signaling reduced the number of quiescent MuSCs generated during five and seven days post injury to 27% (Figure 2.6c-d). Thus, caFGFR1 expression drives the continued expansion of Pax7+ myoblasts *in vivo*, which reduces the number of quiescent MuSCs and delays differentiation in young muscle.

Constitutive FGFR1 MuSC signaling restores old muscle

Responsiveness to FGF signaling is blunted in MuSCs from aged muscle which impairs asymmetric divisions and can lead to a decrease in MuSC numbers. Restoring FGFR1 signaling in cultured MuSCs from aged muscle rescues impaired asymmetric divisions (Bernet et al., 2014). To test if rescuing FGFR1 signaling in MuSCs from aged mice will affect MuSC numbers *in vivo*, we aged mice with or without the caFGFR1

transgene for 24 months (Figure 2.7a). We then gave 24-month-old mice tamoxifen chow for seven days and then fed them doxycycline chow for one month (Figure 2.7b). Twenty-four-month-old mice that express caFGFR1 had significantly more MuSCs in the TA muscle compared to control mice without caFGFR1 expression in MuSCs (Figure 2.7c-d). In mice without caFGFR1 expression in MuSCs there was a decrease in MuSC numbers compared to young controls (Figure 2.3b; 2.7d) whereas there was no difference in MuSC numbers in young and old mice expressing caFGFR1 in MuSCs (Figure 2.3b; 2.7d). These data suggest that rescuing defective FGFR1 signaling in MuSC from aged mice can increase MuSC numbers.

While examining MuSC numbers in the TA muscle from aged mice, we noticed the size of the uninjured TA muscles were larger in caFGFR1 expressing mice than in controls (Figure 2.8a). The average TA wet weights caFGFR1 expressing mice was 44.7mg compared to 39.8mg in controls (Figure 2.8b). The myofiber diameters were larger in caFGFR1 expressing mice compared to controls (Figure 2.8c). This unexpected phenotype led us to examine if the skeletal muscle of old mice expressing caFGFR1 in MuSCs was functionally different than controls. The maximal force capacity of the gastrocnemius muscle in 24-month-old mice was equivalent between animals (Data not shown). However, fatigue resistance was much lower in the EDL muscles from 24-month-old mice expressing caFGFR1 in MuSCs (Figure 2.9a-b). Young mice have a fatigue resistance equivalent to 24-month-old mice expressing caFGFR1; however, fatigue resistance was much greater in 24-month-old mice without caFGFR1 (Figure 2.9a-b). Fatigue resistance can be altered through changes in myofiber types.

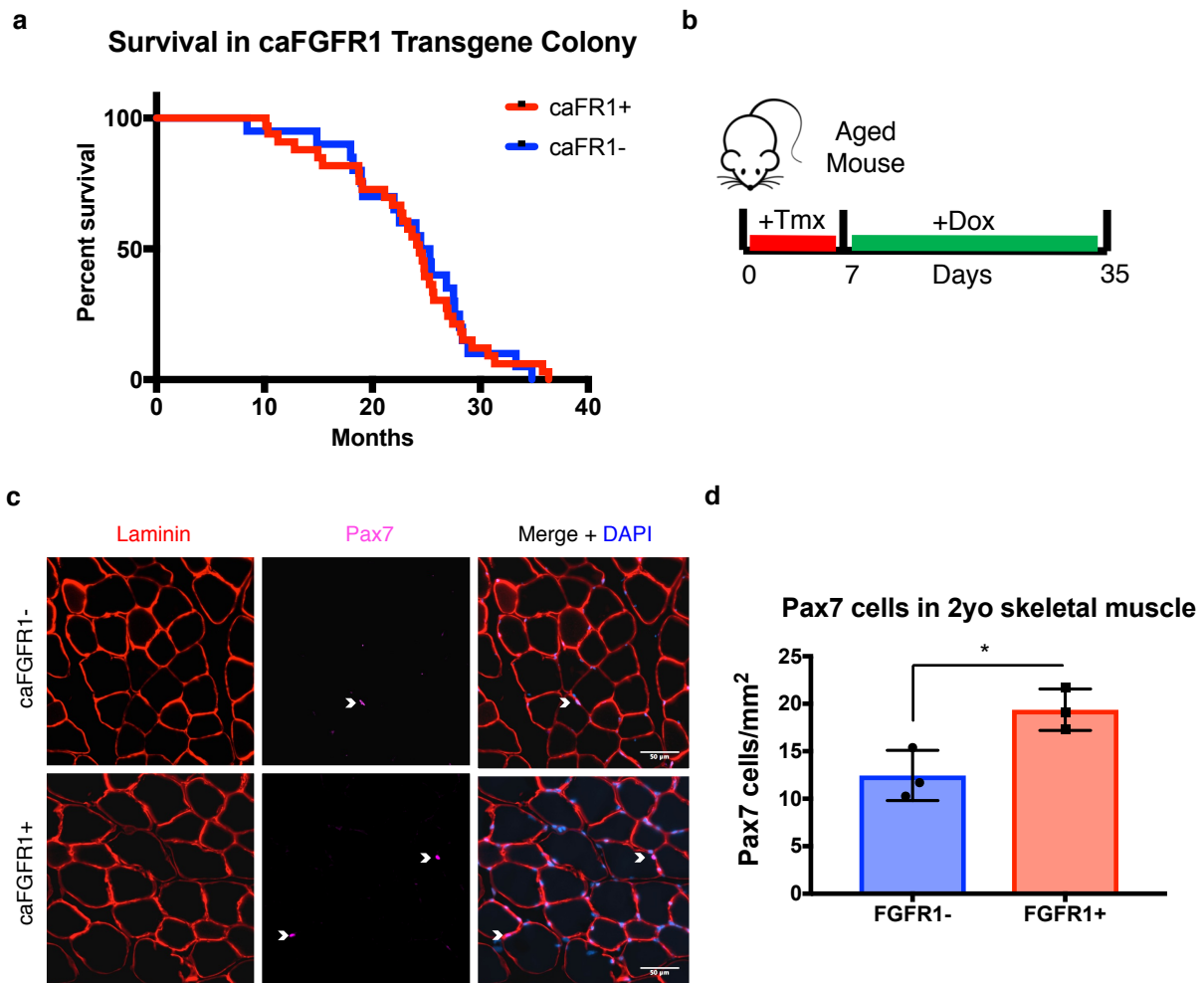


Figure 2.7 – MuSC-specific expression of caFGFR1 in aged muscle increase MuSC numbers

(a) Kaplan-Meier survival curve of uninduced caFGFR1+ and caFGFR1- mice shows no significant difference in survival as mice age. **(b-c)** Two year old (2yo) mice were given tamoxifen chow for 7 days and Doxycycline chow for one month. Tibialis anterior muscles were collected and immunostained for laminin and Pax7. Nuclei were counterstained with DAPI. **(d)** Quantification of Pax7+ MuSC per mm² in TA muscles from (c). n = 3 mice per condition; * = p-value < 0.05

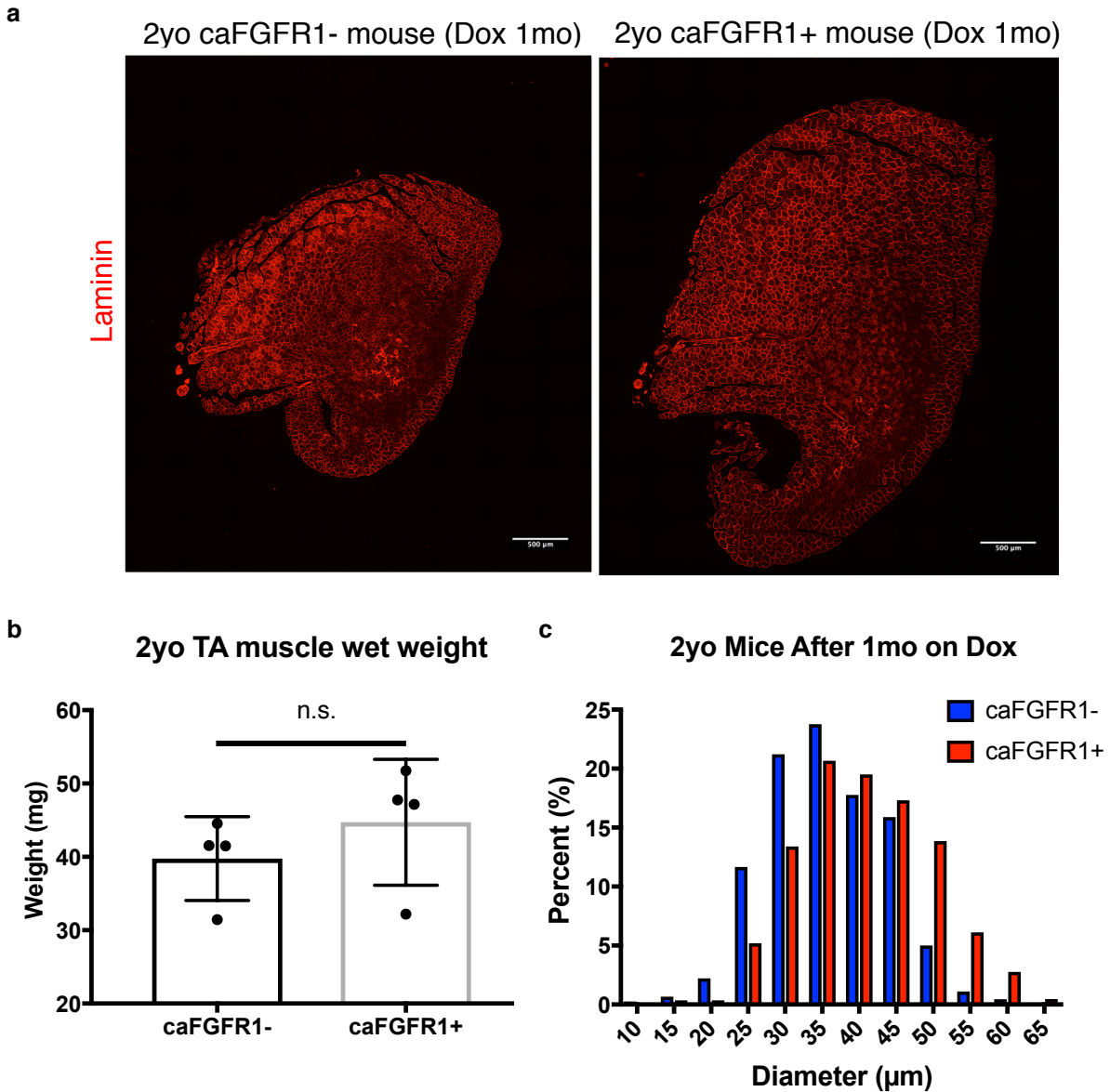


Figure 2.8 – MuSC-specific expression of caFGFR1 in aged muscle increases myofiber size

(a) Two year old (2yo) mice were given tamoxifen chow for 7 days and Doxycycline chow for one month. Tibialis anterior muscles were collected and immunostained for laminin (b) Quantification of wet TA muscle weights from (a). n.s = not significant p-value = >0.05. (c) Minimum Feret Diameter determined by laminin immunoreactivity of 2yo mouse tissue. n = 3 mice per condition.

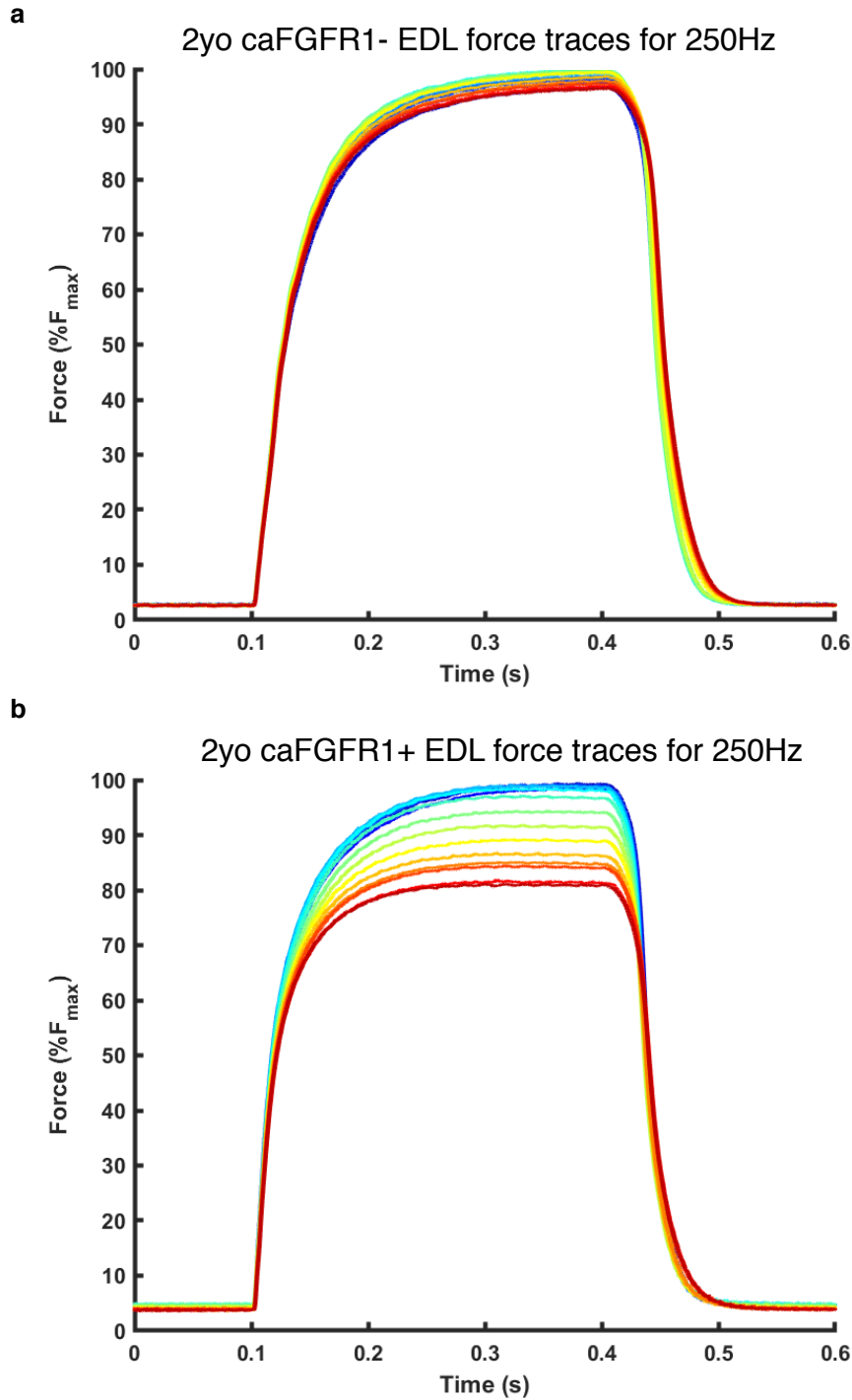


Figure 2.9 – MuSC-specific expression of caFGFR1 restores aged muscle to youthful state

(a-b) Two year old (2yo) mice were given tamoxifen chow for 7 days and Doxycycline chow for one month. EDL muscles were isolated and then repeatedly stimulated with 250Hz every 30 minutes to measure force contraction over time. Blue lines represent early stimulation and red lines represent late stimulations. n = 1 mouse per condition.

For example, a muscle with higher percentage of slow-twitch (Type I) myofibers will be more resistant to fatigue than a muscle with a higher percentage of fast twitch (Type II) myofibers. As muscles age, there is a switch from type II to type I myofibers (Akasaki et al., 2014). Together, these results suggest that expression of caFGFR1 in MuSCs from aged mice can increase MuSC numbers and restore muscle function to a youthful state.

Discussion

Skeletal muscle function and mass decline with age and can lead to increased morbidity and mortality (Landi et al., 2013). While the mechanisms for age-related muscle loss are multifactorial, reduction in the regenerative capacity of muscle is a clear contributor (Brooks and Faulkner, 1990; Day et al., 2010). Previous work has demonstrated that altered FGF signaling in MuSCs from aged muscle may drive the depletion of MuSCs in aged muscle, and thus, reduce the regenerative capacity of aged muscle (Bernet et al., 2014; Chakkalakal et al., 2012; Rozo et al., 2016). The present study aimed to manipulate FGFR1 signaling in MuSC from young and aged mice to understand the *in vivo* effects of FGFR1 signaling in regenerating and aged muscle. We show that increasing FGFR1 signaling in MuSCs has distinct effects on MuSC numbers in young and aged muscle. In MuSCs from young uninjured muscle, increasing FGFR1 signaling has no effect on MuSC numbers. However, in young, regenerating skeletal muscle, constitutive FGFR1 signaling increases MuSC numbers. In contrast, in MuSCs

from aged uninjured skeletal muscle, constitutive FGFR1 signaling increases MuSCs numbers.

FGFR1 signaling as an in vivo repressor of differentiation

A possible mechanism to regulate MuSC numbers during muscle regeneration is through an asymmetric division where one daughter cell becomes a MuSC and the other become a myoblast that can differentiate to rebuild muscle. We propose a model where continuous FGFR1 signaling in activated MuSCs in culture and *in vivo* causes cells to remain in a proliferative state by repressing differentiation (Figure 2.10). In young regenerating muscle – a state where almost all MuSCs are activated – repressing MuSC differentiation through caFGFR1 expression increases the number of Pax7+ cells. This has two significant effects muscle regeneration: (1) it decreases the number of myoblasts capable of differentiation, which delays skeletal muscle regeneration and (2) it decreases the number of quiescent MuSCs generated during early muscle regeneration. Therefore, tuning FGFR signaling is a mechanism to regulate MuSC numbers after a skeletal muscle injury. In young, regenerating skeletal muscle, activation of FGFR1 signaling likely occurs immediately following injury when FGF ligands are released from the extracellular space and from surrounding cell populations (Garrett and Anderson, 1995; Rao et al., 2013). In this environment, as MuSCs divide, FGFR1 signaling is activated in both daughter cells, which drives exponential cell proliferation. As the muscle repairs and the local concentration of FGF is reduced, Pax7+ cells begin to undergo self-renewal divisions, where one daughter

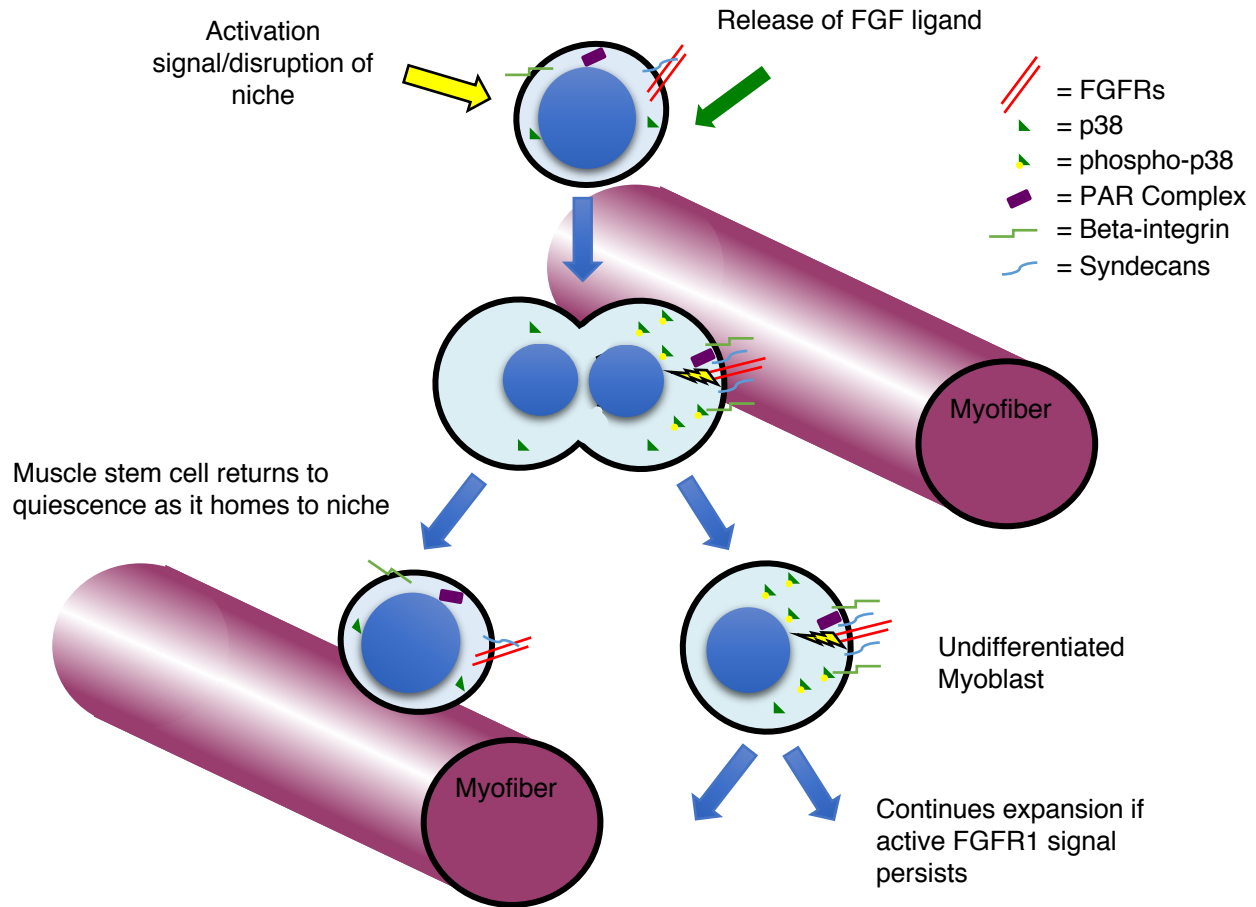


Figure 2.10 – Model for *in vivo* expansion of MuSCs driven by asymmetric FGFR1 signaling.

In activated MuSC, FGFR1 becomes asymmetrically localized. Along with FGFR1, a cadre of co-receptors and signaling molecules becomes asymmetrically localized in activated MuSCs. As the MuSC divides, FGFR1 signaling is concentrated in the daughter cell destined to remain a myoblast while the cell without FGFR1 signaling becomes a quiescent MuSC as it homes to the niche. The myoblast with active FGFR1 signaling will continue to divide asymmetrically until the signal to terminally differentiate overrides FGFR1 signaling. In young *caFGFR1* mice, the continuous FGFR1 signaling drives MuSC expansion at the expense of differentiation, which impairs muscle regeneration. The *caFGFR1* signaling in aged mice rescues precocious differentiation of MuSC by increasing FGFR1 signaling. This increases MuSC numbers and unexpectedly, restores skeletal muscle to a youthful state.

cell becomes quiescent. Negative regulation of the FGFR signaling pathway – for example, though Sprouty-1 – could also provide cell-intrinsic mechanisms to promote the return to quiescence during regeneration (Chakkalakal et al., 2012).

FGFR1 signaling in MuSCs: aged vs young muscle

In young, uninjured skeletal muscle, caFGFR1 expression in MuSCs had no effect on cell numbers, which is consistent with evidence that FGF-signaling does not act as a mitogenic signal in MuSCs but rather permits MuSC proliferation by repressing myogenesis (Clegg et al., 1987; Kudla et al., 1998; Yablonka-Reuveni et al., 2015). Yet in uninjured, aged mice MuSC numbers increased with caFGFR1 expression. This age-related sensitivity to FGFR1 signaling is likely due to the activation state of MuSCs in the aged environment (Bernet et al., 2014; Chakkalakal et al., 2012)(Pawlikowski et al., Submitted). MuSCs in uninjured, aged muscle cycle more frequently during homeostasis than MuSCs from uninjured young muscle (Chakkalakal et al., 2012) and are transcriptionally similar to MuSCs from a young mouse seven days after an injury (Pawlikowski et al., Submitted). MuSCs from aged muscles are in an activated state, similar to MuSCs from a young regenerating muscle and thus, respond to FGFR1 signaling by maintaining the proliferation Pax7+ MuSCs.

But why does increasing FGFR1 signaling in MuSCs from aged muscle increase their numbers? Previous evidence suggests ectopic FGFR1 signaling in MuSCs from aged muscle increases the fraction of asymmetric cell divisions (Bernet et al 2014). Here we show that within activated MuSCs the localization of caFGFR1 protein and subsequent FGFR1 signaling becomes asymmetrically localized, which drives

continued expansion of MuSC in culture and *in vivo*. Continued FGFR1-mediated asymmetric cell division is thus a permissive signal for MuSCs to remain in the cell cycle, whereas loss of FGFR1 signal increases the likelihood of MuSCs to terminally differentiate. MuSCs from aged muscle are activated but have impaired FGFR1 signaling (Bernet et al., 2014; Chakkalakal et al., 2012)(Pawlikowski et al., Submitted), which drives precocious differentiation. Restored FGFR1 signaling in aged animals, via caFGFR1, prevents terminal differentiation by providing a permissive signal for MuSC to remain in the cell cycle. Thus, the increase in MuSC numbers in aged mice expressing caFGFR1 likely acts by promoting asymmetric cell division cycles and blocking terminal differentiation.

FGFR1 signaling in MuSCs alters old muscle tissue

A surprising aspect of this work is that the MuSC-specific expression of caFGFR1 functionally changed aged skeletal muscle tissue. By increasing MuSC numbers in old muscle, through caFGFR1 expression, aged muscle became larger and was less resistant to fatigue than aged controls. These changes make the aged muscle resemble muscle from a younger mouse (Miljkovic et al., 2015), suggesting caFGFR1 expression in MuSCs can restore youthfulness to aged muscle. How caFGFR1 expression only in MuSCs regulates the restoration of aged skeletal muscle tissue is unknown. It is possible that rescuing MuSC numbers has a positive effect on myofibers through an unknown paracrine signal. However, to date no secreted paracrine factor from MuSCs is known to alter myofiber types. Alternatively, MuSCs that express caFGFR1 could

fuse into aged myofibers promote gene expression or signaling pathways towards a more youthful state. Together, this could change the type of myosin genes expressed, which could alter the fiber type from slow-twitch (common in aged muscle) to fast-twitch (common in young muscle) (Miljkovic et al., 2015). Thus, manipulating FGFR1 signaling to increase MuSC numbers and change aged muscle function opens a potentially new avenue of therapeutic intervention for sarcopenia.

Methods

Mice

Mice were bred and housed according to National Institutes of Health (NIH) guidelines for the ethical treatment of animals in a pathogen-free facility at the University of Colorado at Boulder (Wild-type, Pax7^{iresCre}, ROSA26^{LSLrtTA} and caFGFR1 transgenic lines). The University of Colorado Institutional Animal Care and Use Committee (IACUC) approved all animal protocols and procedures. Wild-type mice were C57Bl/6 (Jackson Labs, ME, USA) and Pax7^{iresCre} mice (Murphy et al., 2011) and caFGFR1 transgenic mice (Cilvik et al., 2013) were previously described. Crossing mice generated conditional Pax7^{iresCre}; ROSA26^{LSLrtTA}; caFGFR1 mice. For experiments on young mice, cells and tibialis anterior (TA) muscles were isolated from 3-6-month-old male and female Pax7^{iresCre}; ROSA26^{LSLrtTA}; caFGFR1 mice. For experiments on aged mice, TA muscles were isolated from 24-month-old male and female Pax7^{iresCre};

ROSA26^{LSLrtTA}; caFGFR1 mice. Control mice were age and sex matched from the mice and crosses described above.

Mouse injuries and tamoxifen injections

Mice at 3-6 months old were anesthetized with isofluorane and the left TA muscle was injected with 50 μ L of 1.2% BaCl₂ and then the injured and contralateral TA muscles were harvested at the indicated time points. Intraperitoneal (IP) administration of tamoxifen (Sigma), re-suspended in sterile corn oil (Sigma), was given to 3-6-month-old mice at a volume of 0.075mg of tamoxifen per gram of mouse weight. In 24-month-old mice IP tamoxifen was given for the three days and then mice were switched to tamoxifen chow.

Isolation and immunofluorescence of primary muscle stem cells

Gastrocnemius, extensor digitorum longus (EDL), TA and all other lower hindlimb muscles were dissected from experimental and control mice. The muscle groups from both hind limbs were minced with dissection scissors, separated and digested in 9mL of F12-C (Gibco) with penicillin/streptavidin (Gibco) and 1000uL 10X collagenase (Worthington) for 60 minutes at 37°C with shaking every 10 minutes. Equal parts F12-C with penicillin/streptavidin and 15% horse serum (growth media) was added to the digest. Cells in the digest were filtered through 100 μ m, 70 μ m and 40 μ m filters. The cells was centrifuged at 1500rpm and the pellet was resuspended in 20mL growth media. The cells were plated onto two (Corning) 10cm tissue culture plate with Matrigel in

10mL of growth media. Cells were incubated in growth media with FGF-2 (50nM working concentration) for 72 hours at 37°C in 6% O₂, 5% CO₂. If cells were not lysed for RNA and protein collection cells were fixed for immunofluorescence.

For immunostaining, cells were fixed with 4% paraformaldehyde for 10 minutes at room temperature. Cells were then permeabilized with 0.25% Triton-X100 (Sigma) in PBS containing 2% bovine serum albumin (Sigma) for 60 min at RT. Incubation with primary antibody occurred at 4°C overnight followed by incubation with secondary antibody at room temperature (RT) for 1hr. Primary antibodies included mouse anti-Pax7 (Developmental Studies Hybridoma Bank, University of Iowa, USA) at 1:750, rabbit anti-myc-tag (CellSignaling) at 1:400, chicken anti-syndecan4 (Developmental Studies Hybridoma Bank, University of Iowa, USA) at 1:1000 and a mouse anti-phosphoFGFR1 (CellSignaling) at 1:100. Alexa secondary antibodies (Molecular Probes) were used at a 1:1000 dilution. For analysis that included EdU detection, EdU staining was completed prior to antibody staining using the Click-iT EdU Alexa fluor 488 detection kit (Molecular Probes) following manufacturer protocols. Cells were incubated with 1 µg/mL DAPI for 10 min at room temperature then mounted in Mowiol supplemented with DABCO (Sigma-Aldrich) or ProLong Gold (Thermo) as an anti-fade agent.

Isolation and immunofluorescence of primary myofibers

Individual extensor digitorum longus myofibers were isolated cultured and immunostained according to (Vogler et al., 2016). Briefly, hindlimbs were dissected,

connective tissue removed, and muscle groups separated followed by enzymatic digestion in 400-U/mL collagenase at 37 °C for 1.5 h. Collagenase was inactivated by the addition of Ham's F-12C supplemented with 15 % horse serum. Individual extensor digitorum longus myofibers were gently isolated by trituration and either immediately fixed in 4 % paraformaldehyde for 10 minutes or maintained in Ham's F-12C supplemented with 15 % horse serum and 50nM FGF-2 at 6 % O₂ prior to fixation and immunostaining. Immunostaining was performed using transfer baskets described in Vogler et al., 2016 and used solutions and antibodies identical to primary muscle stem cell immunofluorescence.

Immunofluorescence staining of tissue sections

TA or gastrocnemius muscles were dissected, fixed on ice for 2hrs with 4% paraformaldehyde, and then transferred to PBS with 30% sucrose at 4°C overnight. Muscle was mounted in O.C.T. (Tissue-Tek®) and cryo-sectioning was performed on a Leica cryostat to generate 10µm thick sections. Tissues and sections were stored at -80°C until staining. Tissue sections were post-fixed in 4% paraformaldehyde for 10 minutes at room temperature (RT) and washed three times for 5 min in PBS. Immunostaining with anti-Pax7, anti-Laminin and anti-eMHC antibodies required heat-induced epitope retrieval where post-fixed slides were placed in citrate buffer, pH 6.0, and subjected to 6 min of high pressure-cooking in a Cuisinart model CPC-600 pressure cooker. Immunostaining with anti-myc-tag did not require heat-induced epitope retrieval. For immunostaining, tissue sections were permeabilized with 0.25% Triton-X100

(Sigma) in PBS containing 2% bovine serum albumin (Sigma) for 60 min at RT. Incubation with primary antibody occurred at 4°C overnight followed by incubation with secondary antibody at room temperature (RT) for 1hr. Primary antibodies included mouse anti-Pax7 (Developmental Studies Hybridoma Bank, University of Iowa, USA) at 1:750, rabbit anti-laminin (Sigma-Aldrich) at 1:200, rabbit anti-myc-tag (CellSignaling) at 1:200 and a mouse anti-eMHC (Developmental Studies Hybridoma Bank, University of Iowa, USA) at 1:5. Alexa secondary antibodies (Molecular Probes) were used at a 1:1000 dilution. For analysis that included EdU detection, EdU staining was completed prior to antibody staining using the Click-iT EdU Alexa fluor 488 detection kit (Molecular Probes) following manufacturer protocols. Sections were incubated with 1 µg/mL DAPI for 10 min at room temperature then mounted in Mowiol supplemented with DABCO (Sigma-Aldrich) or ProLong Gold (Thermo) as an anti-fade agent.

Cell culture.

Primary Muscle Stem Cells: After initial isolation, primary myoblasts were maintained on Matrigel-coated tissue culture plastic plates or gelatin-coated coverslips at 37°C with 6% O₂, 5% CO₂ in growth media as described above. Media was changed only during cell passaging. To promote myoblast fusion, cells at 75% confluency were washed three times with PBS and media switched to DMEM (Gibco) with 5% horse serum (Gibco), 1% penicillin/streptavidin and 1% Insulin-Transferrin-Selenium (Gibco).

Primary Myofibers: After initial isolation

Microscopy and image analyses

Images were captured on a Nikon inverted spinning disk confocal microscope. Objectives used on the Nikon were: 10x/0.45NA Plan Apo, 20x/0.75NA Plan Apo and 40x/0.95 Plan Apo. Confocal stacks were projected as maximum intensity images for each channel and merged into a single image. Brightness and contrast were adjusted for the entire image as necessary. Both muscle stem cell numbers and average myofiber diameter were counted manually using Fiji ImageJ. Images were processed using Fiji ImageJ.

EdU Incorporation in mice and cells

For mouse experiments, 5-ethynyl-2'-deoxyuridine (EdU – Life Technologies) was dissolved in sterile water with dextrose to give final concentrations of 0.5 μ g/mL EdU and 1% dextrose. Water was given to mice for the described number of days. For primary culture experiments, cells were incubated with 10 μ M 5-ethynyl-2'-deoxyuridine (EdU – Life Technologies) for two hours.

Functional fatigue resistance assays

Ex vivo assessment of fatigability of EDL muscles were performed as described in Park et al., 2012. In brief, mice at 24 months old were anesthetized with isoflurane and the right EDL muscles were dissected. Muscles were bathed in Ringer's Solutions. Surgical knots were tied at both ends of the EDLs and mounted on a PowerLab force transducer chamber incubated in oxygenated Tyrode solution. EDL muscles were

equilibrated and then electrically stimulated with 250Hz every 30 minutes to measure the percent maximal force generated. The stimulation was repeated overnight to measure the change in percent maximal force over time.

Primers for caFGFR1 detection by PRC

FGFR3 TMD – FGFR1 TKD spanning primers:

FR3-FR1-FW: AGCTACGGGGTGGTCTTCTT

FR3-FR1-RV: AACCAGGAGAACCCCAGAGT

Chapter 3:

TDP-43 and RNA form amyloid-like myo-granules in skeletal muscle regeneration

Adapted from: Vogler, T. O., Wheeler, J. R., Nguyen, E. D., ... Olwin. B. B. & Parker, R.
TDP-43 and RNA form amyloid-like myo-granules in regenerating
muscle. *Nature*, 563(7732), 508 (2018).

Summary

A dominant histopathological feature in neuromuscular diseases including amyotrophic lateral sclerosis and inclusion body myopathy is cytoplasmic aggregation of the RNA-binding protein TDP-43. Although rare protein-misfolding mutations in TDP-43 often cause protein aggregation, most patients do not have a TDP-43 mutation suggesting aggregates of wild-type TDP-43 arise by an unknown mechanism. Here we show TDP-43 is an essential protein for normal skeletal muscle formation that unexpectedly forms cytoplasmic, amyloid-like oligomeric assemblies, termed myo-granules, during skeletal muscle regeneration in mice and humans. Myo-granules bind mRNAs encoding sarcomeric proteins and are cleared as myofibers mature. Although myo-granules occur during normal skeletal muscle regeneration, myo-granules can seed TDP-43 amyloid fibrils *in vitro*, and are increased in a mouse model of inclusion body myopathy. Therefore, heightened assembly or decreased clearance of functionally normal myo-granules could be the source of cytoplasmic TDP-43 aggregates common to neuromuscular disease.

Introduction

TAR DNA-binding Protein 43 (TDP-43) is a ubiquitously expressed DNA and RNA-binding protein involved in several aspects of RNA metabolism, such as RNA stability, splicing and transport (Alami et al., 2014; Ayala et al., 2011; Buratti and Baralle, 2008; Kawahara and Mieda-Sato, 2012; Volkening et al., 2009). TDP-43 is predominantly considered a nuclear protein, where cytoplasmic localization of TDP-43 is a histopathological hallmark of degenerative neuromuscular diseases (Küsters et al., 2009; Neumann et al., 2006; Wehl et al., 2008). However, a number of studies show TDP-43 regulates RNA in the cytosol of healthy cells. In primary neurons, TDP-43 forms cytoplasmic ribonucleoproteins (RNPs) granules that transport mRNA along axons and dendrites (Ayala et al., 2008; Fallini et al., 2012). The role of TDP-43 in neuronal RNP assembly and function are mediated by its direct interactions with other RNA-binding proteins, such as, heterogenous nuclear ribonucleoprotein (hnRNP) A/B, PABPC1, fused in sarcoma (FUS) and ataxin-2 (Buratti et al., 2005; D'Ambrogio et al., 2009; Elden et al., 2010; Freibaum et al., 2010; Kawahara and Mieda-Sato, 2012; Kim et al., 2010). However, beyond neurons, the function of TDP-43 and its role in RNP assemblies are largely unknown.

The function and aggregation of the TDP-43 in multinucleated skeletal muscle cells (myofibers) is of interest for two reasons. First, TDP-43 aggregates accumulate in the skeletal muscle of patients with inclusion body myopathy (IBM), oculopharyngeal muscular dystrophy (OPMD), and distal myopathies (Küsters et al., 2009; Wehl et al., 2008). These aggregates appear similar to the cytoplasmic TDP-43 aggregates found in

the neurons of patients with amyotrophic lateral sclerosis (ALS) and frontotemporal lobar degeneration (FTLD), suggesting a common mechanism in muscle and neurons leading to histopathological, cytoplasmic TDP-43 aggregation (Neumann et al., 2006; Renton et al., 2014; Weihl et al., 2008). Second, reducing TDP-43 levels leads to age-related muscle weakness in mice (Kraemer et al., 2010), muscle degeneration and sarcomere disruption in zebrafish (Schmid et al., 2013), and age-related muscle weakness in *Drosophila* wing muscles (Diaper et al., 2013; Llamusi et al., 2013). Given the requirement for TDP-43 in muscle function, and its potential to form cytoplasmic aggregates in muscle diseases, we examined TDP-43 function during normal mammalian skeletal muscle formation.

Results

Cytoplasmic TDP-43 myo-granules

We first examined the subcellular distribution of TDP-43 in cultured skeletal muscle cells and found abundant nuclear TDP-43 in C2C12 myoblasts, a mouse muscle cell line (Figure 3.1a)(Rodriguez-Ortiz et al., 2013). However, during differentiation of C2C12 myoblasts and isolated primary mouse myoblasts into multinucleated myotubes, we observed an increase in cytoplasmic TDP-43 by immunofluorescence and by subcellular fractionation (Figure 3.1a-e). Further, live cell single molecule imaging of HALO-tagged TDP-43 revealed increased cytosolic HALO-TDP-43 in differentiating myotubes compared to myoblasts (Figure 3.1f-k).

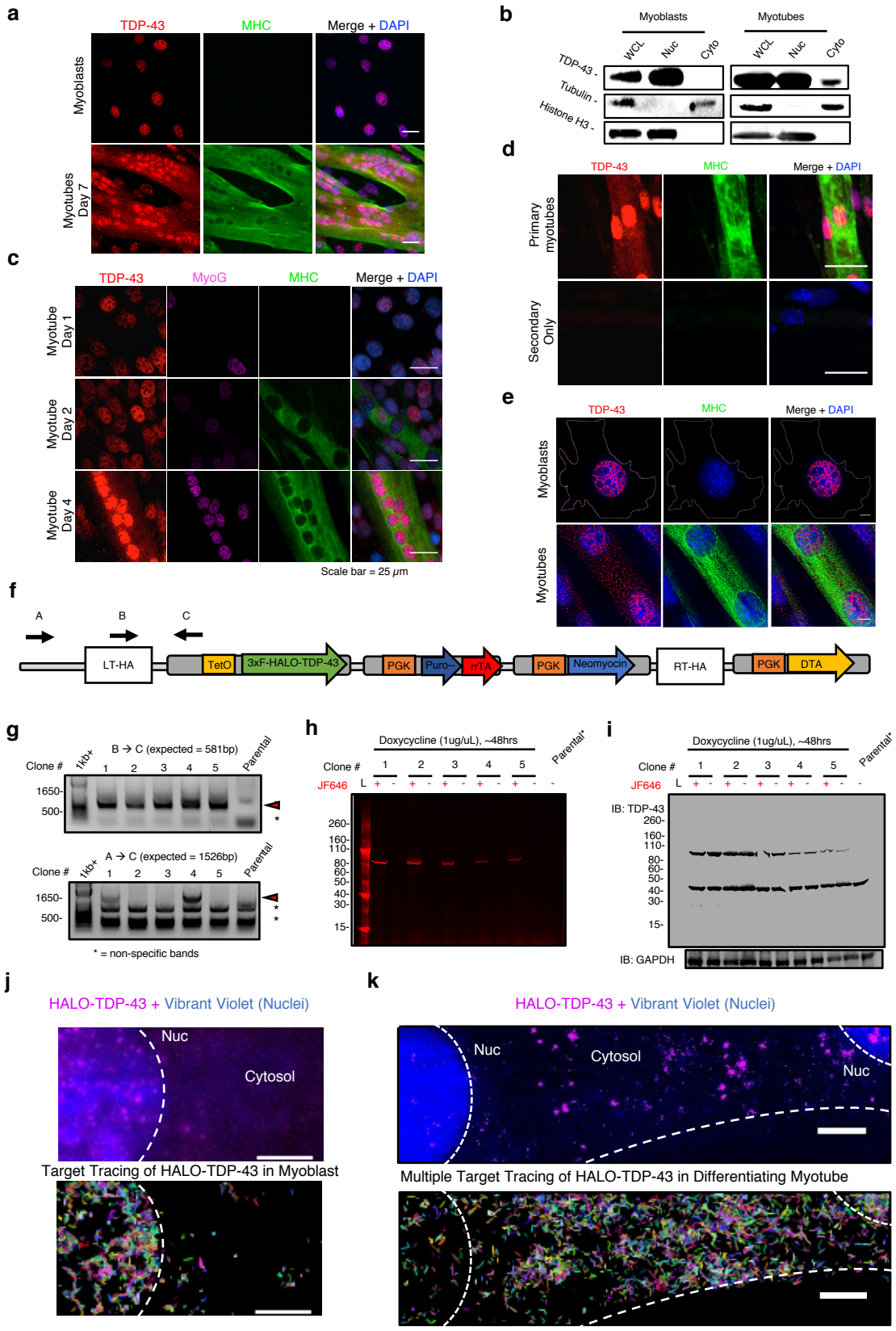


Figure 3.1. See next page for caption.

Figure 3.1. Increased cytosolic TDP-43 during normal skeletal muscle formation

(a) Nuclear localization of TDP-43 immunofluorescence in C2C12 myoblasts and both nuclear and cytoplasmic localization in C2C12 myotubes differentiated for 7 days ($n = 3$ independent experiment). Myosin heavy chain (MHC) identifies differentiated cells. Scale bar is $25\mu\text{m}$ **(b)** Subcellular fractionation reveals increased cytosolic TDP-43 in differentiating myotubes (Cyto MB, $5.0 \pm 2.1\%$; Cyto MT, $19.7 \pm 3.1\%$; $n=3$ biologically independent experiments giving similar results, unpaired two-tailed t-test, $p\text{-value} = 2.0 \times 10^{-3}$). **(c)** Time-course of TDP-43 immunoreactivity during skeletal muscle differentiation ($n = 3$ independent experiments with similar results). Myogenin (MyoG) immunoreactivity (magenta) and MHC immunoreactivity (green), identify differentiated cells. Nuclei counterstained with DAPI. Scale bar is $25\mu\text{m}$ **(d)** TDP-43 immunoreactivity in primary myotubes derived from muscle stem cells differentiated in culture for 4 days ($n = 3$ independent experiments with similar results). Images for a secondary antibody control on the lower panel. Scale bar is $25\mu\text{m}$. **(e)** Deconvolution microscopy of C2C12 myotubes differentiated for 5 days reveal punctate TDP-43 immunoreactivity in myosin heavy chain (MHC)-positive myotubes ($n=3$ independent experiments with similar results). **(f)** CRISPR/Cas9-mediated genomic integration of tetracycline inducible HALO-TDP-43 into the ROSA26 safe harbor locus in C2C12 myoblasts. **(g)** PCR of C2C12 myoblast gDNA for the presence of the HALO-TDP-43 construct (top panel) and for integration into the ROSA26 locus (bottom panel) using the primers mapped in (f) ($n=3$ independent experiments with similar results). Red arrowheads point to the expected PCR product for ROSA26 integration. Subsequent live-imaging experiments were performed using clones 1 and 4. **(h)** Detection of fluorescently labeled HALO-tagged TDP-43 in C2C12 myoblasts following induction resolved on SDS-PAGE. Janelia Fluor® 646 (JF646) ($n = 3$ independent experiments with similar results). **(i)** Detection of both HALO-tagged TDP-43 and endogenous TDP-43 in selected C2C12 cell clones ($n=3$ independent experiments with similar results). **(j)** Representative myoblast and **(k)** multinucleated myotube image of individual HALO-TDP-43 molecules. Top panels are taken from start of acquisition (frame 1). Nuclei (Nuc) and cytosolic borders are demarcated with white dotted lines ($n=3$ independent experiments with similar results). Lower panels show dynamic mapping of single TDP-43 molecule tracks using multiple target tracing Matlab script (Serge et al., 2008). Vibrant Violet was used to detect myonuclei. Scale is $5\mu\text{m}$.

We next examined the subcellular distribution of TDP-43 in uninjured tibialis anterior muscle and tibialis anterior muscle that was chemically injured with barium chloride (BaCl_2) and allowed to regenerate (Figure 3.2a) (Caldwell et al., 1990; Hardy et al., 2016). Although we observed primarily nuclear TDP-43 in uninjured muscle, at five days post-injury (dpi) TDP-43 was upregulated and in both the myonuclei and cytoplasm of newly forming myofibers identified by embryonic myosin heavy chain (eMHC) immunoreactivity (Figure 3.2b, Figure 3.3a). Super resolution microscopy reveals TDP-43 is predominately localized to myonuclei in uninjured myofibers, while in regenerating myofibers, cytoplasmic TDP-43 localizes to regions surrounding eMHC (Figure 3.2c), which are sites of newly formed sarcomeres (Webster et al., 1988). By 10 dpi, cytosolic TDP-43 levels decline and localize around the centrally-located nuclei, while by 30 dpi, TDP-43 re-localizes to the nucleus (Figure 3.2b, d, Figure 3.3b). Thus, cytosolic TDP-43 increases during skeletal muscle cell formation in culture and in mice.

Since cytoplasmic TDP-43 localization is associated with pathological aggregation, we asked if the cytoplasmic TDP-43 identified in skeletal muscle formation adopts a higher order, oligomeric state. We detected an increase in UREA-insoluble TDP-43 in myotubes compared to myoblasts and observed higher molecular weight SDS-resistant TDP-43 assemblies unique to differentiating myotubes by SDD-AGE (Semi-Denaturing Detergent Agarose Gel Electrophoresis) (Figure 3.3c, d). Further, immunoprecipitation of TDP-43 from myotubes and from tibialis anterior mouse muscle at 5dpi, followed by electron microscopy (EM) reveals the presence of 50-250 nm assemblies that are not detected in undifferentiated myoblasts or in uninjured skeletal

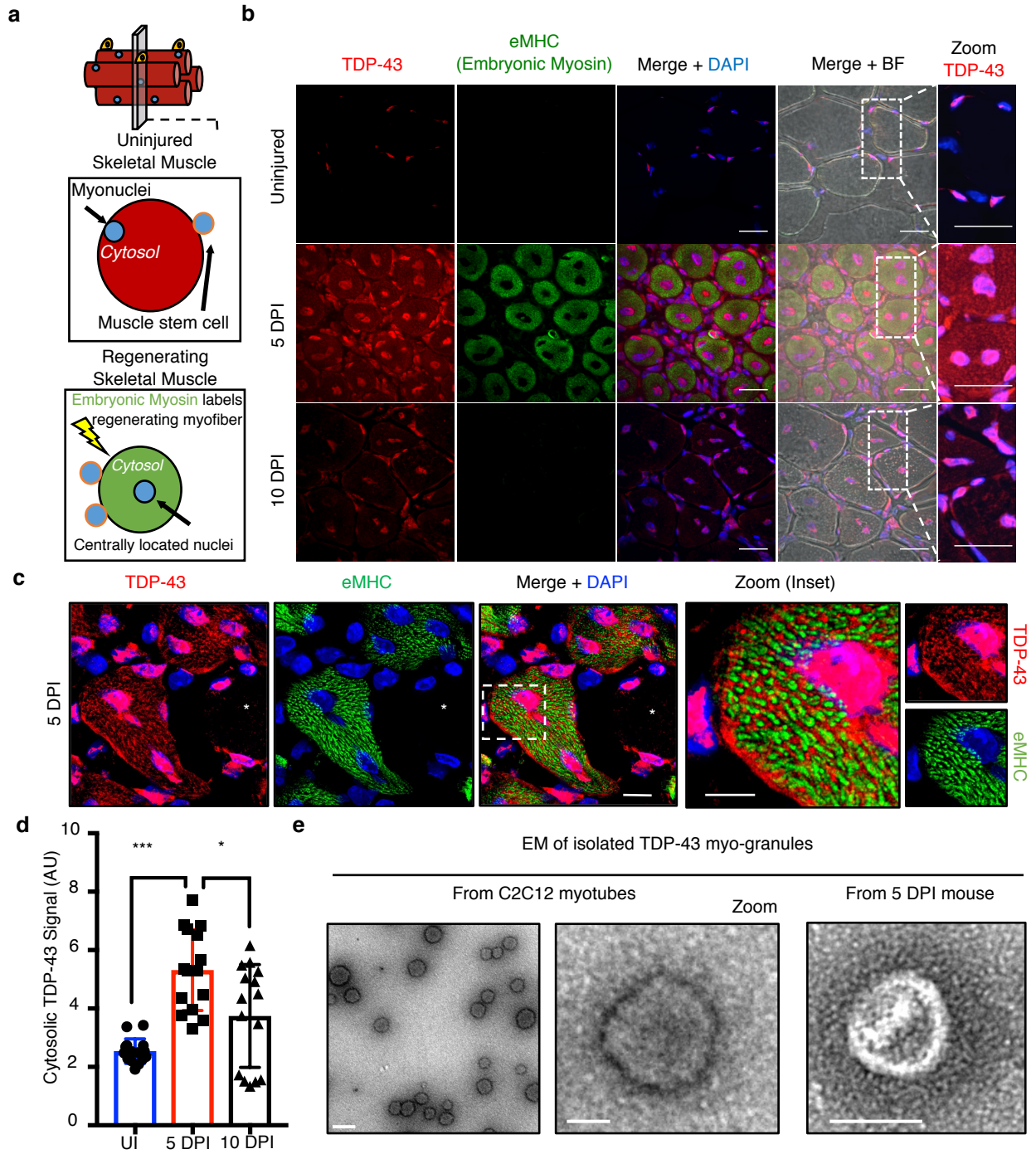


Figure 3.2. See next page for caption.

Figure 3.2. TDP-43 adopts higher-ordered state during normal skeletal muscle formation.

(a) Schematic for regeneration of skeletal muscle injuries in wild type mice. **(b)** TDP-43 immunoreactivity following BaCl₂-induced tibialis anterior (TA) muscle injury. Embryonic myosin heavy chain (eMHC) in regenerating myofibers with nuclei counterstained with DAPI. Scale bar is 25μm in merged and zoom panels (n = 5 mice per condition providing similar results). **(c)** Super resolution imaging of TDP-43 immunoreactivity around nascent sarcomeres in the cytoplasm during muscle regeneration. Scale bar is 10μm in merged panels and 5μm in zoom panels. Asterisk identifies an uninjured myofiber lacking eMHC and TDP-43 cytosolic signal. Nuclei are counterstained with DAPI (n=3 biologically independent experiments providing similar results) **(d)** Quantification of cytoplasmic TDP-43 signal in skeletal muscle myofibers using unpaired two-tailed t-tests. 5dpi vs UI p-value = 4.36×10^{-8} (***) ; 5dpi vs 10dpi p-value = 0.011(*) ; 10dpi vs UI p-value = 0.015 (not shown) (n=3 biological replicates, n=5 myofibers per replicate). p-values are unpaired two-tailed t-tests for each individual comparison. Data are mean ± s.d. **(e)** Electron microscopy of myo-granules isolated by TDP-43 immunoprecipitation from C2C12 myotubes and from mouse 5dpi tibialis anterior muscle (n=3 biologically independent experiments providing similar results).

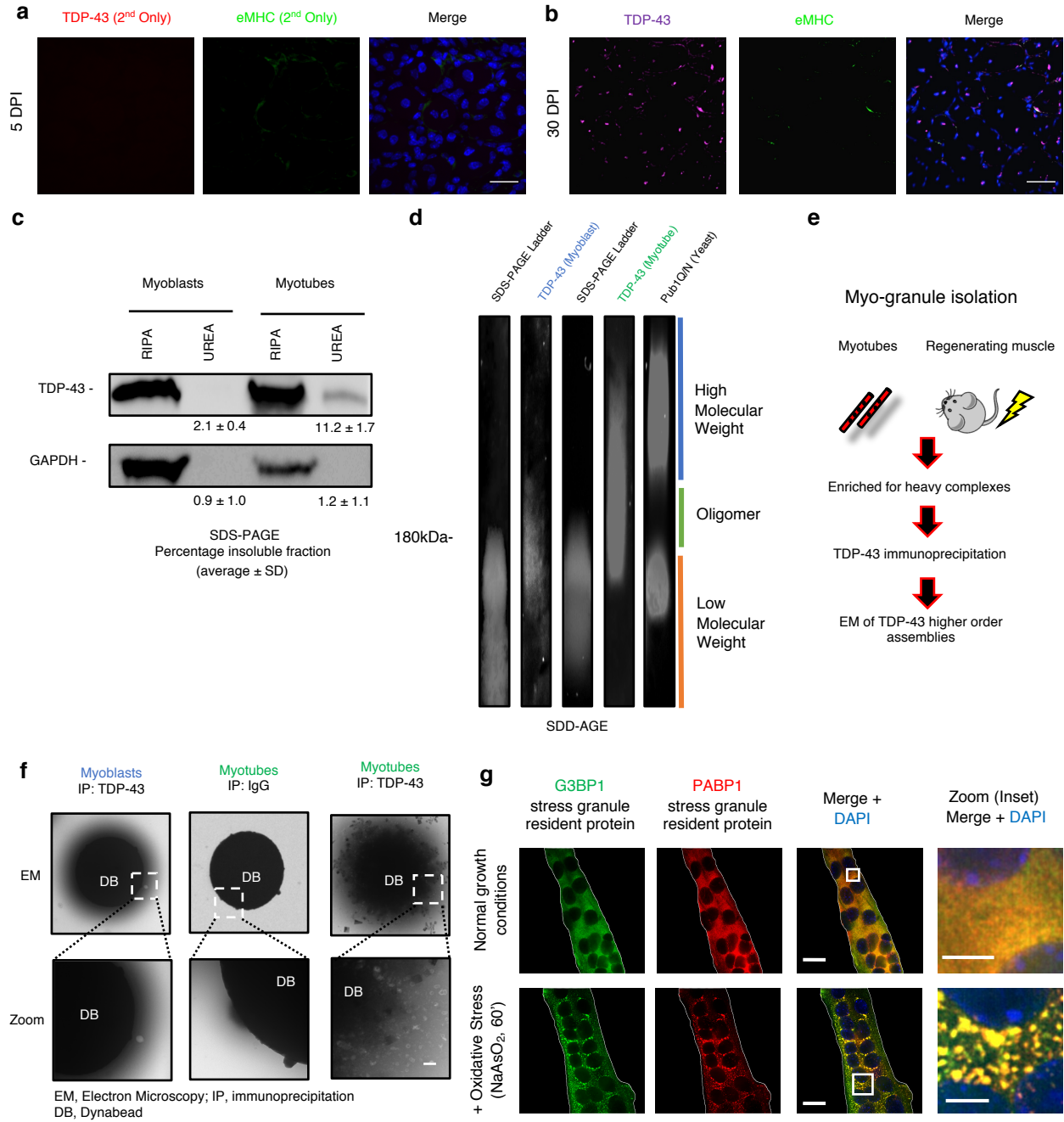


Figure 3.3. See next page for caption.

Figure 3.3. During muscle formation TDP-43 adopts a higher-order state distinct from stress granules.

(a) A secondary antibody control for 5 dpi TDP-43 staining in TA muscle sections. (n = 5 mice per condition providing similar results). eMHC (embryonic myosin heavy chain) immunoreactivity in regenerating myofibers with nuclei counterstained with DAPI. **(b)** Immunoreactive TDP-43 in 30dpi TA muscle sections with nuclei counterstained with DAPI (n = 4 mice). Scale bar is 50 μm . **(c)** RIPA-UREA assay reveals presence of a urea insoluble TDP-43 fraction isolated from C2C12 myotubes differentiated for 7 days but not in C2C12 myoblasts (n=3 independent experiments, each giving similar results, unpaired two-tailed t-test, p-value = 0.0008). GAPDH remains RIPA-soluble in both myoblasts and myotubes (n = 3 independent experiments, each giving similar results, unpaired two-tailed t-test, p-value = 0.7443) **(d)** Higher molecular weight SDS-resistant TDP-43 assemblies present in differentiating C2C12 myotubes resolved by SDD-AGE (Semi-Denaturing Detergent Agarose Gel Electrophoresis) (n = 3 independent experiments). Pub1 Q/N-GFP from yeast forms higher molecular weight SDS-resistant assemblies than TDP-43 assemblies. **(e)** Schematic for the isolation of myo-granules containing TDP-43 during skeletal muscle formation **(f)** Immunoprecipitation (IP) of TDP-43 on dynabeads (DB) reveals oligomers isolated from C2C12 myotubes but absent in myoblasts as observed by electron microscopy (EM) (n = 3 independent experiments). **(g)** Stress granule formation in multinucleated myotubes derived from C2C12 cells. Immunofluorescence using antibodies against stress granule proteins, G3BP1 and Pabp1, after \pm NaAsO₂ treatment for 60min (n=3 independent experiments, each giving similar results). Zoom represents magnified inset. Scale bars are 5 μm and 20 μm , respectively.

muscle (Figure 3.2e, Figure 3.3e, f). The EM structure is similar to previously characterized TDP-43 oligomers, albeit roughly two-fold larger in diameter (Johnson et al., 2009). To exclude the possibility that the TDP-43 assemblies in skeletal muscle are stress granules we assayed C2C12 myotubes for the stress granule markers G3BP1 and Pabp1. Stress granules were not present during normal myotube formation (Figure 3.3g). Thus, during muscle formation, TDP-43 exists as a component of an SDS-resistant oligomeric assembly distinct from stress granules, which we refer to as “myo-granules.”

Myo-granules are amyloid-like assemblies

Their SDS-resistance suggests myo-granules have amyloid-like properties, which is supported by two observations. First, X-ray diffraction on lyophilized myo-granules revealed a diffraction pattern with a 4.8 Å reflection, indicating a beta-rich complex that is not observed in control samples. Myo-granules lacked a 10 Å reflection implying a lack of mated cross beta-sheets, similar to previously described amyloid-like oligomers (Figure 3.4a, Figure 3.5a, b) (Sangwan et al., 2017). Second, immunopurified myo-granules from C2C12 myotubes and regenerating mouse tibialis anterior muscle are also immunoreactive for A11, a conformation specific antibody that recognizes beta-rich structures including amyloid-like oligomers (Figure 3.5c-h) (Kayed et al., 2003).

Similar to TDP-43, A11 immunoreactivity increases in myotubes in culture and in regenerating mouse tibialis anterior muscle (Figure 3.5i-k). In developing myotubes in culture, A11 immunoreactivity is cytoplasmic and correlates with cytoplasmic TDP-43 immunoreactivity (Figure 3.6a-c). During muscle regeneration, A11 immunoreactivity

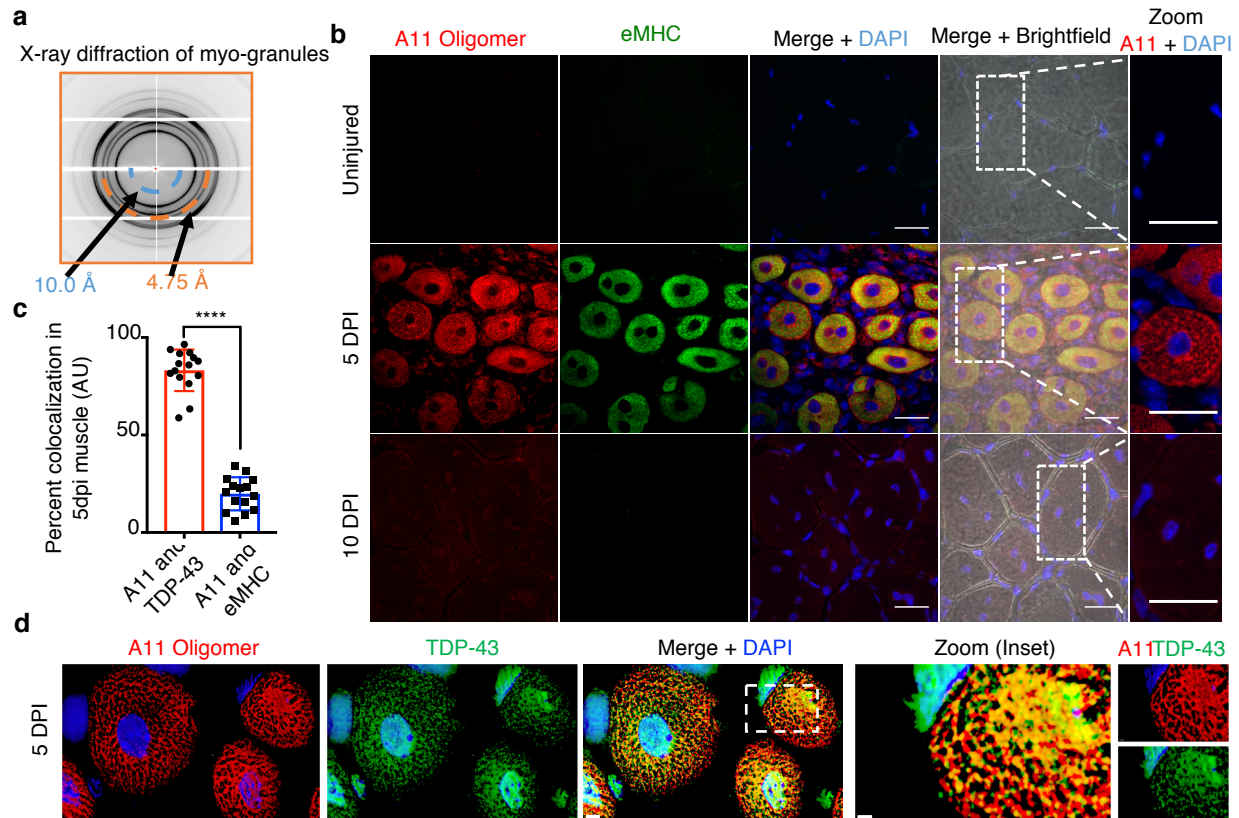


Figure 3.4. Myo-granules containing TDP-43 are amyloid-like RNP oligomers.

(a) X-ray diffraction on myo-granules immunoprecipitated from C2C12 myotubes. Two rings at $\sim 4.8 \text{ \AA}$ (orange) and $\sim 10 \text{ \AA}$ (blue) are drawn on the bottom half to highlight locations of these reflections. One sample per condition was used. Two diffraction images at different rotations were taken per sample and each image gave similar results. **(b)** A11 immunoreactivity during TA muscle regeneration and uninjured muscle ($n = 4$ mice per condition). Regenerating myofibers are immunoreactive for eMHC. Scale bars = $25 \mu\text{m}$. **(c)** Quantification of A11 and TDP-43 co-localization and A11 and eMHC co-localization in 5 dpi skeletal muscle. Unpaired two-tailed t-test (***) p -value = 6.3×10^{-17} . $n = 3$ mice, $n = 5$ myofibers per mouse. Data are mean \pm s.d. **(d)** Representative deconvolution image of A11 and TDP-43 co-localization in 5dpi mouse TA myofibers quantified in (c). Scale bar is $3 \mu\text{m}$ and $1 \mu\text{m}$ (zoomed inset) $n = 3$ mice providing similar results.

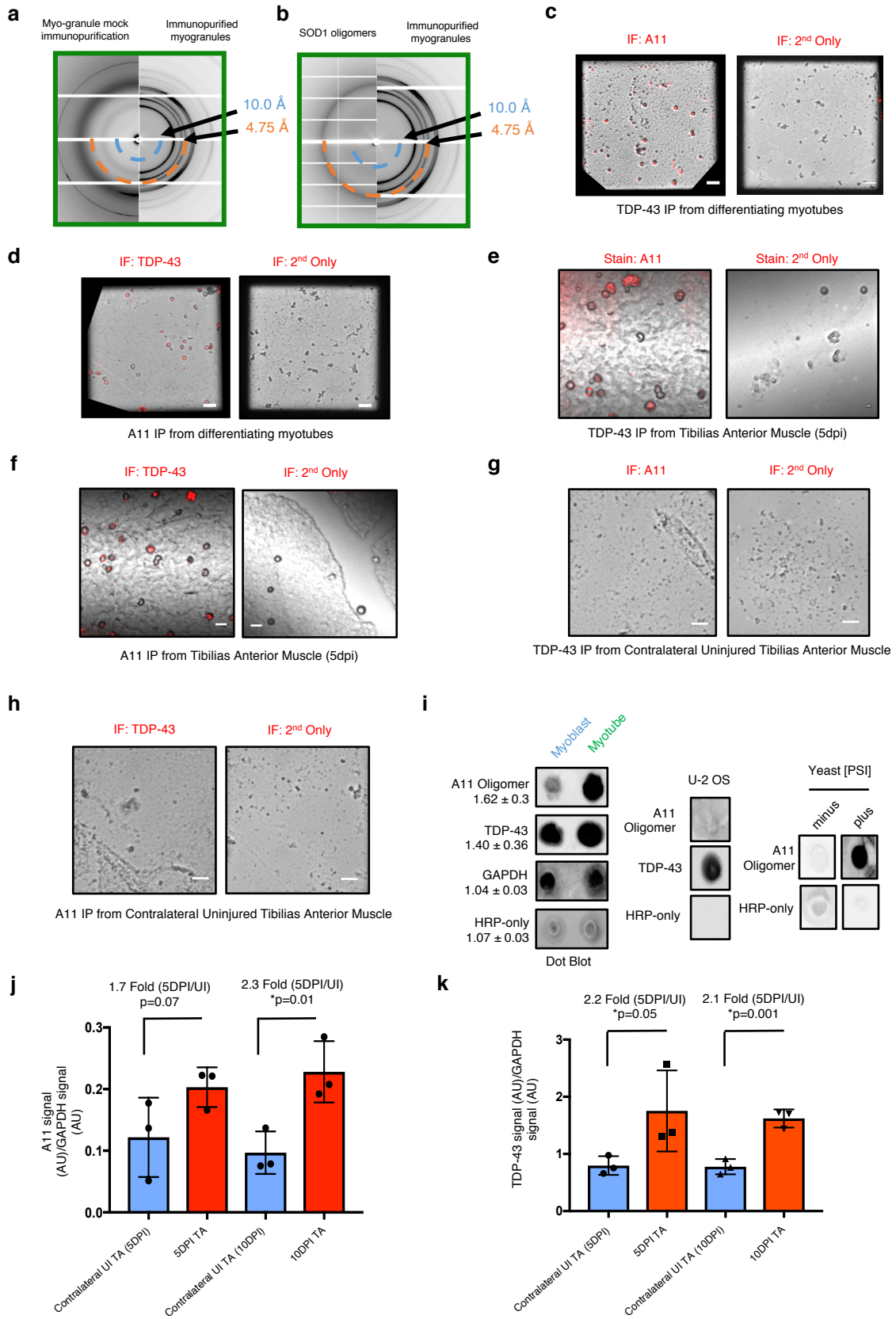


Figure 3.5. See next page for caption.

Figure 3.5. Myo-granules isolated from cells and mice contain TDP-43 and are amyloid-like oligomers

(a-b) X-ray diffraction on immunoprecipitated myo-granules (right half of both panels) compared to the diffraction of mock IgG immunoprecipitation (left half of panel a) and to the diffraction of super oxide dismutase 1 (SOD1) amyloid oligomers (left half of panel b). In all diffraction patterns two rings at ~ 4.8 Å and ~ 10 Å are drawn on the bottom half to highlight absence of an ~ 4.8 Å reflection in the mock immunoprecipitation and a similar ~ 4.8 Å reflection with a ~ 10 Å reflection absence in the SOD1 diffraction. One sample per condition was used. Two diffraction images at different rotations were taken per sample and each image gave similar results. **(c)** Complexes immunopurified using TDP-43 or **(d)** A11 isolated from C2C12 myotubes are immunoreactive for A11 and TDP-43 respectively, while immunopurified TDP-43 or A11 myo-granules immunostained with secondary antibodies lack signal (red) ($n=3$ independent experiments). Scale bar is $1 \mu\text{m}$. **(e)** Complexes immunopurified using TDP-43 or **(f)** A11 isolated from 5 dpi TA muscle are immunoreactive for A11 and TDP-43 respectively, while immunopurified TDP-43 or A11 myo-granules immunostained with secondary antibodies lack signal (red) ($n=3$ mice). Scale bar is $0.05 \mu\text{m}$. **(g)** TDP-43 immunopurified complexes isolated from an uninjured tibialis anterior muscle (contralateral to the 5dpi muscle) reveal no complexes with an A11 oligomeric confirmation ($n = 3$ mice). Scale bar is $0.05 \mu\text{m}$. **(h)** A11 immunopurified complexes from an uninjured tibialis anterior muscle (contralateral to the 5dpi muscle) reveal no complexes containing TDP-43 ($n = 3$ mice). Scale bar is $0.05 \mu\text{m}$. **(i)** Dot blot A11 immunoreactivity in C2C12 cells differentiated into myotubes as compared to myoblasts. Quantification reflects fold change in dot blot signal from myoblast to myotube. Data are mean \pm s.d. ($n=3$ independent experiments) **(j)** Quantification of dot blot signal for A11 conformation complexes and TDP-43 **(k)** during skeletal muscle regeneration at 5dpi and at 10dpi compared to contralateral uninjured TA muscle and normalized to HRP-only signal. Quantification reflects fold change in dot blot signal. Data are mean \pm s.d., $n = 3$ mice, p-value are unpaired two-tailed t-test.

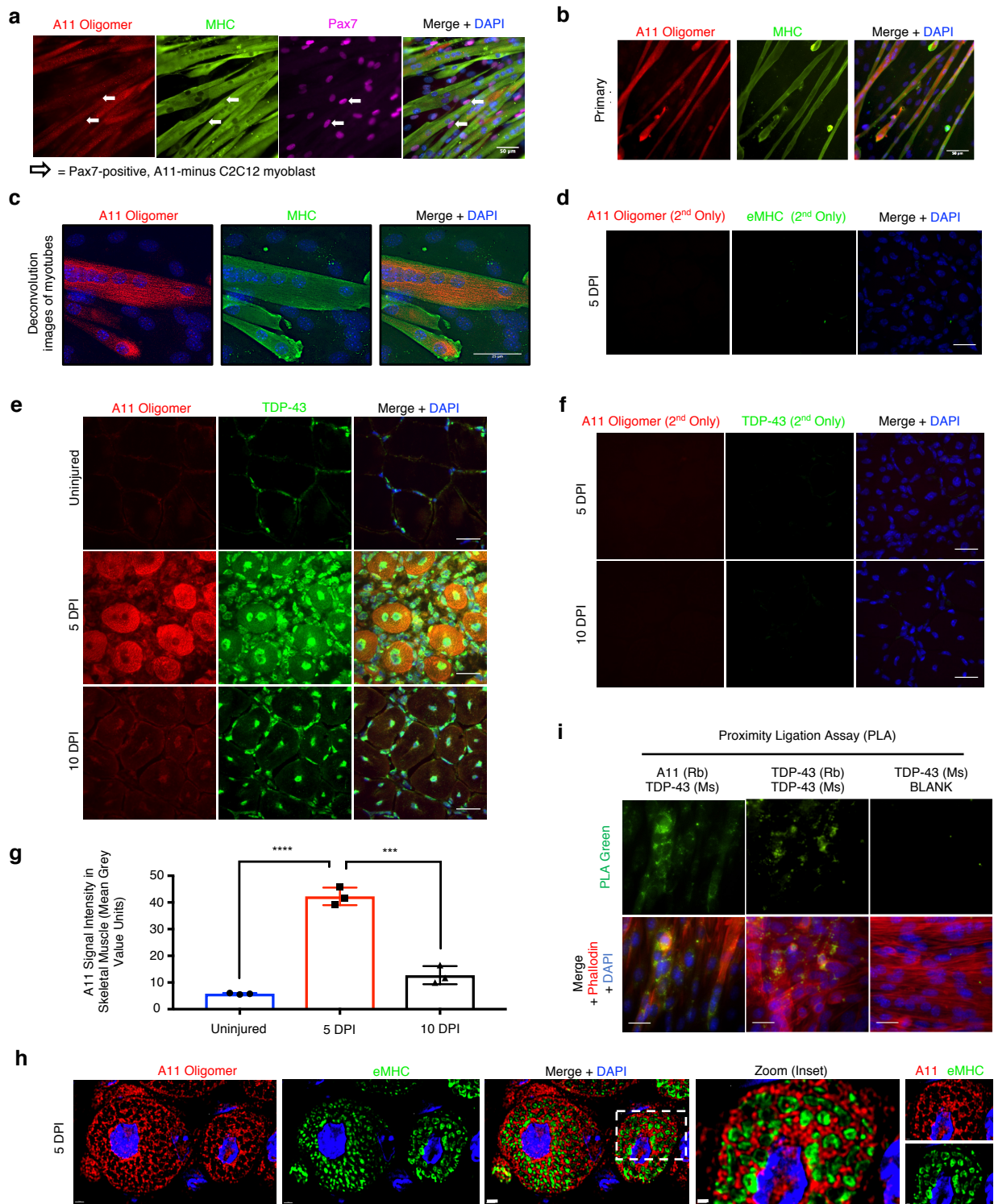


Figure 3.6. See next page for caption.

Figure 3.6. Myo-granules in skeletal muscle contain TDP-43 and are amyloid-like oligomers.

(a) C2C12 myotubes differentiated for 7 days reveal strong A11 immunoreactivity in myosin heavy chain (MHC)-positive myotubes but no A11 immunoreactivity in undifferentiated Pax7-positive myoblasts (n=3 independent experiments). **(b)** Muscle stem cells isolated from 4-month old C57/BL6 mice were differentiated in culture for 5 days and reveal cytoplasmic and nuclear immunoreactivity for A11 oligomer. Myotubes are immunoreactive for MHC (n = 3 mice). **(c)** Deconvolution microscopy of C2C12 myotubes differentiated for 7 days reveal punctate A11 staining in myosin heavy chain (MHC)-positive myotubes but no A11 signal in undifferentiated myoblasts (n=3 independent experiments). **(d)** Secondary antibody control for 5 dpi A11 in TA muscle sections. Nuclei counterstained with DAPI. Scale bars are 25 μm (n = 4 mice). **(e)** Representative images of A11 and TDP-43 colocalization in uninjured, 5 dpi and 10 dpi tibialis anterior muscle (n=3 mice). **(f)** Secondary antibody control for 5 dpi and 10dpi A11-TDP-43 colocalization in TA muscle section reveals lack of signal. Nuclei counterstained with DAPI. Scale bars are 25 μm (n = 3 mice). **(g)** Quantification of A11 signal intensity in myofibers from (e). Unpaired two-tailed t-test for uninjured vs 5dpi p-value = 4.4×10^{-5} (****); 5dpi vs 10dpi p-value = 4.1×10^{-4} (***); 10dpi vs uninjured p-value = 0.024 (not shown). n = 3 mice per condition, n = 10 myofibers averaged per mouse. Data are mean \pm s.d. **(h)** Representative deconvolution image of A11 and eMHC immunoreactivity in 5dpi mouse TA myofibers quantified in Fig. 2c (n = 3 mice providing similar results). Scale bar is 2 μm and 0.8 μm (zoomed inset). **(i)** Proximity ligation assays (PLAs) reveal complexes of TDP-43 and A11 (green) in C2C12 myotubes. A PLA positive control with two antibodies that recognize different epitopes of TDP-43 are positive, whereas complexes are absent if one primary antibody is omitted (n = 3 independent experiments per condition).

correlates with TDP-43 cytoplasmic immunoreactivity increasing in the cytoplasm at 5dpi but dissipating by 10dpi (Figure 3.4b, Figure 3.6d-g). At 5dpi in mice, more than 80% of A11 immunoreactivity is co-localized with cytosolic TDP-43 immunoreactivity (Figure 3.4c, d, Figure 3.6h). Further, cytoplasmic TDP-43 exists as a component of an A11-reactive complex revealed by proximity ligation assays in differentiating C2C12 myotubes (Figure 3.6i). These observations argue cytoplasmic myo-granules contain TDP-43 in an amyloid-like oligomer conformation during skeletal muscle formation.

Myo-granules contain sarcomeric mRNAs

As TDP-43 is an RNA-binding protein, we examined if myo-granules include RNA. Immunoprecipitation of myo-granules with TDP-43 or A11 antibodies followed by oligo-dT Northern blot analysis reveals that TDP-43 and A11 associate with mRNA in myotubes (Figure 3.7a). To identify the mRNAs bound by TDP-43 during muscle formation, we constructed transcriptome-wide maps of TDP-43 binding sites in undifferentiated myoblasts and in myotubes using eCLIP (enhanced UV crosslinking and immunoprecipitation) (Figure 3.7b-e) (Van Nostrand et al., 2016). We identified a total of 556 binding sites across 174 genes for myoblasts and a total of 975 binding sites across 320 genes for myotubes as significantly enriched over size matched input (SMinput, which reflects all RNA-protein interactions in the input). The binding sites were highly correlated between biological replicates, revealed enrichment for the TDP-43 UG-rich consensus sequence, exhibited thousands of reproducible CLIP clusters by irreproducible discovery rate analysis, and identified known TDP-43 mRNA targets including the 3' UTR of TDP-43 (Figure 3.7f-h) (Ayala et al., 2011). We also observed

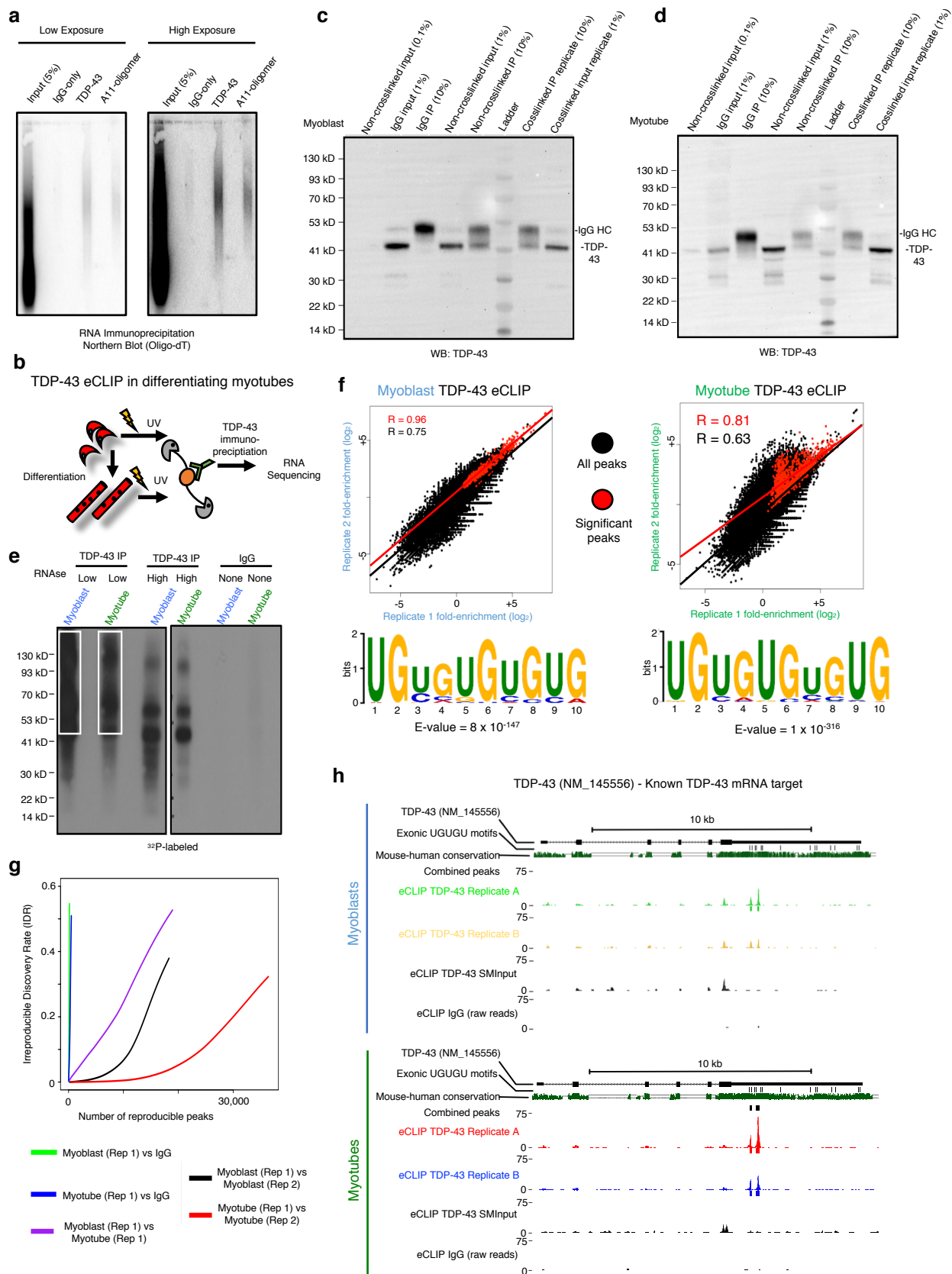


Figure 3.7. See next page for caption.

Figure 3.7. TDP-43 eCLIP on skeletal muscle myoblasts and myotubes.

(a) RNA immunoprecipitation (RIP) from C2C12 myotubes, followed by oligo-dT Northern blot reveals A11 and TDP-43 associate with poly-A RNA ($n = 3$ biologically independent samples). **(b)** Schematic of enhanced CLIP (eCLIP) protocol for cultured C2C12 myoblasts and myotubes. **(c)** Immunoprecipitation of TDP-43 complexes used for eCLIP in C2C12 myoblast ($n = 2$ biologically independent samples). **(d)** Same as in (B) but for C2C12 myotubes ($n = 2$ biologically independent samples). **(e)** Autoradiogram of ^{32}P -labeled TDP-43 - RNA complexes fractionated by PAGE. White box indicates the area cut and used for eCLIP library preparation ($n=1$ library prepared per condition). **(f)** Scatterplots indicate correlation between significant TDP-43 eCLIP peaks in biological replicates. Scatterplot represents fold enrichment for each region in TDP-43 eCLIP relative to paired size matched input (SMInput) with significant peaks in red ($p \leq 10^{-8}$ over SMIput). P-values for each peak to determine significance were calculated by Yates' Chi-Square test (Perl) or Fisher Exact Test (R computing software) when the expected or observed read number was below five¹⁶. For myoblasts R values calculated using $n = 511137$ non-significant peaks and $n = 596$ significant peaks. For myotubes R values calculated using $n = 413368$ non-significant peaks and $n = 1501$ significant peaks. UG-rich motif is significantly enriched in clusters from ORFs and UTRs (p-value determined by DREME software tool). **(g)** Irreproducible discovery rate (IDR) analysis comparing peak fold enrichment across indicated datasets. **(h)** TDP-43 eCLIP reveals TDP-43 binds to 3'UTR of TDP-43 transcript in myoblasts (top panel) and myotubes (bottom panel) ($n=3$ biologically independent experiments giving similar results).

that the mRNAs bound to TDP-43 changed significantly during skeletal muscle differentiation (Figure 3.8a).

A majority of the TDP-43 binding sites in myoblasts and myotubes are in exons of protein coding transcripts, suggesting TDP-43 may be associating with mature mRNAs (Figure 3.9a, Figure 3.8b, c). In contrast, TDP-43 binding sites in neurons were predominantly mapped to introns (Polymenidou et al., 2011; Tollervey et al., 2011). The difference may reflect cell state, where TDP-43 binds more processed cytoplasmic RNAs in newly forming tissue and more nuclear, intronic RNA in post-mitotic mature cells. Connectome and gene ontology analysis of TDP-43 exonic target transcripts in myotubes, which are likely to constitute interactions with cytoplasmic mRNAs, revealed TDP-43 binds to a network of transcripts associated with the sarcomere (Figure 3.9b, Figure 3.8a). TDP-43 target RNAs identified by eCLIP in myotubes often have multiple TDP-43 exonic binding sites in close proximity (Tollervey et al., 2011). For example, in the titin mRNA numerous TDP-43 exon binding sites are distributed across the transcript, and within single exons we observed multiple UG-rich stretches with several TDP-43 binding sites (Figure 3.8d). These observations argue TDP-43 adopts new functionality during myogenesis by binding to structural mRNAs required for skeletal muscle formation, while retaining canonical nuclear functions such as splicing and nuclear cytoplasmic shuttling.

To validate that the sarcomeric mRNAs identified by eCLIP bind to cytoplasmic TDP-43 during muscle formation we used single molecule fluorescence in situ hybridization (smFISH). We found that TDP-43 protein co-localizes with mRNAs for

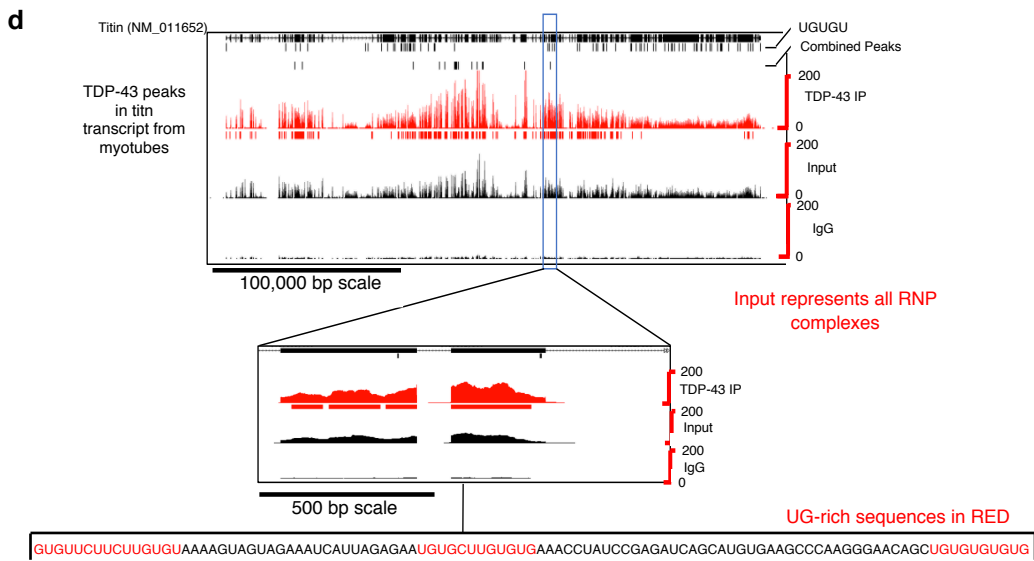
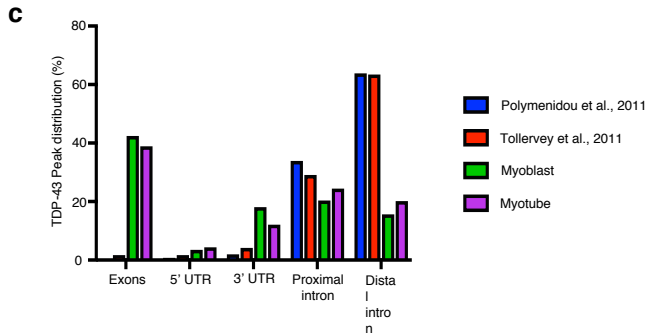
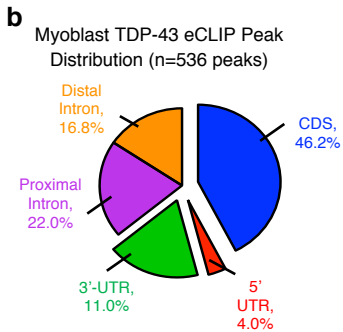


Figure 3.8. See next page for caption.

Figure 3.8. TDP-43 binds to mRNAs that encode sarcomeric proteins during muscle formation.

(a) Myoblast (left column), myotube (middle column) and shared (right column) connectome analysis for all TDP-43 eCLIP peaks (top row) and TDP-43 exonic peaks (bottom row). **(b)** TDP-43 binds predominantly in exons of protein coding RNAs in C2C12 myoblasts. **(c)** Peak distribution for significantly enriched TDP-43 peak locations in myoblasts and myotubes across the transcriptome reveal increased exonic and 3'-UTR association compared to neuronal TDP-43 peaks identified in Polymenidou et al., 2011 and in Tollervey et al., 2011. **(d)** Identification of multiple TDP-43 binding sites across and within exons of Titin. Zoomed region is representative of multiple UG-rich sequences within single exon (n=3 biologically independent experiments giving similar results).

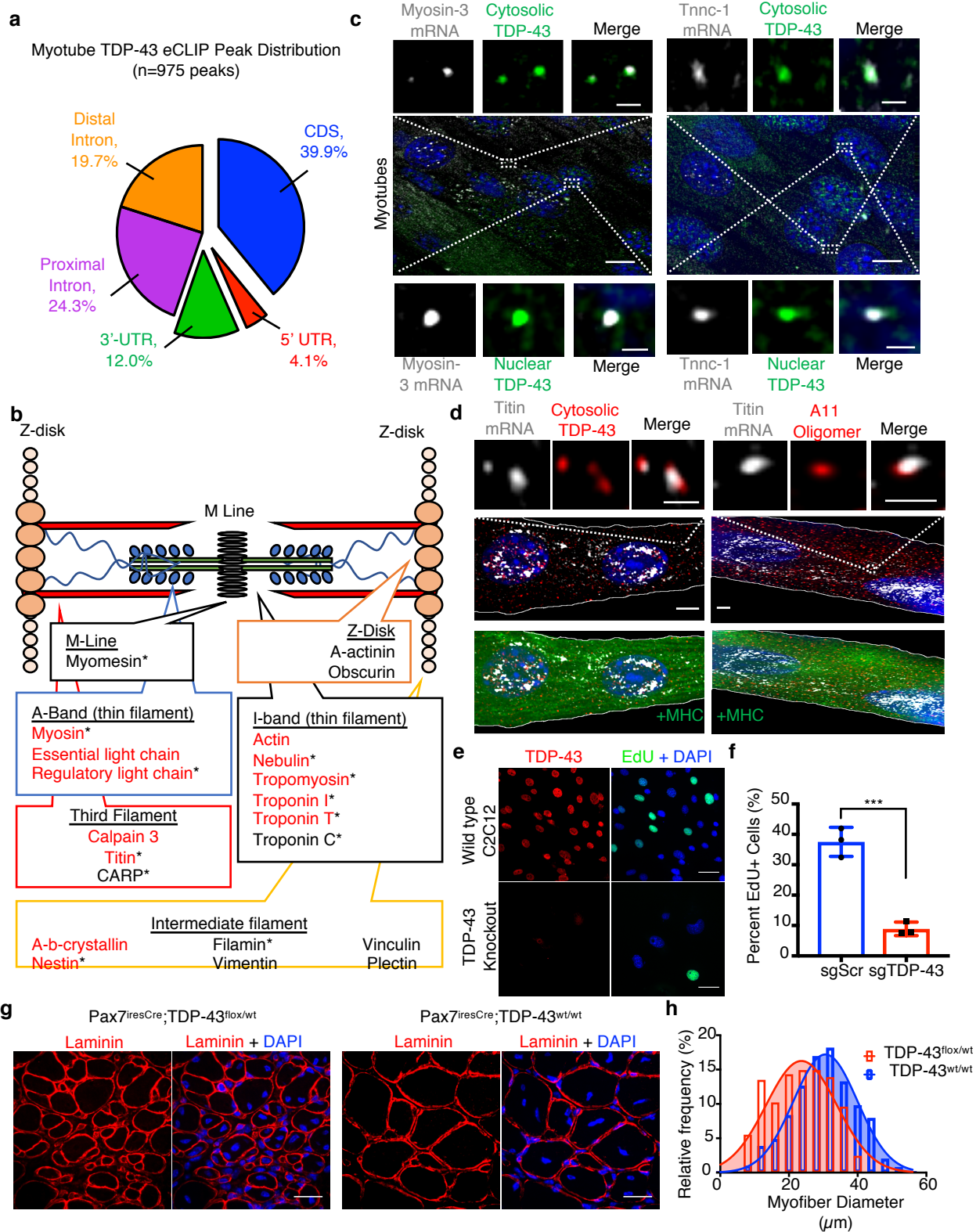


Fig 3.9. TDP-43 binds select sarcomeric mRNA transcripts during muscle formation.

(a) Distribution of TDP-43 RNA binding identified by eCLIP in C2C12 myotubes **(b)** TDP-43 eCLIP myotube exonic peaks identified in select sarcomeric mRNA transcripts. All listed genes are found in at least one eCLIP replicate, * = identified in two replicates, red = gene associated with muscle disease. Sarcomere schematic is adapted from Laing and Nowak, 2005. **(c)** Single molecule FISH (smFISH) for embryonic myosin heavy chain (Myosin-3) and Troponin C1 (Tnnc1) mRNA co-localized with cytoplasmic and nuclear TDP-43 immunoreactivity in C2C12 myotubes (n=3 biologically independent experiments). **(d)** SmFISH for Titin mRNA co-localized with both A11 and TDP-43 immunoreactivity in cytoplasm of myosin heavy chain-positive C2C12 myotubes (n=3 biologically independent experiments). Scale bar is 10 μ m for merged panels, 0.5 μ m for insets for (c, d). Representative images of CRISPR-Cas9 TDP-43 scramble sgRNA (top panel) and TDP-43 knockout sgRNA (bottom panel) C2C12 cells showing TDP-43 immunoreactivity and EdU incorporation. Scale bar is 50 μ m. Cells counterstained with DAPI (n=3 biologically independent experiments each giving similar results). **(f)** Quantification of EdU incorporation in TDP-43 knockout (sgTDP-43) and scramble (sgScr) C2C12 cells after 7 days in culture (n = 3 independent experiments). Unpaired two-tailed t-test *** p-value = 0.0007. Data are mean \pm s.d. **(g)** Representative images at 10 dpi regenerating TA muscle reveals reduced myofiber feret diameter in TDP-43 haploinsufficient Pax7^{iresCre}TDP-43^{Flox/WT} mice. Laminin immunoreactivity identifies myofibers and nuclei are counterstained with DAPI. Scale bar is 50 μ m (n = 3 mice per condition). **(h)** Myofiber feret diameter frequency distribution in Pax7^{iresCre}TDP-43^{Flox/WT} mice at 10dpi compared to Pax7^{iresCre}TDP-43^{WT/WT} controls (> 450 myofibers quantified per condition from n = 3 mice).

myosin-3 and troponin-c in the cytoplasm of myotubes (Figure 3.9c). In addition, smFISH for titin mRNA reveals co-localization of both TDP-43 and A11 immunoreactivity with titin mRNA in myotubes (Figure 3.9d). These observations demonstrate TDP-43 binds to sarcomeric mRNAs in the cytosol, and can form A11-positive myo-granules in association with those mRNAs, perhaps because of the high local concentration of TDP-43 proteins on a single mRNA molecule (Afroz et al., 2017; Tollervey et al., 2011).

The association of TDP-43 myo-granules with sarcomeric mRNAs during muscle formation is analogous to the role of TDP-43 in forming cytoplasmic neuronal messenger ribonucleoprotein (mRNP) granules for local translation of mRNAs in neurons (Alami et al., 2014). Consistent with this similarity, mass spectrometry of purified myo-granules identified 356 proteins enriched in proteins involved in RNA localization and translation, which overlaps with the TDP-43 interactome (Freibaum et al., 2010) and the neuronal RNA granule proteome (Fatimy et al., 2016). (Figure 3.10a-d, Table 3.1, 3.2). Myo-granules include valosin containing protein (VCP), a protein linked to neuromuscular degeneration (Taylor, 2015), which we validated by co-localization of VCP with A11 and TDP-43 in the cytoplasm of regenerating muscle (Figure 3.10e). However, hnRNPA2B1, an RNA-binding protein associated with neuromuscular degeneration (Kim et al., 2013), is not identified in myo-granules and remains nuclear during muscle regeneration (Figure 3.10f). Therefore, myo-granules associate with a specific set of proteins that may help localize and regulate sarcomeric mRNAs during skeletal muscle formation.

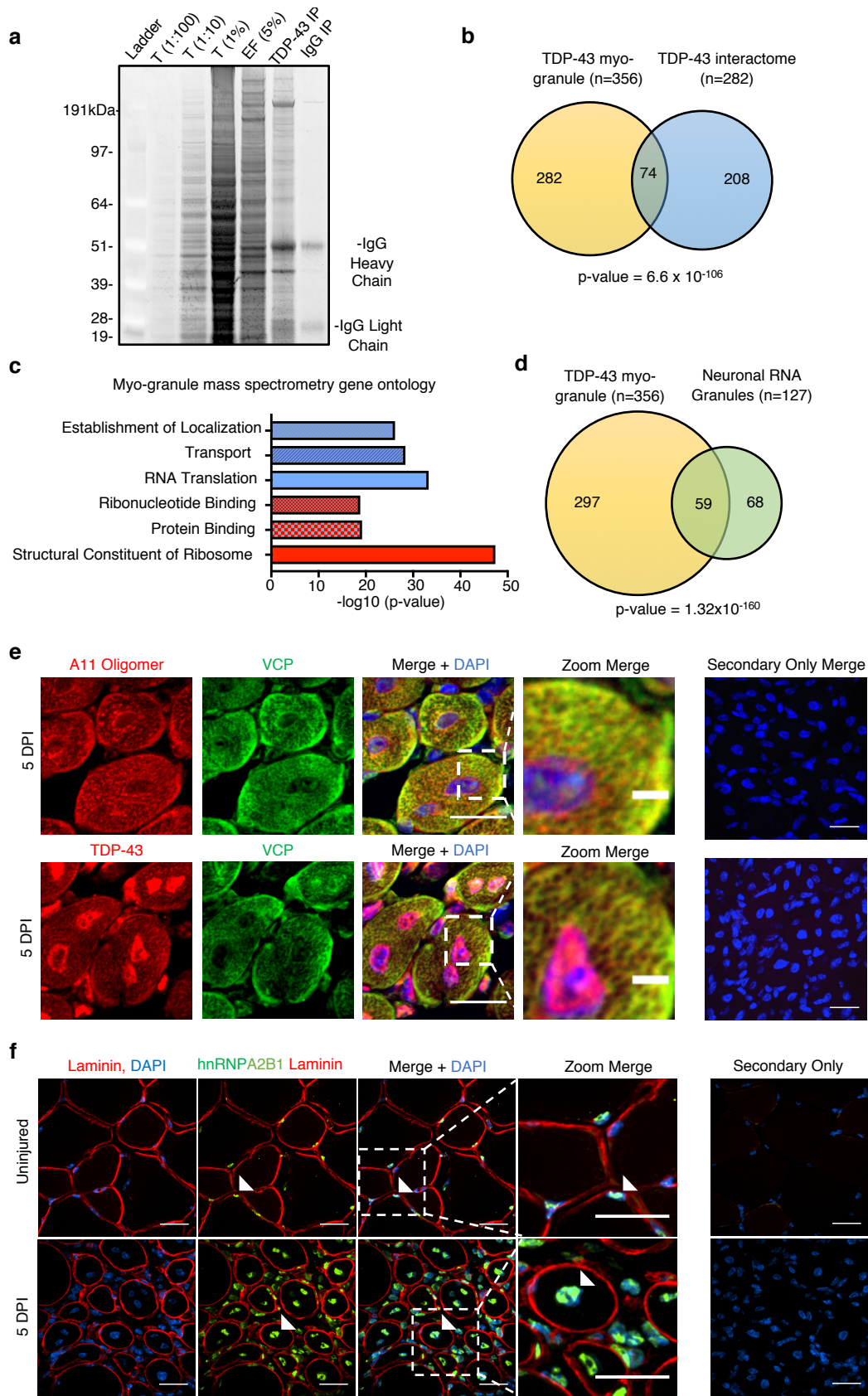


Figure 3.10. See next page for caption.

Figure 3.10. Myo-granule protein composition.

(a) SDS-PAGE gel stained with SYPRO Ruby reveals enrichment for select proteins during fractionation of total cell lysate (T) from C2C12 myotubes, enriched fraction (EF) and TDP-43 immunoprecipitation (IP) (n=3 biologically independent experiments giving similar results). TDP-43 IP and IgG control IP are representative of the fractions used for mass spectrometry. **(b)** Venn diagram showing significant overlap between the myo-granule proteome and TDP-43 interactome (defined by Freibaum et al., 2010) (p-value determined using hypergeometric test). **(c)** Gene Ontology of myo-granules reveals enrichment for processes relating to the localization and translation of RNA (n=356 proteins, p-value determined using hypergeometric test with Benjamini & Hochberg False Discovery Rate (FDR) correction). **(d)** Venn diagram showing significant overlap between myo-granules and neuronal RNA granule proteomes (defined by El Fatimy et al., 2016) (p-value determined using hypergeometric test). **(e)** VCP, a top hit in the myo-granule proteome, colocalizes with cytoplasmic TDP-43 and A11 signal in 5dpi mouse skeletal muscle (n = 3 mice). **(f)** The RNA-binding protein hnRNPA2B1 is not associated with the myo-granule proteome and remains localized to myonuclei in injured (5 dpi) and uninjured tibialis anterior muscle (n = 3 mice).

Tubulin beta-5 chain	Ras-related protein Rap-1A	Integrin alpha-7;integrin alpha-7 heavy chain;integrin alpha-7 light chain
Myosin-1;Myosin-4	ATP synthase subunit gamma;ATP synthase subunit gamma, mitochondrial	Barrier-to-autointegration factor;Barrier-to-autointegration factor, N-terminally processed
ATP synthase subunit d, mitochondrial	60S ribosomal protein L27	Extradil 17-beta-dehydrogenase L2
ATP synthase subunit alpha;ATP synthase subunit alpha	40S ribosomal protein S27;40S ribosomal protein S27-like	40S ribosomal protein S16
Filamin-A	Monofunctional C1-tetrahydrofolate synthase, mitochondrial	GTP-binding nuclear protein Ran;GTP-binding nuclear protein Ran, testis-specific isoform
ATP synthase-coupling factor 6, mitochondrial	Ras-related protein Rab-18	Dihydrolipoylysine-residue acetyltransferase component of pyruvate dehydrogenase complex
Vimentin	NAD(P) transhydrogenase, mitochondrial	Sodium-coupled neutral amino acid transporter 2
40S ribosomal protein S2	Nucleolin	Translocation protein SEC63 homolog
Tubulin beta-4B chain	Ras-related protein Rab-2A	Calcium/calmodulin-dependent protein kinase type II subunit gamma
DnaJ homolog subfamily A member 2	Erythrocyte band 7 integral membrane protein	NADH dehydrogenase [ubiquinone] 1 alpha subcomplex subunit 10, mitochondrial
Cytoskeleton-associated protein 4	Calponin-3	ATPase family AAA domain-containing protein 1
60S ribosomal protein L4	Ras-related protein Rab-8	NADH-cytochrome b5 reductase 1
Aldehyde dehydrogenase, mitochondrial	Peroxisomal membrane protein PEX14	Sterol O-acyltransferase 1
60S ribosomal protein L7	Ras-related protein Rab-6A;Ras-related protein Rab-6B	Tubulin alpha-4A chain
60S ribosomal protein L7a	Tripartite motif-containing protein 72	Apoptosis-inducing factor 1, mitochondrial
Ribosomal protein;60S ribosomal protein L10a	T-complex protein 1 subunit theta	Long-chain-fatty-acyl-CoA ligase 3;Long-chain-fatty-acyl-CoA ligase 4
60S ribosomal protein L13	Integrin beta-1	AP-2 complex subunit alpha-1
60S ribosomal protein L10;60S ribosomal protein L10-like	Ras-related C3 botulinum toxin substrate 1	Golgi apparatus protein 1
60S acidic ribosomal protein P2	Kinesin-1 heavy chain	Calcium-transporting ATPase
Dolichyl-diphosphooligosaccharide--protein glycosyltransferase subunit 1	Cleft lip and palate transmembrane protein 1 homolog	Plasminogen
Cytoplasmic dynein 1 heavy chain 1	60S ribosomal protein L31	5.8 kDa mitochondrial proteolipid
Tubulin beta-6 chain	Ubiquitin carboxyl-terminal hydrolase	Cytochrome c oxidase subunit 6B1
60S acidic ribosomal protein P0	Calcium-binding mitochondrial carrier protein ScaMc-1	60S ribosomal protein L37a
ADP/ATP translocase 1	Fatty acyl-CoA reductase 1	40S ribosomal protein S23
60S ribosomal protein L23	S-formylglutathione hydrolase	60S ribosomal protein L23a
Leucine-rich repeat-containing protein 59	40S ribosomal protein S14	tubulin alpha-1C chain
Four and a half LIM domains protein 1	Apolipoprotein O	DnaJ homolog subfamily C member 11
Galectin-1	Vesicle-associated membrane protein 3	Fibronectin type III domain-containing protein 3B
Phosphoglycerate kinase 1	Histone H2A;Histone H2A type 2-C;Histone H2A type 2-A	Translocation protein SEC62
40S ribosomal protein S3a	Galectin;Galectin-3	Acetyl-CoA acetyltransferase, mitochondrial
Cysteine-rich protein 2	V-type proton ATPase subunit B, brain isoform	Protein OIL1
Stomatin-like protein 2, mitochondrial	Signal peptidase complex subunit 1	NADH dehydrogenase [ubiquinone] 1 subunit C2
Long-chain specific acyl-CoA dehydrogenase, mitochondrial	60S ribosomal protein L18a	CDGSH non-sulfur domain-containing protein 2
60S ribosomal protein L32	60S ribosomal protein L30	Protein FAM162A
40S ribosomal protein S17	60S ribosomal protein L27a	NADH dehydrogenase [ubiquinone] iron-sulfur protein 3, mitochondrial
ATP synthase subunit O, mitochondrial	Histone H1.4	Adenylate kinase isoenzyme 1
Histone H4	Glutathione S-transferase P 1;Glutathione S-transferase P 2	28S ribosomal protein S23, mitochondrial
Electron transfer flavoprotein subunit alpha, mitochondrial	Pyruvate dehydrogenase E1 component subunit beta, mitochondrial	Saccharopine dehydrogenase-like oxidoreductase
ATP synthase F(0) complex subunit B1, mitochondrial	CDGSH iron-sulfur domain-containing protein 1	Dolichyl-diphosphooligosaccharide--protein glycosyltransferase 48 kDa subunit
Tubulin alpha-1A chain;Tubulin alpha-3 chain	Asparityl/asparaginy beta-hydroxylase	Transmembrane 9 superfamily member 2
Prohibitin	ATP-dependent RNA helicase DDX1	60S ribosomal protein L8
Sarcalumenin	Cytochrome b5 type B	Myosin-6;Myosin-7
Titin	MICOS complex subunit Mic19	Prollyl 4-hydroxylase subunit alpha-1
78 kDa glucose-regulated protein	Ras GTPase-activating-like protein IQGAP1	Amine oxidase [flavin-containing] A
Heat shock cognate 71 kDa protein	Isocitrate dehydrogenase [NADP], mitochondrial	Tubulin beta-2B chain;Tubulin beta-2A chain
MICOS complex subunit Mic60	40S ribosomal protein S11	Calcium-binding mitochondrial carrier protein Aralar1
Trifunctional enzyme subunit alpha	Coatomer subunit alpha;Coatomer subunit alpha;Xenin;Proxenin	Peptidyl-RNA hydrolase 2, mitochondrial
Calnexin	Protein-glutamine gamma-glutamyltransferase 2	NADH dehydrogenase [ubiquinone] 1 alpha subcomplex subunit 3
Fibronectin;Anastellin	Ras-related protein Rab-5C;Ras-related protein Rab-5B	Troponin T, fast skeletal muscle
Chloride intracellular channel protein 1	40S ribosomal protein S26	Myosin-11
Heat shock protein HSP 90-beta	Myoferlin	Coatomer subunit beta
Clathrin heavy chain;Clathrin heavy chain 1	HF2 cell-surface antigen heavy chain	Myosin light chain 1/3, skeletal muscle isoform
40S ribosomal protein S24	Coiled-coil domain-containing protein 47	Synaptic vesicle membrane protein VAT-1 homolog
40S ribosomal protein S8	Alpha-enolase	beta-hydroxyacyl-CoA dehydrogenase type-2
40S ribosomal protein S6	Calcium uniporter protein, mitochondrial	40S ribosomal protein S9
ATP synthase subunit e, mitochondrial	Vesicle-associated membrane protein-associated protein A	40S ribosomal protein S20
Dolichyl-diphosphooligosaccharide--protein glycosyltransferase subunit 2	Neural cell adhesion molecule 1	Eukaryotic translation initiation factor 2 subunit 3, Y-linked
40S ribosomal protein S7	ATP-dependent 6-phosphofructokinase, muscle type	Cytochrome c oxidase subunit 4 isoform 1, mitochondrial
60S ribosomal protein L36	39S ribosomal protein L12, mitochondrial	NADH dehydrogenase [ubiquinone] flavoprotein 3, mitochondrial
Mitochondrial 10-formyltetrahydrofolate dehydrogenase	Annexin A2;Annexin	Cytoplasmic dynein 1 light intermediate chain 1
Phosphate carrier protein, mitochondrial	Endoplasmic	Brain acid soluble protein 1
60S ribosomal protein L24	Mitochondrial import receptor subunit TOM70	Nestin
Histone H1.5	Succinate dehydrogenase [ubiquinone] flavoprotein subunit, mitochondrial	Vesicle-associated membrane protein-associated protein B
Ras-related protein Rab-7a	Heterogeneous nuclear ribonucleoprotein A3	60S ribosomal protein L14
Myosin regulatory light chain 2, skeletal muscle isoform	Bassoon	Syntaxin-12
60 kDa heat shock protein, mitochondrial	MICOS complex subunit Mic27	Heterogeneous nuclear ribonucleoprotein K
Leucine-rich PPR motif-containing protein, mitochondrial	Aconitate hydratase, mitochondrial	Voltage-dependent calcium channel subunit alpha-2/delta-1
Heterogeneous nuclear ribonucleoprotein U	Myc box-dependent-interacting protein 1	26S proteasome non-ATPase regulatory subunit 2
NADH dehydrogenase [ubiquinone] 1 beta subcomplex subunit 9	ATP synthase protein 8	Heterogeneous nuclear ribonucleoprotein D0
40S ribosomal protein S15a	Flotillin-2	39S ribosomal protein L41, mitochondrial
40S ribosomal protein S18	Dihydrolipoylysine-residue succinyltransferase component	Flotillin-1
Guanine nucleotide-binding protein (G(i)) subunit alpha-2	NADH dehydrogenase [ubiquinone] iron-sulfur protein 4, mitochondrial	Sphingolipid delta(4)-desaturase DES1
Histone H1.2	Hexokinase-2	Monocarboxylate transporter 1
Alpha-crystallin B chain	T-complex protein 1 subunit zeta	Ras-related protein Rab-5A
Polyadenylate-binding protein 1	40S ribosomal protein S19	Plasminogen receptor (RT)
Desmin	NADH dehydrogenase [ubiquinone] 1 alpha subcomplex subunit 8	Electron transfer flavoprotein subunit beta
Protein S100-A11	Protein sel-1 homolog 1	Actin-related protein 3
40S ribosomal protein S25	Heat shock protein beta-1	Transmembrane and coiled-coil domain-containing protein 1
Unconventional myosin-1c	Lon protease homolog, mitochondrial	Mineralocorticoid receptor
60S ribosomal protein L6	PRA1 family protein 3	Hexokinase-1
60S ribosomal protein L13a	Complement component 1 Q subcomponent-binding protein, mitochondrial	FAS-associated factor 2
Very-long-chain enoyl-CoA reductase	Transforming protein RhoA	Unconventional myosin-1xb
ATP synthase subunit f, mitochondrial	DnaJ homolog subfamily A member 1	Calpain-2 catalytic subunit
Pyruvate-5-carboxylate reductase 2	Calsequestrin;Calsequestrin-2	Reticulon-2
Cytochrome b-c1 complex subunit 7	Cytochrome c oxidase subunit 5B, mitochondrial	Medium-chain specific acyl-CoA dehydrogenase, mitochondrial
D-3-phosphoglycerate dehydrogenase	40S ribosomal protein S13	Leukocyte surface antigen CD47
Cytochrome c oxidase subunit NDUF4A	Selenoprotein T	Nodal modulator 1
26S protease regulatory subunit 6A	I4-3-3 protein zeta/delta	ATP-binding cassette sub-family F member 2
Sequestosome-1	Erlin-2	28S ribosomal protein S15, mitochondrial
NADH dehydrogenase [ubiquinone] iron-sulfur protein 6, mitochondrial	39S ribosomal protein L1, mitochondrial	Serine/threonine-protein phosphatase PP1-gamma catalytic subunit
Insulin-like growth factor 2 mRNA-binding protein 3	Succinate dehydrogenase [ubiquinone] iron-sulfur subunit, mitochondrial	Surfeit locus protein 4
TAR DNA-binding protein 43	Protein ERGIC-53	Dysferlin
Triosephosphate isomerase	LETM1 and EF-hand domain-containing protein 1, mitochondrial	ATP-dependent 6-phosphofructokinase, liver type
Ribonuclease inhibitor	Catrin light chain A	Paspilipyl-protein isomerase C
Mitotic nuclear division protein 1 homolog	NADH dehydrogenase [ubiquinone] flavoprotein 1, mitochondrial	beta-oxoglutarate dehydrogenase, mitochondrial
Transitional endoplasmic reticulum ATPase	Proctatin regulatory element-binding protein	Mitochondrial inner membrane protein OXA1L
60S ribosomal protein L3	ATPase family AAA domain-containing protein 3	Sorting and assembly machinery component 50 homolog
Cytochrome c1, heme protein, mitochondrial	Cytochrome c oxidase subunit 5A, mitochondrial	ER membrane protein complex subunit 1
Prohibitin-2	Wolframin	Heparan sulfate 2-O-sulfotransferase 1
Ras-related protein Rab-14	Mitochondrial import inner membrane translocase subunit Tim10	Calcium uptake protein 1, mitochondrial
40S ribosomal protein S5	T-complex protein 1 subunit epsilon	Sodium/potassium-transporting ATPase subunit alpha-1
Profilin;Profilin-1	Trifunctional enzyme subunit beta, mitochondrial;3-ketoacyl-CoA thiolase	39S ribosomal protein L27, mitochondrial
Up-regulated during skeletal muscle growth protein 5	28S ribosomal protein S36, mitochondrial	Protein transport protein SecE1 subunit beta
3-ketoacyl-CoA thiolase, mitochondrial	NADH dehydrogenase [ubiquinone] 1 alpha subcomplex subunit 5	NADH dehydrogenase [ubiquinone] 1 beta subcomplex subunit 7
Protein LY6C	Malectin	OCLIA domain-containing protein 1
Eukaryotic initiation factor 4A-I	Signal recognition particle receptor subunit beta	Alpha-1,3/1,6-mannosyltransferase ALG2
NADH-ubiquinone oxidoreductase 75 kDa subunit, mitochondrial	V-type proton ATPase 16 kDa proteolipid subunit	Acyl-coenzyme A thioesterase 9, mitochondrial

Table 3.1. See next page for caption.

Table 3.1. Myo-granule protein composition. Mass spectrometry of isolated TDP-43 containing myo-granules compared to IgG control IP (n=3 biological independent experiments).

TDP-43 Myo-granule and Neuronal Granule Proteome Properties

Property	TDP-43 Myo-granule (n = 356)	P-Value	Neuronal RNA Granule (n = 127)	P-Value
Proteins with RNA-Binding Activity*	129	1.02×10^{-32}	94	3.41×10^{-82}
Proteins with Prion-like Domain**	11	-	10	-
Proteins with LARKS***	9	-	4	-
Proteins with ATPase Activity	22	4.68×10^{-11}	0	n/s

Table 3.2. Myo-granule properties identified by mass spectrometry

Protein properties of TDP-43 myo-granules (n=356 proteins) and neuronal RNA granules (n=127 proteins) (El Fatimy et al., 2016). Statistical analysis was performed using hypergeometric distribution to determine chance overlap between two lists. *RNA-Binding Activity defined by Castello et al., 2010. **Prion-like Domain containing proteins defined using PLAAC (Lancaster et al., 2014) and only proteins with a positive coreSCORE were used in the analysis. ***Top 400 proteins rich in LARKS (low-complexity, aromatic-rich kinked segments) were searched (Hughes et al., 2018) and used in the analysis.

TDP-43 is essential for muscle formation

If TDP-43 containing myo-granules are sarcomeric mRNPs, then genetic depletion of TDP-43 may disrupt skeletal muscle myofiber formation. CRISPR-Cas9-mediated deletion of TDP-43 in C2C12 cells arrested growth of C2C12 myoblasts leading to cell death and preventing myoblast differentiation (Figure 3.9e, f, Figure 3.11a). Since TDP-43 appears essential for myoblast proliferation and survival, we asked whether removing one copy of the TDP-43 gene in muscle stem cells using Pax7^{iresCre} recombination impaired muscle regeneration (Figure 3.11b, c) (Chiang et al., 2010; Murphy et al., 2011). The myofiber size and muscle stem cell number is unaffected when one copy of TDP-43 is deleted from muscle stem cells (Figure 3.11d-f). However, following injury, mice with one TDP-43 allele in muscle stem cells have significantly smaller myofibers than in wild type mice (Figure 3.9g, h, Figure 3.11g-i). Since there was no detectable change in a muscle stem cell numbers when one TDP-43 allele was deleted, we posit the regeneration defect is in part due to loss of TDP-43 function during myofiber formation. Thus, TDP-43 is essential for skeletal muscle cell differentiation in culture and required for skeletal muscle regeneration.

Myo-granules in humans and disease

To determine if cytoplasmic TDP-43 and myo-granules are conserved in human muscle regeneration, we examined human muscle biopsies from patients with different clinical and pathological features of necrotizing myopathy. In each patient, we observed increased cytoplasmic TDP-43 and A11 amyloid oligomer staining in the regenerating muscle, suggesting myo-granules form in regenerating human myofibers and are not

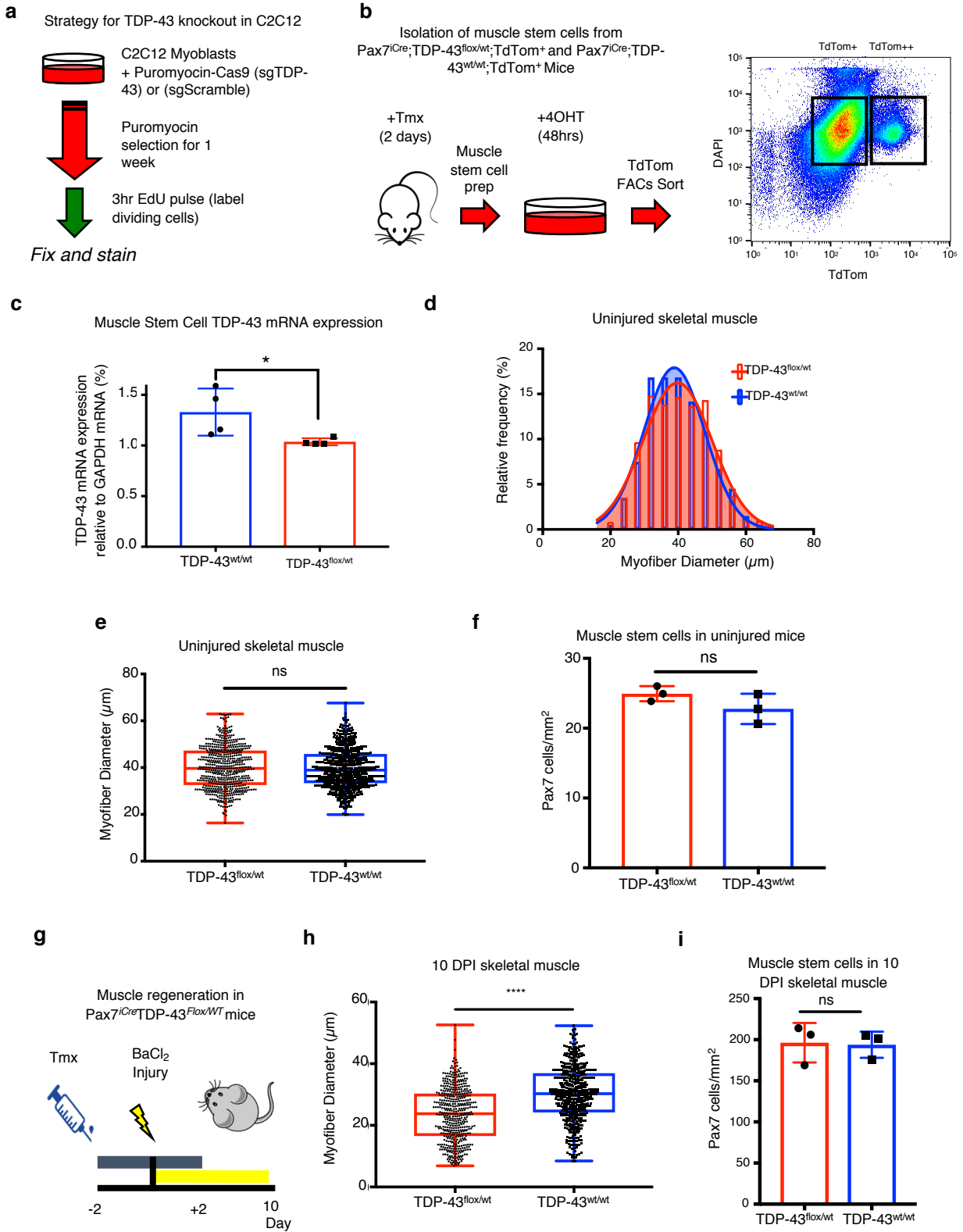


Figure 3.11. See next page for caption.

Figure 3.11. TDP-43 is an essential protein for skeletal muscle formation.

(a) Schematic for the approach used to knockout TDP-43 and quantify C2C12 myoblast proliferation. **(b)** Schematic for the isolation and fluorescence activated cell sorting (FACS) of muscle stem cells from $Pax7^{iCre};TDP-43^{Flox/WT}TdTom^+$ and $Pax7^{iCre};TDP-43^{WT/WT}TdTom^+$ mice. (>125k muscle stem cells collected per mouse from two populations defined in (b) as $TdTom^+$ and $TdTom^{++}$). **(c)** TDP-43 mRNA expression relative to GAPDH mRNA expression from isolated, $TdTom^+$ and $TdTom^{++}$ muscle stem cells from (b). (n = 4 independent experiments (each a mean of technical triplicates) from n = 2 mice). Unpaired, two-tailed t-test (*) p-value = 0.0469). **(d)** Myofiber feret diameter frequency distribution in uninjured $Pax7^{iresCre}TDP-43^{Flox/WT}$ mice compared to $Pax7^{iresCre}TDP-43^{WT/WT}$ controls (n = 3 mice, 600 myofibers quantified per condition). **(e)** Quantification of myofiber feret diameter in (c). Box plot horizontal bars represent mean, 25th and 75th percentile \pm minima/maxima from n = 600 myofibers from n = 3 mice per condition. Unpaired, two-tailed, t-test p-value = 0.5925 is not significant (n.s.)) **(f)** Pax7+ muscle stem cell numbers in uninjured $Pax7^{iresCre}TDP-43^{Flox/WT}$ mice compared to $Pax7^{iresCre}TDP-43^{WT/WT}$ controls (Data are mean \pm s.d., n = 3 mice, Unpaired two-tailed, t-test p-value = 0.1963 (n.s.)). **(g)** Schematic for TDP-43 depletion in Pax7+ muscle stem cells during muscle regeneration in $Pax7^{iresCre}TDP-43^{Flox/WT}$ and $Pax7^{iresCre}TDP-43^{WT/WT}$ mice (Tmx, Tamoxifen). **(h)** Quantification of myofiber feret diameter at 10 dpi in muscle stem cell TDP-43 haploinsufficient mice compared to wild type control box plot horizontal bars represent mean, 25th and 75th percentile \pm minima/maxima from n = 489 myofibers from n = 3 mice per condition. Unpaired, two-tailed, t-test (****) p-value = 2.3×10^{-30} . **(i)** Similar Pax7+ muscle stem cell numbers at 10 dpi in muscle stem cell TDP-43 haploinsufficient mice compared to controls. Data are mean \pm s.d. from n = 3 mice, Unpaired two-tailed, t-test p-value = 0.89 (n.s.).

present in non-regenerating myofibers (Figure 3.12, Figure 3.13a). It is possible that myo-granules formed during normal regeneration may seed the aggregates seen in human muscle diseases.

Since myo-granules containing TDP-43 form during human skeletal muscle regeneration and TDP-43 aggregates are found in skeletal muscle diseases, then the increased regeneration occurring in diseases may promote TDP-43 aggregation. Indeed, cytoplasmic TDP-43 aggregates in skeletal muscle diseases are often seen in myofibers with centrally-located nuclei, a hallmark of regeneration (Küsters et al., 2009; Salajegheh et al., 2009). Therefore, we tested whether cytoplasmic myo-granules accumulate in newly regenerated myofibers of VCP mutant mice, a model of multisystem proteinopathy (MSP) and IBM characterized by TDP-43 aggregation (Custer et al., 2010). When uninjured VCP mutant and wild-type mice were treated with 5-ethynyl-2'-deoxyuridine (EdU), which identifies actively regenerating myofibers containing newly fused nuclei arising from muscle stem cells, VCP mutant mice possessed more EdU+ centrally-located myonuclei compared to VCP wildtype mice (Figure 3.13b, c). Moreover, in the myofibers with EdU+ centrally-located nuclei, we detect increased cytoplasmic TDP-43 and A11 amyloid oligomer staining, correlating the cytoplasmic TDP-43 aggregation with increased muscle regeneration in VCP mutant mice (Figure 3.14a, b, Figure 3.13d, e).

Consistent with the hypothesis that myo-granules may seed the aggregates seen in disease, myo-granules isolated from C2C12 myotubes were capable of transitioning to a Thioflavin-T (ThioT)-positive aggregate (amyloid-like fibers) over time (Figure 3.14c,

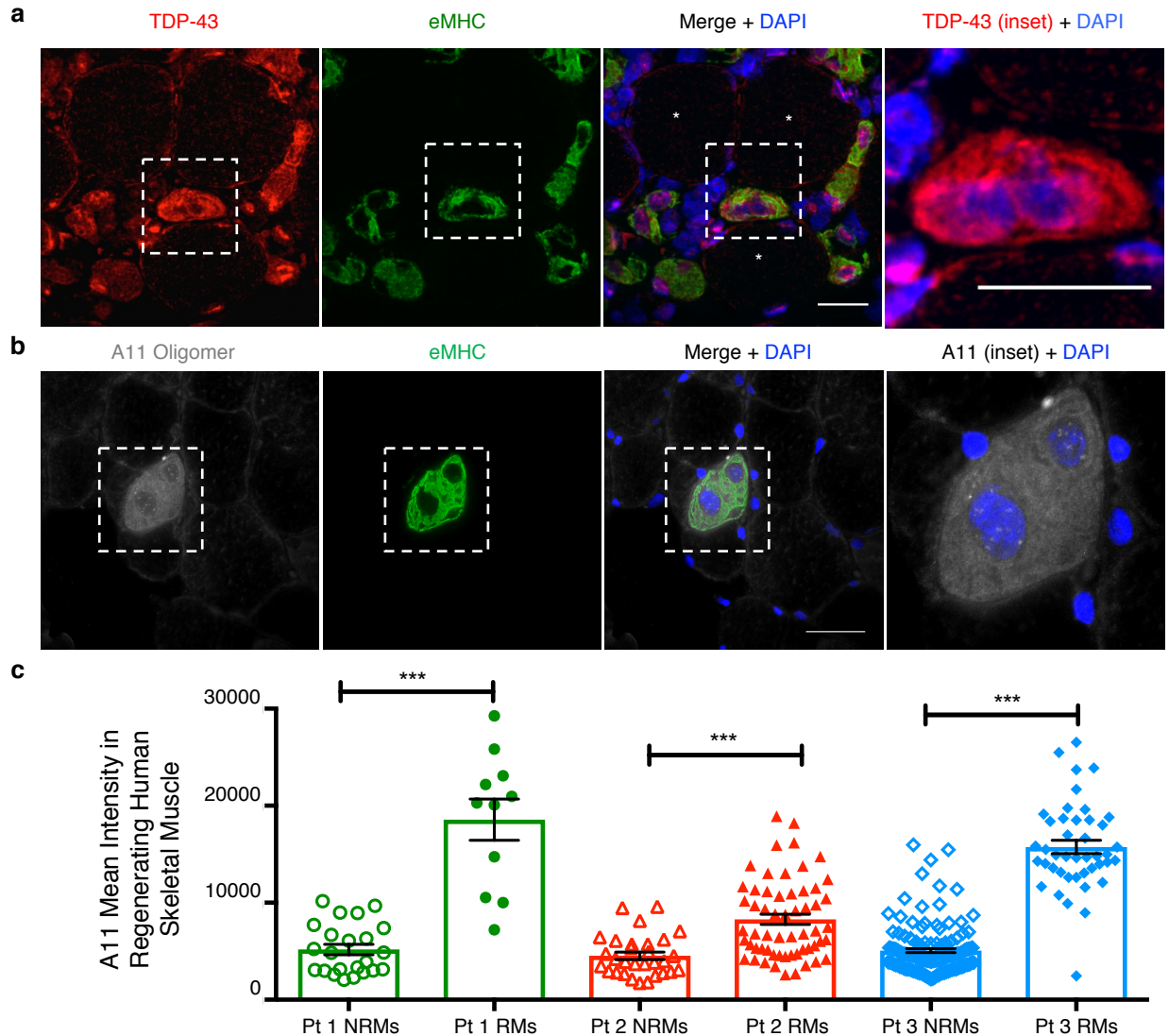


Fig. 3.12. Myo-granules form during human muscle regeneration.

(a) Representative image of cytoplasmic TDP-43 in regenerating human skeletal muscle from patient with necrotizing myopathy, n = 3 skeletal muscle biopsies from three individual patients gave similar results (scale bar is 50 μ m). (b) Representative image of A11 immunoreactivity in regenerating human skeletal muscle from patient with necrotizing myopathy, n = 3 skeletal muscle biopsies from three individual patients gave similar results (scale bar is 100 μ m). (c) Quantification of A11 immunoreactive intensity in regenerating myofibers (RM = eMHC+) compared to non-regenerating myofibers (NRMs = eMHC-) from three patients (Pt) with necrotizing myopathy. Unpaired two-tailed t-test used for each individual comparison: For Pt 1 NRMs (n = 23) vs RMs (n = 11) *** p-value = 2.54 x 10⁻⁹; For Pt 2 NRMs (n = 31) vs RMs (n = 59) *** p-value = 7.89 x 10⁻⁶; For Pt 3 NRMs (n = 146) vs RMs (n = 44) *** p-value = 6.17 x 10⁻⁴⁹. Data are mean \pm s.e.m.

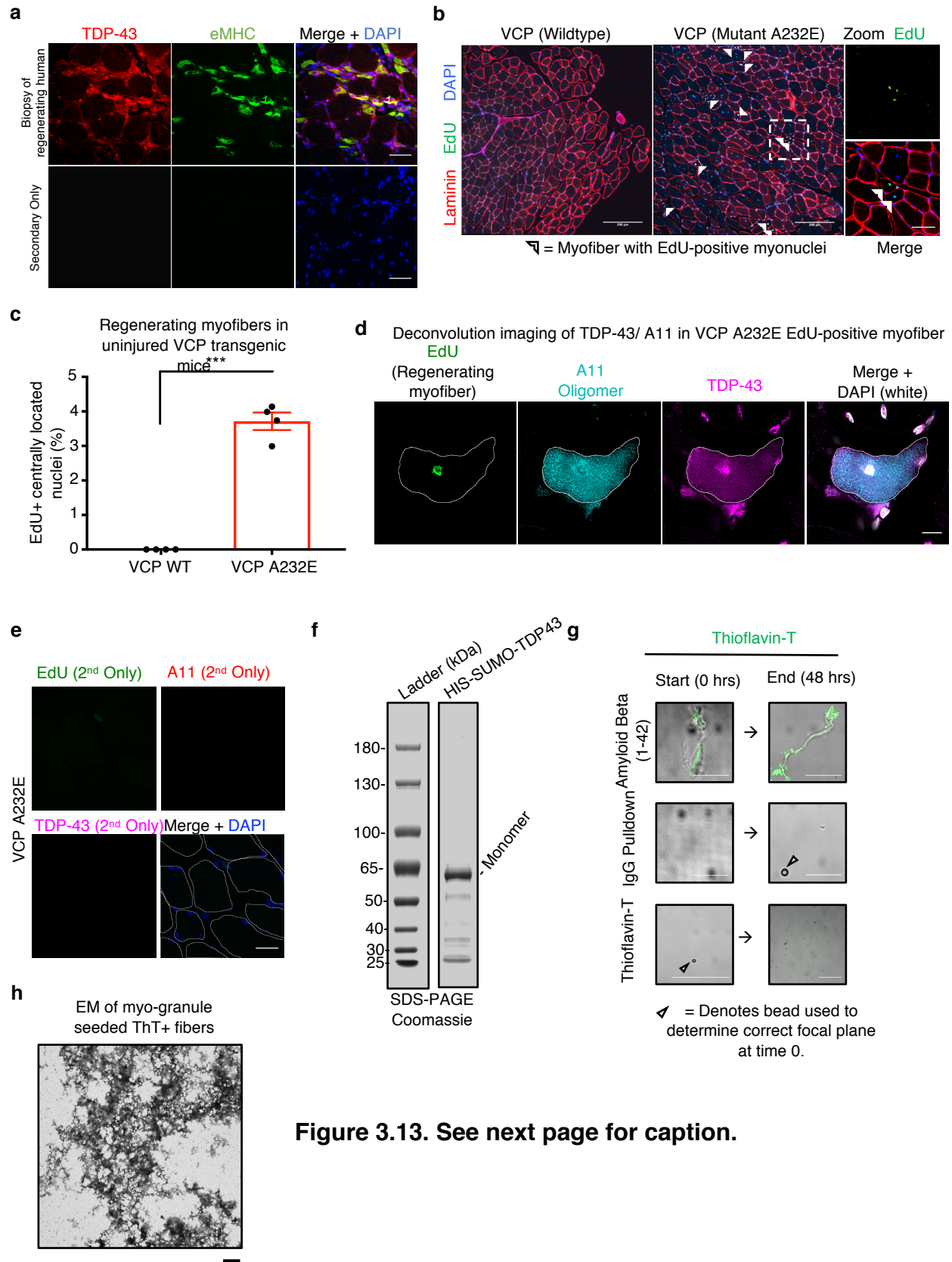


Figure 3.13. See next page for caption.

Figure 3.13. Myo-granules that seed amyloid-like fibres are increased in human muscle regeneration and in multisystem proteinopathy.

(a) Representative image of TDP-43 immunoreactivity (top panel) and secondary antibody only control (bottom panel) in regenerating human skeletal muscle from patient with necrotizing myopathy. N = 3 independent experiments on n = 3 independent patient biopsies each giving similar results. Scale bar is 50 μ m). **(b)** Representative tibialis anterior cross-section images of uninjured VCP A232E and VCP WT mice labeled with EdU after 21 days of EdU given in the drinking water to mark division and fusion of muscle stem cells, visualized for laminin immunoreactivity to identify myofibers and stained with DAPI to identify nuclei. Arrowheads indicate myofibers with EdU+ centrally-located myonuclei (n = 3 mice each giving similar results). Scale bar is 200 μ m and 50 μ m in inset. **(c)** Quantification of myofibers with EdU+ centrally-located myonuclei in VCP-A232E and VCP-WT mice. Data is mean \pm s.d., n = 4 >1000 myofibers quantified per genotype mice per condition, (unpaired, two-tailed, t-test p-value = 6.5 x10⁻⁶). **(d)** Representative deconvolution image of A11 and TDP-43 co-localization in a regenerating myofiber from a VCPA232E TA muscle (n = 3 mice each giving similar results). Scale bar is 10 μ m **(e)** Secondary antibody control for uninjured VCP-A232E TA muscle section reveals lack of signal. Nuclei counterstained with DAPI and myofibers are outlined in white (n = 4 mice each giving similar results). Scale bar is 25 μ m. **(f)** Coomassie stained recombinant HIS-SUMO-TDP-43 used for Thioflavin-T assays resolved by SDS-PAGE (n=3 biologically independent experiments each giving similar results). **(g)** Thioflavin T (ThioT) incorporation reveals ThioT-positive amyloid-like fibers for recombinant A β ₁₋₄₂ and absence of ThioT signal for both IgG pulldown control and ThioT alone (n=3 biologically independent experiments each giving similar results). Scale bar is 10 μ m. **(e)** Representative transmission electron microscopy image (zoomed out from Fig 5e) of ThioT-positive fibers formed from isolated myo-granules (n=3 biologically independent experiments). Scale bar is 1 μ m.

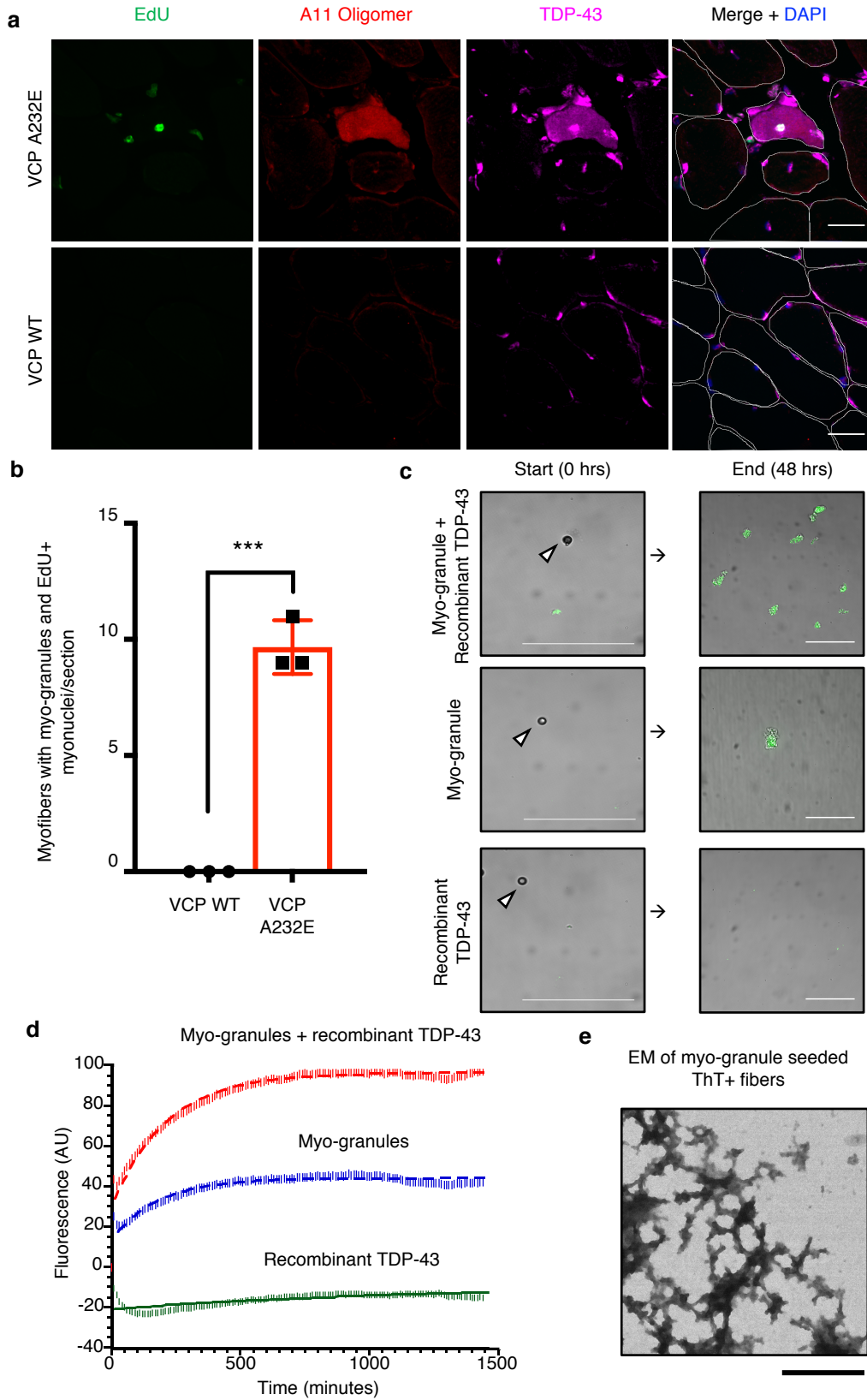


Figure 3.14. See next page for caption.

Figure 3.14. Myo-granules are increased in VCP disease and are capable of seeding amyloid-like fibers.

(a) Uninjured VCP A232E tibialis anterior muscle (top panel) and uninjured VCP wild type (WT) tibialis anterior muscle (bottom panel) probed for EdU incorporation into centrally-located nuclei and immunostained for A11 and TDP-43. Cells counterstained with DAPI and myofibers outlined in white. Scale bar is 25 μ m. **(b)** Quantification of myofibers with EdU+ centrally-located myonuclei, A11 immunoreactivity and cytoplasmic TDP-43 in VCP-A232E and VCP-WT mice, (n = 3 mice, 1 tibialis anterior cross section quantified per mouse), unpaired two-tailed t-test p-value = 1.3×10^{-4} . Data are mean \pm s.d. **(c)** Representative images of purified myo-granules from C2C12 myotubes incubated with or without recombinant TDP-43 and Thioflavin-T (ThioT) reveals formation of higher order ThioT-positive amyloid-like fibers. Scale bar is 25 μ m (n=3 biologically independent experiments). **(d)** Plot of kinetics for fiber aggregation determined by ThioT incorporation measured in 10-minute intervals. Rates derived by fitting time points to single exponential rate equation: Myo-granule + recombinant TDP-43 ($R^2 = 0.96$; $k_{\text{obs}} \times 10^{-4} \text{ (min}^{-1}\text{)} = 47 \pm 1.6$; Myo-granule ($R^2 = 0.92$; $k_{\text{obs}} \times 10^{-4} \text{ (min}^{-1}\text{)} = 56 \pm 2.9$; Recombinant TDP-43 ($R^2 = 0.47$; $k_{\text{obs}} \times 10^{-4} \text{ (min}^{-1}\text{)} = 8.5 \pm 4.9$) (n=3 biologically independent experiments, background corrected arbitrary units, AU). **(e)** Representative transmission electron microscopy images of ThioT-positive fibers formed from isolated myo-granules (n=3 biologically independent experiments). Scale bar is 1 μ m.

d). Moreover, addition of recombinant TDP-43 to isolated myo-granules increased the amount of ThioT-positive aggregates formed without affecting their initial rate of assembly (Figure 3.14c, d, Figure 3.13f, g). Electron microscopy of ThioT-positive TDP-43 aggregates formed from myo-granules reveals fibrous structures morphologically similar to previously reported TDP-43 amyloid fibers (Figure 3.14e) (Mompeán et al., 2015). This suggests that the failure to clear myo-granules during normal muscle formation may seed the formation of cytoplasmic TDP-43 aggregates in diseased muscle. Whether the oligomerization of TDP-43 in myo-granules involves its N-terminal oligomerization domain (Afroz et al., 2017), the C-terminal prion-like domain that is prone to aggregation and fiber formation (Chen et al., 2010; Igaz et al., 2009), or both, remains to be established.

Discussion

We uncover two important properties of TDP-43 in the formation of skeletal muscle. First, TDP-43 is an essential protein that associates with select sarcomeric mRNAs and localizes to sites of newly forming sarcomeres during skeletal muscle formation. Second, TDP-43 is a component of a higher order, amyloid-like myo-granule assembled during normal skeletal muscle formation. Purified myo-granules from cultured myotubes are capable of seeding amyloid-like fibrils *in vitro* suggesting a link between the normal biological functions of TDP-43 and pathological TDP-43 aggregates.

We propose a model whereby myo-granules containing TDP-43 are increased in damaged tissues with elevated regeneration, thereby enhancing the possibility of amyloid fiber formation and/or aggregation of TDP-43 in disease (Figure 3.15). Since the triggering event in this model is elevated muscle regeneration, it explains why TDP-43 aggregates occur in genetically diverse diseases including IBM (Salajegheh et al., 2009), which can be caused by mutations in the ubiquitin segregase VCP (Custer et al., 2010), OPMD, caused by Ala expansions in PABPN1 (Küsters et al., 2009), and DMRV, caused by mutations in the UDP-N-acetylglucosamine 2-epimerase gene (GNE) (Nishino et al., 2002). Moreover, the seeding of TDP-43 aggregates by TDP-43 oligomers may also occur in neurons since reversible cytoplasmic TDP-43 accumulation occurs in models of acute neuronal injury *in vivo* (e.g. axotomy or traumatic brain injury) (Moisse et al., 2009; Wiesner et al., 2018). TDP-43 aggregates are also frequently observed on autopsy in neurologically normal elderly individuals (Nascimento et al., 2018). The age-dependent accumulation of TDP-43 aggregates may be caused by a failure to clear TDP-43, or other amyloid-like assemblies that formed during tissue repair. Over a lifetime, failures in proteostatic control mechanisms, including autophagy or endocytosis (Elobeid et al., 2016; Liu et al., 2017a; Wilson et al., 2013), could increase the likelihood that functional, amyloid-like assemblies transition into pathological aggregates.

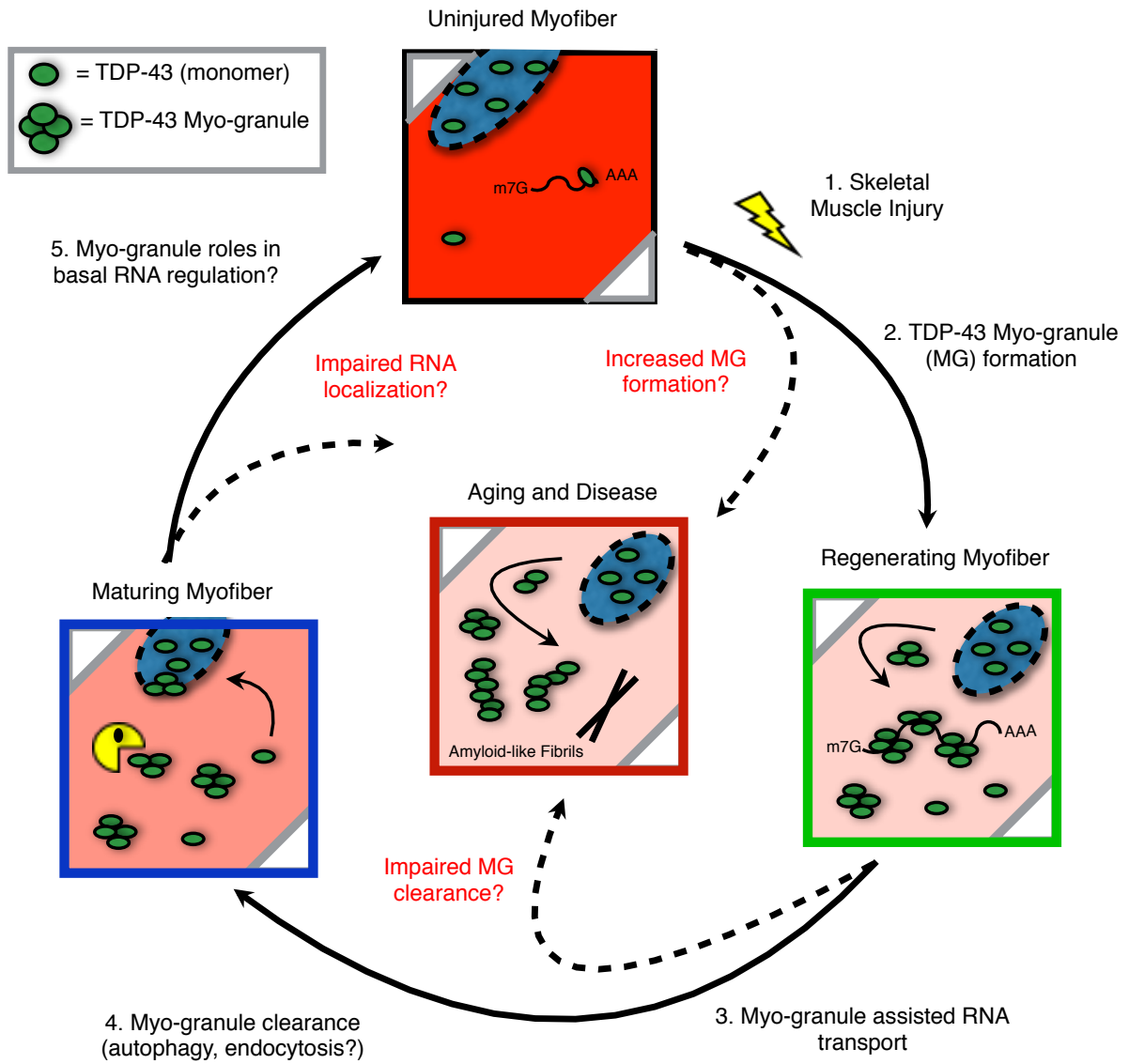


Figure 3.15. Myo-granules in normal skeletal muscle regeneration and in disease.

Schematic of TDP-43 oligomerization and aggregation in wild type, aging and diseased skeletal muscle myofibers.

Methods

Mice

Mice were bred and housed according to National Institutes of Health (NIH) guidelines for the ethical treatment of animals in a pathogen-free facility at the University of Colorado at Boulder (Wild-type, Pax7^{iresCre}, TDP-43^{flox/flox} and VCP-A232E lines). The University of Colorado Institutional Animal Care and Use Committee (IACUC) approved all animal protocols and procedures. Wild-type mice were C57Bl/6 (Jackson Labs, ME, USA) and VCP-A232E, VCP-WT (Custer et al., 2010), and TDP-43^{flox/flox} mice (Chiang et al., 2010) were previously described. Crossing mice into Pax7^{iresCre} mice (Murphy et al., 2011) generated conditional TDP-43^{flox/WT} mice. Cells and tibialis anterior (TA) muscles were isolated from 3-6-month-old male and female wild-type and Pax7^{iresCre}; TDP-43^{flox/WT} mice. TA or gastrocnemius muscles were isolated from 9-month-old male VCP-A232E mice. Control mice were age and sex matched from the mice and crosses described above.

Mouse Injuries and Tamoxifen injections

Mice at 3-6 months old were anesthetized with isoflurane and the left TA muscle was injected with 50 μ L of 1.2% BaCl₂ and then the injured and contralateral TA muscles were harvested at the indicated time points. Intraperitoneal (IP) administration of tamoxifen (Sigma), re-suspended in sterile corn oil (Sigma), was given to 3-6-month-old mice at a volume of 0.075mg of tamoxifen per gram of mouse weight.

Human Muscle Biopsy Tissue

Under an IRB-approved protocol at Johns Hopkins University, a clinical muscle biopsy database was searched for patients who were clinically diagnosed with rhabdomyolysis and/or pathologically diagnosed with necrotizing myopathy with evidence of myofiber regeneration. Patient muscle tissue leftover from diagnostic biopsy was stored frozen at -80 C for less than two years, and samples were cyrosectioned for immunohistochemical analysis.

Immunofluorescence staining of tissue sections

TA or gastrocnemius muscles were dissected, fixed on ice for 2hrs with 4% paraformaldehyde, and then transferred to PBS with 30% sucrose at 4°C overnight. Muscle was mounted in O.C.T. (Tissue-Tek®) and cryo-sectioning was performed on a Leica cryostat to generate 10µm thick sections. Tissues and sections were stored at -80°C until staining. Tissue sections were post-fixed in 4% paraformaldehyde for 10 minutes at room temperature (RT) and washed three times for 5 min in PBS. Immunostaining with anti-Pax7, anti-Laminin, anti-eMHC, anti-TDP-43 and A11 antibodies required heat-induced epitope retrieval where post-fixed slides were placed in citrate buffer, pH 6.0, and subjected to 6 min of high pressure-cooking in a Cuisinart model CPC-600 pressure cooker. For immunostaining, tissue sections were permeabilized with 0.25% Triton-X100 (Sigma) in PBS containing 2% bovine serum albumin (Sigma) for 60 min at RT. Incubation with primary antibody occurred at 4°C overnight followed by incubation with secondary antibody at room temperature (RT) for

1hr. Primary antibodies included mouse anti-Pax7 (Developmental Studies Hybridoma Bank, University of Iowa, USA) at 1:750, rabbit anti-laminin (Sigma-Aldrich) at 1:200, rabbit anti-TDP-43 (ProteinTech) at 1:200, mouse anti-TDP-43 (Abcam) at 1:200, rabbit A11 (Sigma-Aldrich) at 1:200, mouse anti-VCP (ThermoFisher Scientific) at 1:400 and a mouse anti-eMHC (Developmental Studies Hybridoma Bank, University of Iowa, USA) at 1:5. Alexa secondary antibodies (Molecular Probes) were used at a 1:1000 dilution. For analysis that included EdU detection, EdU staining was completed prior to antibody staining using the Click-iT EdU Alexa fluor 488 detection kit (Molecular Probes) following manufacturer protocols. Sections were incubated with 1 µg/mL DAPI for 10 min at room temperature then mounted in Mowiol supplemented with DABCO (Sigma-Aldrich) or ProLong Gold (Thermo) as an anti-fade agent.

Isolation of Primary Muscle Stem Cells

Gastrocnemius, extensor digitorum longus (EDL), TA and all other lower hindlimb muscles were dissected from wild-type mice. The muscle groups from both hind limbs were separated and digested in 3.6mL of F12-C (Gibco) with penicillin/streptavidin (Gibco) and 400uL 10X collagenase (Worthington) for 90 minutes at 37°C on a slow rotisserie. In a biosafety cabinet, muscles were settled for 5 minutes, undisturbed, and then as much of the liquid was removed without disturbing the muscle groups. F12-C with penicillin/streptavidin and 15% horse serum was added and the muscles rocked for 1 minute. Then, 3mL of growth media was added to each tube (F12-C with penicillin/streptavidin, 15% horse serum (Gibco), 20% fetal bovine serum (Sigma), 1%

Chick Embryo Extract (Antibody Production Services Ltd.). The digest was poured onto a (Corning) 10cm tissue culture plate with Matrigel in 10mL of growth media. Growth media was added as necessary to keep the muscle chunks submerged. Muscles chunks were incubated in growth media with FGF-2 (50nM working concentration) for 72 hours at 37°C in 6% O₂, 5% CO₂. After 72 hours, muscle stem cells have migrated out onto the Matrigel and the muscle chunks and media were removed. The plate containing attached muscle stem cells was rinsed with sterile PBS and 10mL warm growth media added supplemented with 50nM FGF-2. Colonies of myoblasts formed by 4 days of culture and were expanded by passaging with 0.25% Trypsin-EDTA (Sigma).

Cell culture.

Primary Muscle Stem Cells: After initial isolation, primary myoblasts were maintained on Matrigel-coated tissue culture plastic plates or gelatin-coated coverslips at 37°C with 6% O₂, 5% CO₂ in growth media as described above. Media was changed only during cell passaging. To promote myoblast fusion, cells at 75% confluency were washed three times with PBS and media switched to DMEM (Gibco) with 5% horse serum (Gibco), 1% penicillin/streptavidin and 1% Insulin-Transferrin-Selenium (Gibco). To induce stress granule formation, primary myotubes were stressed with 0.5mM sodium arsenite for 1hr at 37°C.

C2C12 cells: Immortalized murine myoblasts (American Type Culture Collection) were maintained on uncoated standard tissue culture plastic or gelatin-coated coverslips at 37°C with 5% CO₂ in DMEM with 20% fetal bovine serum and 1%

penicillin/streptavidin. To promote myoblast fusion when the C2C12 cells reached confluence, they were switched to 5% horse serum, 1% penicillin/streptavidin and 1% Insulin-Transferrin-Selenium in DMEM. To induce stress granule formation, C2C12 myotubes were stressed with 0.5mM sodium arsenite for 1hr at 37°C.

U-2 OS: Human osteosarcoma cells were maintained in DMEM, High Glucose, GlutaMAX with 10% fetal bovine serum, 1% penicillin/streptomycin, and 1mM sodium pyruvate at 37°C/5% CO₂.

Yeast: BY4741 yeast was transformed with a single plasmid expressing Pub1Q/N-GFP (pRP1689) were grown at 30°C in minimal media with 2% glucose as a carbon source and with leucine dropout to maintain the plasmid. SUP35 [PSI+] (5V-H19A) and SUP35 [psi-] (yAV831) stains were grown in minimal media supplemented with a complete set of amino acids and 2% Dextrose at 30°C.

Immunofluorescence Staining of Cells and Proximity Ligation Assay

Primary and immortalized cells were washed with PBS in a laminar flow hood and fixed with 4% Paraformaldehyde for 10 min at room temperature in a chemical hood. Cells were permeabilized with 0.25% Triton-X100 in PBS containing 2% bovine serum albumin (Sigma) for 1 hour at RT. Incubation with primary antibody occurred at 4°C overnight followed by incubation with secondary antibody at room temperature for 1hr. Primary antibodies included mouse anti-Pax7 (Developmental Studies Hybridoma Bank, University of Iowa, USA) at 1:750, rabbit anti-TDP-43 (ProteinTech) at 1:200, mouse anti-TDP-43 (Abcam) at 1:200, rabbit A11 (Sigma-Aldrich) at 1:200, and a

mouse anti-MHC (MF-20, Developmental Studies Hybridoma Bank, University of Iowa, USA) at 1:1. Alexa secondary antibodies (Molecular Probes) were used at a 1:1000 dilution. All antibodies were diluted in with 0.125% Triton-X100 in PBS containing 2% bovine serum albumin. For analysis that included EdU detection, EdU staining was completed prior to antibody staining using the Click-iT EdU Alexa fluor 488 detection kit (Molecular Probes) following the manufacturer's protocol. Cells were incubated with 6.6mM Phalloidin (Thermo Scientific) for 20 minutes and/or 1 µg/mL DAPI for 10 min at room temperature then mounted in Mowiol supplemented with DABCO (Sigma-Aldrich) as an anti-fade agent. For the proximity ligation assay, samples were incubated with indicated antibodies at the concentrations listed above. Secondary antibody incubation and Duolink proximity ligation assays were performed according to the manufacturer's protocol (Sigma).

Subcellular fractionation

Nuclear/ cytosolic fractionation was performed according to established protocol (Burke and Sullivan, 2017) to determine localization of soluble TDP-43 in C2C12 myoblasts and differentiating myotubes. In brief, myoblasts or differentiating myotubes (day 4) were trypsinized, washed with phosphate-buffered solution (PBS), and pelleted by centrifugation at 1000xg, 5 min. Cells were subsequently washed in PBS and divided into a whole lysate fraction (WCL, 1/3 total) or a cytosolic/ nuclear fraction (Cyto/Nuc, 2/3 total). Both cellular fractions were pelleted by centrifugation at 1000xg, 5 mi. The WCL fraction was suspended into RIPA buffer [50 mM Tris pH 7.5, 1% NP-40, 0.5%

sodium deoxycholate, 0.05% SDS, 1 mM EDTA, 150 mM NaCl, protease inhibitors (Roche)] and placed on ice. The Cyto/ Nuc fraction was suspended in a hypotonic lysis buffer [10mM Tris HCL 7.5, 10mM NaCl, 3mM MgCl₂, 0.5% NP40, protease inhibitors (Roche)] and placed on ice for 4 minutes. Nuclei were then pelleted by centrifugation at 500xg for 5 minutes. The supernatant [cytosolic fraction (Cyto)] was removed. The pellet [nuclear fraction] was then suspended in nuclear lysis buffer [50mM Tris HCL 7.4, 120mM NaCl, 1% SDS, 1mM EDTA, 50mM DTT, protease inhibitors (Roche)]. Nuclei were lysed with 5 passages through an 18G needle. Cellular debris was cleared from collected fractions with centrifugation at 1000xg, 5min. Equal volumes (20uL) of fractions were then resolved on a 4-12% Bis-Tris SDS-PAGE and transferred to nitrocellulose membrane (Bio-Rad). Western blotting was performed according to standard procedures.

Single Molecule Imaging of endogenous HALO-TDP-43

A tetracycline inducible HALO-Tagged (Promega) TDP-43 fusion protein was knocked into the ROSA26 safe harbor locus using CRISPR/Cas9 (Platt et al., 2014). Knock-in cells were selected using puromycin and proper genomic integration was confirmed by PCR and western blotting. For live cell single molecule imaging studies, puromycin-resistant myoblasts or differentiating myotubes were grown on collagen treated, 35mm imaging dishes (MatTek). HALO-TDP-43 was induced for 48hrs using doxycycline (1 μ g/mL). HALO-TDP-43 molecules were labeled with 50pM JF646 dye (a generous gift from Luke Lavis) for 15 minutes in culture media (Grimm et al., 2015).

After the pulse, cells were washed three times with media and incubated with Vibrant Violet (1:400) containing media to visualize myonuclei for at least 1 hour prior to image acquisition. All single molecule live imaging was performed under HILO conditions (highly inclined and laminated optical sheet) on a Nikon N-STORM microscope equipped with TIRF illuminator, an environmental chamber, two iXon Ultra 897 EMCCD cameras (Andor), a 100x oil-immersion objective (Nikon, NA = 1.49), two filter wheels, appropriate filter sets, and 405 nm (20mW), 488 nm (50 mW), 561 nm (50 mW), and 647 nm (125 mW) laser lines (Tokunaga et al., 2008). Differentiating myotubes were identified by visualizing fused myonuclei with 405nm laser line (1% laser power). To image HALO-TDP-43, cells were imaged continuously with 647nm (40% laser power) for 15s at an effective frame rate of 100 frames per s. Single particle tracks were generated using Matlab.

Biochemical characterization of TDP-43 during myogenesis

RIPA/urea solubility assays were conducted as previous described (Mackenzie et al., 2017). In brief, C2C12 myoblasts and myotubes were lysed with RIPA buffer (50 mM Tris pH 7.5, 1% NP-40, 0.5% sodium deoxycholate, 0.05% SDS, 1 mM EDTA, 150 mM NaCl). Protein concentrations were determined using BCA assay (Thermo Scientific) according to standard procedures. Lysates were centrifuged at 18,000 x g for 20 minutes at 4°C. The supernatant represented the RIPA soluble fraction while the pellet was solubilized in 7M Urea in TBE and represents the UREA soluble fraction. Western blotting was performed following resolution of protein lysates on SDS-PAGE.

Semi-Denaturing Detergent Agarose Gel Electrophoresis (SDD-AGE) was conducted as previously described (Halfmann and Lindquist, 2008). In brief, C2C12 myoblasts and myotubes were lysed with RIPA buffer, protein concentrations were standardized using BCA assay, diluted to 1X in loading buffer (2X TAE, 20% glycerol, 8% SDS, bromophenol blue) and separated across a 1.5% agarose gel containing 0.1% SDS. Gels were transferred by capillary transfer overnight to nitrocellulose in TBS. Standard western blotting procedures were performed.

Fractionation of TDP-43 oligomers across sucrose gradients (10–35%) was performed by adopting a previously described method (Wheeler et al., 2016, 2017). Fractions were collected and equal volume was loaded for SDD-AGE analysis. Immunoprecipitation followed by scanning electron microscopy of TDP-43 SDS-resistant fraction was performed as below.

Dot blots on C2C12 protein lysates or whole muscle lysates were conducted according to standard procedures (Fang et al., 2014). Both C2C12 cells and whole muscle were lysed in RIPA buffer, protein concentrations were normalized using BCA and were spotted onto nitrocellulose membranes.

Isolation of myo-granules

A protocol for isolating myo-granules from myotubes was modified from existing protocols for isolating heavy RNP complexes (Jain et al., 2016; Wheeler et al., 2017). In brief, myotubes or whole TA muscle were lysed under non-denaturing conditions using CHAPS lysis buffer (10 mM Tris-HCl pH 7.5, 1 mM MgCl₂, 1 mM EGTA, 0.5% CHAPS,

10% glycerol, 1 mM PMSF, 1 mM DTT) or RIPA buffer and spun to remove heavy cellular debris (250xg, 5 minutes). Successive centrifugation was used to enrich for heavy complexes (18,000xg, 20 minutes). The pellet was resuspended into immunoprecipitation buffer (10mM Tris HCL 7.5; 25mM NaCl; 0.005% NP40) to create an “myo-granule enriched fraction”. The enriched fraction was precleared for 30 minutes with immunoprecipitation buffer equilibrated dynabeads and then incubated overnight with antibodies against either TDP-43 (Proteintech) or A11 (Thermo Scientific). Myo-granules were immunopurified on equilibrated dynabeads, washed in immunoprecipitation buffer, and eluted using Pierce Gentle Ag/Ab Buffer (Thermo Scientific) as previously described (Fang et al., 2014). Buffer was exchanged using a 10K MW spin column (Millipore Amicon).

RNA extraction and oligo-dT Northern analysis of myo-granules

RNA was isolated from myo-granules bound to dynabeads by Trizol extraction followed by ethanol precipitation as previously described (Khong et al., 2018). RNA was run on a 1.25% formaldehyde agarose gel, transferred to nitrocellulose membrane and hybridized with a α P³² labeled oligo-dT probe at room temperature overnight. Membrane was exposed on phosphorimager screen either for 1 hour (low exposure) or overnight (high exposure) and imaged on a Typhoon FLA 9500 phosphorimager.

Electron Microscopy

Electron microscopy sample preparation and image acquisition was performed as previously described unless otherwise specified (Winey et al., 2014). For experiments wherein immunofluorescence on EM grids was performed, Carbon type B 300 mesh Copper TEM grids (Ted Pella) were Poly-Lysine (Sigma) treated for 30 minutes, washed three times in phosphate buffered saline (PBS), and immunopurified myo-granules (diluted 1:50) were adhered to grid for 1 hour at room temperature. TEM grids with myo-granules were blocked in 3% bovine serum albumin (BSA) for 1 hour at room temperature. Primary antibody incubation was performed at 1:100 dilution in 3% BSA for 1 hour at room temperature. Grids were then washed three times in PBS and incubated with secondary antibodies at 1:250 dilution in 3% BSA. Secondary only controls were performed at the same concentration without addition of primary antibody. Grids were washed three times with PBS and placed onto microscopy slides. Images were acquired using a DeltaVision Elite microscope with a 100X objective. Grids were stained with uranyl acetate and immunopositive myo-granules were examined by TEM.

Myo-granule Electron Diffraction

Lyophilized myo-granules and SOD1 segment oligomers (prepared as in (Sangwan et al., 2017)) were mounted for diffraction by dipping a nylon loop in glycerol and sticking some of the lyophilized sample to the glycerol (Lovci et al., 2013). Samples were carefully aligned to avoid the nylon loop entering the X-ray beam when diffraction images were taken. All samples were shot at the Advanced Photon Source (Argonne National Laboratory, Lemont, IL) beamline 24-E with a 50-micron aperture. Samples

were rotated 5 degrees over a 4 second exposure at 295K and images analyzed with ADXV.

TDP-43 eCLIP-seq

C2C12 myoblasts were seeded at 6×10^6 cells per 15 cm plate, grown 24hrs at 37°C, 5% CO₂ and either harvested (undifferentiated myoblasts) or differentiated in differentiation media for 7 days. TDP-43 enhanced CLIP (eCLIP) was performed according to established protocols (Van Nostrand et al., 2016).

In brief, TDP-43-RNA interactions were stabilized with UV crosslinking (254 nm, 150mJ/cm²). Cell pellets were collected and snap frozen in liquid N₂. Cells were thawed, lysed in eCLIP lysis buffer (50 mM Tris-HCl pH 7.4, 100 mM NaCl, 1% NP-40, 0.1% SDS, 0.5% sodium deoxycholate, and 1x protease inhibitor) and sonicated (Bioruptor). Lysate was RNase I (Ambion, 1:25) treated to fragment RNA. Protein-RNA complexes were immunoprecipitated using indicated antibody. One size-matched input (SMInput) library was generated per biological replicate using an identical procedure without immunoprecipitation. Stringent washes were performed as described, RNA was dephosphylated (FastAP, Fermentas), T4 PNK (NEB), and a 3' end RNA adaptor was ligated with T4 RNA ligase (NEB). Protein-RNA complexes were resolved on an SDS-PAGE gel, transferred to nitrocellulose membranes, and RNA was extracted from membrane. After RNA precipitation, RNA was reverse transcribed using SuperScript IV (Thermo Fisher Scientific), free primer was removed, and a 3' DNA adaptor was ligated onto cDNA products with T4 RNA ligase (NEB). Libraries were PCR amplified and dual-

indexed (Illumina TruSeq HT). Pair-end sequencing was performed on Illumina NextSeq sequencer.

Bioinformatics and Statistical analysis

Read processing and cluster analysis for TDP-43 eCLIP was performed as previously described (Van Nostrand et al., 2016). Read processing and cluster analysis for TDP-43 eCLIP was performed as previously described. Briefly, 3' barcodes and adapter sequences were removed using standard eCLIP scripts. Reads were trimmed, filtered for repetitive elements, and aligned to the mm9 reference sequence using STAR. PCR duplicate reads were removed based on the read start positions and random sequence. Bigwig files for genome browser display were generated based on the location of the second of the paired end reads. Peaks were identified using the encode_branch version of CLIPPER (Lovci et al., 2013) using the parameter “-s mm9.” Peaks were normalized against size matched input by calculating fold enrichment of reads in IP versus input, and were designated as significant if the number of reads in the IP sample was greater than in the input sample, with a Bonferroni corrected Fisher exact p-value less than 10^{-8} .

Microscopy and image analyses

Images were captured on a Nikon inverted spinning disk confocal microscope or a DeltaVision Elite microscope. Objectives used on the Nikon were: 10x/0.45NA Plan Apo, 20x/0.75NA Plan Apo and 40x/0.95 Plan Apo. Confocal stacks were projected as

maximum intensity images for each channel and merged into a single image. Brightness and contrast were adjusted for the entire image as necessary. Both muscle stem cell numbers and average fiber diameter were counted manually using Fiji ImageJ.

Objectives used on the DeltaVision Elite microscope were 100X using a PCO Edge sCMOS camera. At least 3 images were taken for each experiment comprising of 8 or 10 Z-sections each. Images were processed using Fiji ImageJ. For super resolution imaging, microscopy was performed using a Leica TCS SP8 White Light Laser with 63x 1.4 NA Oil objective coupled to HyVolution (SVI Huygens based deconvolution) and special Leica Hybrid Detectors. Image quantification was performed using Imaris imaging software.

Sequential immunofluorescence and single molecule FISH

Sequential immunofluorescence (IF) and smFISH on fixed myotubes was performed as recently described (Khong et al., 2018). Briefly, C2C12 myotubes were differentiated for 7 days in differentiation media, fixed in 4% paraformaldehyde (4%) for 10 minutes, and washed in PBS. The following antibodies were used for immunofluorescence: rabbit anti-TDP-43 (Proteintech, 1:400), rabbit anti-A11 oligomer (Thermo Fisher Scientific, 1:400), goat anti-rabbit Alexa 647 (Abcam, 1:1000), goat anti-mouse IgG1 Alexa 488 (Thermo Fisher Scientific, 1:1000). All IFs were performed sequentially except for staining with mouse anti-myosin heavy chain, F59 (DSHB) which was diluted (1:10) in hybridization buffer. Custom Stellaris FISH probes were designed

against mouse Titin, Myosin-3, Troponin C1 and labeled with Quasar 570 Dye using Stellaris RNA FISH Probe Designer (Biosearch Technologies, Petaluma, CA).

Mass spectroscopy

Mass spectrometry was performed as previously described (Jain et al., 2016). In brief, samples were immunoprecipitated on dynabeads as described above. Samples were washed with 0.1 M ammonium bicarbonate (ABC), and resuspended in 100 μ L of 0.1 M ABC, 0.2% sodium deoxycholate, 6M guanidine HCL. Samples were reduced and alkylated with 5 mM TCEP, 40 mM chloroacetamide at 65 °C for 20 min in darkness. Samples were trypsinized with 0.5 μ g of trypsin at 37 °C for overnight. Proteolysis reaction was quenched by acidification using formic acid. Deoxycholic acid was removed by phase-transfer using ethyl acetate, as previously described (Yeung and Stanley, 2010). Tryptic peptides were desalted using in-house stop-and-go extraction (STAGE) tips, speed-vac to dryness, and samples were stored at -80 °C.

Samples were resolved by UPLC in the direct injection mode using a Waters nanoACQUITY system. Samples were resuspended in 12 μ L of buffer A (0.1% formic acid/water), of which 5 μ L (42% of total) was loaded onto a Symmetry C18 nanoACQUITY trap column (130 Å, 5 μ m, 180 μ m 20 mm) with 15 μ L/min of 99.5% buffer A and 0.5% buffer B (0.1% formic acid/acetonitrile) for 3 min. Samples were then eluted and resolved on a BEH130 C18 analytical column (130 Å, 1.7 μ m, 75 μ m x 250 mm) using a gradient with 3-8% buffer B between 0-3 min, 8-28% buffer B between 2-185 min, and 28-60% buffer B between 185-190 min (0.3 μ L/min). MS/MS was

performed using an LTQ Orbitrap Velos, scanning MS between 400–1800 m/z (1×10^6 ions, 60,000 resolution) in FT, and selecting the 20 most intense MH₂²⁺ and MH₃³⁺ ions for MS/MS in LTQ with 180 s dynamic exclusion, 10 ppm exclusion width, repeat count = 1. Maximal injection time was 500 ms for FT precursor scans with one microscan, and 250 ms for LTQ MS/MS with one microscan and AGC 1×10^4 . The normalized collision energy was 35%, with activation Q=0.25 for 10 ms.

Raw data from mass spectrometry were processed using MaxQuant/Andromeda (ver 1.5.0.12) (Cox and Mann, 2008; Cox et al., 2011) and searched against Uniprot mouse database (downloaded on October 2015, 46,471 entries) with common contaminant entries. The search used trypsin specificity with maximum two missed cleavages, included carbamidomethylation on Cys as a fixed modification, and N-terminal acetylation and oxidation on Met as variable modifications. Andromeda used seven ppm maximum mass deviation for the precursor ion, and 0.5 Da as MS/MS tolerance, searching eight top MS/MS peaks per 100 Da. False discovery rates were set to 0.01 for both protein and peptide identifications, with seven amino acid minimum peptide length, and two minimum total peptides.

TDP-43 CRISPR-Cas9 knockout and EdU incorporation

CRISPR-Cas9 knockout was performed in C2C12 myoblasts. Single guide RNA (sgRNA) against TDP-43 (5'- GTGTATGAGAGGAGTCCGAC) were designed using (crispr.mit.edu) and cloned into pSpCas9(BB)-2A-Puro (PX459). T7 endonuclease assays (T7EN) was used to confirm correct targeting to the TDP-43 locus. C2C12

myoblasts were transfected with JetPrime using standard protocols. Myoblasts were selected with puromycin (1 $\mu\text{g}/\text{mL}$) for one week. C2C12 myoblasts were incubated with 10 μM 5-ethynyl-2'-deoxyuridine (EdU – Life Technologies) for three hours. Cells were washed, fixed and stained using the methods described above.

Recombinant TDP-43 Purification

Full-length human TDP-43 was subcloned into pE-SUMO (LifeSensors). His6-SUMO N-terminally tagged TDP-43 was transformed in BL21(DE3)RIL *E. coli*, which were grown up from an overnight culture in LB-amp at 37°C until an OD₆₀₀ of 0.3 was reached. At this time, the culture was shifted to 15°C and grown until the OD₆₀₀ was 0.4-0.5. TDP-43 was then induced with 1mM IPTG for 16 hours at 15°C. The *E. coli* cells were then lysed by sonication on ice in 50mM HEPES (pH 7.5), 2% Triton X-100, 500mM NaCl, 30mM imidazole, 5% glycerol, 2mM β -mercaptoethanol, and protease inhibitors (cOmplete, EDTA-free, Roche). TDP-43 was purified over Ni-NTA agarose beads (Qiagen) and eluted from the beads using 50mM HEPES (pH 7.5), 500 mM NaCl, 300mM imidazole, 5% glycerol, and 5mM DTT. The protein was subsequently buffer exchanged into 50mM HEPES (pH 7.5), 500mM NaCl, 5% glycerol, and 5mM DTT, flash frozen in liquid N₂, and stored as aliquots in -80°C until use. Protein concentration was determined by Bradford assay (Bio-Rad). The purity of TDP-43 was confirmed on a 4-20% polyacrylamide gel.

Thioflavin-T incorporation

Myo-granules were isolated from myotubes and diluted in phosphate buffered saline. Three separate biological replicates were performed constituting purification from three separate myotube cultures. 25 μ M Thioflavin-T (Abcam) was added to recombinant 15 μ M HIS-SUMO-TDP-43, myo-granule, or myo-granule plus recombinant 15 μ M HIS-SUMO-TDP-43. Surface denaturation was performed with continuous shaking at 37°C with Thioflavin-T incorporation monitored every 10 minutes at 495 nm after excitation at 438 nm on a Gen5 microplate reader (BioTek). Raw fluorescence values obtained for experimental conditions were background subtracted and plotted as a function of time. The resulting curves were fit to following single exponential rate equation (Equation 1) using Kaleidagraph (Synergy Software).

$$\text{Equation 1: } -A * e^{(-k_{obs} * t)} + B$$

where A is amplitude, k_{obs} (min^{-1}) is single exponential rate constant, and B represents maximal amount of fluorescence detected (Smith and Jackman, 2011).

Accession Numbers

Enhanced CLIP data has been deposited in the GEO

(<https://www.ncbi.nlm.nih.gov/geo/query/acc.cgi?acc=GSE106553>) under accession number GEO: GSE106553.

Chapter 4:

hnRNPA2B1 in Normal Skeletal Muscle Formation and Regeneration

Summary

RNA binding proteins regulate many aspects of RNA metabolism and mutations in these proteins cause numerous degenerative diseases. The nuclear RNA-binding protein, heterogeneous nuclear ribonucleoprotein A2B1 (hnRNPA2B1) is mutated in the degenerative disease, multisystem proteinopathy (MSP). Mutations cause abnormal aggregation and cytoplasmic localization of hnRNPA2B1 in skeletal muscle cells (myofibers) of patients with MSP. The cytoplasmic aggregates of hnRNPA2B1 are thought to be toxic and impair the normal functions of hnRNPA2B1. However, the role of hnRNPA2B1 in healthy skeletal muscle is unknown. Here we show hnRNPA2B1 is upregulated during normal skeletal muscle regeneration and binds primarily to the 3' UTR of a distinct class of RNAs that regulate splicing in skeletal muscle. Knockout of hnRNPA2B1 does not alter the proliferation of muscle progenitor cells (myoblasts) but delays skeletal muscle differentiation and muscle formation. These observations suggest an unexplored role for hnRNPA2B1 as a regulator of splicing during skeletal muscle differentiation. Thus, the loss of RNA splicing regulation could be a driver for muscle degeneration in diseases where hnRNPA2B1 is mutated or dysfunctional.

Introduction

Heterogeneous nuclear ribonucleoprotein A2B1 (hnRNPA2B1) is a multifunctional, nuclear RNA-binding protein that plays a variety of roles in RNA metabolism such as RNA splicing, polyadenylation, translation and export (Glisovic et al., 2008; Keene, 2007; Martinez et al., 2016; Nguyen et al., 2018). Mutations in hnRNPA2B1 result in cytoplasmic hnRNPA2B1 aggregates in the neurons and skeletal muscle myofibers of patients with multisystem proteinopathy (MSP) (Kim et al., 2013; Li et al., 2016). Additionally, cytoplasmic hnRNPA2B1 aggregates are found in patients with amyotrophic lateral sclerosis (ALS) (Martinez et al., 2016), limb- girdle muscular dystrophy (LGMD) (Bengoechea et al., 2015) and oculopharyngeal muscular dystrophy (OPMD) (Fan and Rouleau, 2003). The mutations of hnRNPA2B1 found in neuromuscular diseases occur in the C-terminal low complexity domain (LCD) and increase the aggregation potential of hnRNPA2B1. The cytoplasmic aggregates of hnRNPA2B1 are thought to be a key driver of neuromuscular degeneration (Kim et al., 2013).

The relationship between pathological hnRNPA2B1 aggregates and the normal function of hnRNPA2B1 remains poorly understood. Characterization of hnRNPA2B1 in neurons led to the hypothesis that mutations in the LCD caused cytosolic mislocalization and aggregation of hnRNPA2B1. This has a two-pronged effect on cells: (1) it impairs the normal nuclear function of hnRNPA2B1 to interact with RNA and (2) it increases the aggregation of hnRNPA2B1 resulting in the formation of toxic amyloid-like aggregates (Kim et al., 2013; Martinez et al., 2016). While these studies have

broadened our understanding of hnRNPA2B1 RNA targets and the role of hnRNPA2B1 in neurons, the functional role of wild-type hnRNPA2B1 and a detailed description of the RNA-binding targets of hnRNPA2B1 in skeletal muscle is lacking.

A paralogous RNA-binding protein to hnRNPA2B1, hnRNPA1, is a crucial protein for RNA splicing and is found in pathological aggregates of muscle diseases (Li et al., 2016). Knockout of hnRNPA1 causes embryonic lethality due to severe muscle defects. However, hnRNPA2B1 did not compensate for the loss of hnRNPA1, suggesting these two proteins may have distinct functions in skeletal muscle (Liu et al., 2017b). Here, we explored the basic properties of hnRNPA2B1 in wild type skeletal muscle. We find hnRNPA2B1 is a highly expressed RNA-binding protein in skeletal muscle formation, which binds to a unique subset of RNA transcripts linked to the regulation of splicing. Loss of hnRNPA2B1 impairs skeletal muscle differentiation and formation. Thus, the loss of RNA splicing regulation could be a driver for the muscle degeneration in diseases where hnRNPA2B1 is mutated or dysfunctional.

Results

Cytoplasmic localization and aggregation of hnRNPA2B1, similar to related RBPs such as TDP-43, is a pathological hallmark of several degenerative skeletal muscle diseases (Bengoechea et al., 2015; Fan and Rouleau, 2003; Kim et al., 2013). We hypothesized that analogous to TDP-43, which localizes to the cytosol during normal formation (Vogler et al., 2018), hnRNPA2B1 redistribution to the cytosol may be a part of normal physiological process during muscle regeneration. To test this, we examined

the subcellular distribution of hnRNPA2B1 in uninjured tibialis anterior muscle and tibialis anterior muscle that was chemically injured with barium chloride (BaCl₂) and allowed to regenerate (Caldwell et al., 1990). In uninjured tibialis anterior muscle, hnRNPA2B1 is localized to the nucleus, similar to TDP-43 (Figure 4.1a). At five days post injury, hnRNPA2B1 remains localized to the nucleus and is not found in the cytoplasm like TDP-43 (Figure 4.1b). Although the localization does not change, expression of hnRNPA2B1 increases in both Pax7+ muscle progenitor cells and myonuclei during regeneration (Figure 4.1a, b). Then as skeletal muscle repairs, hnRNPA2B1 levels decrease and return to near uninjured levels (Figure 4.1a-d). This specific increase in protein levels during muscle regeneration suggests that hnRNPA2B1 is important for the formation of new muscle. However, the localization of hnRNPA2B1 in muscle regeneration appears to differ from TDP-43.

The observation that hnRNPA2B1 increases during muscle regeneration suggested that hnRNPA2B1 has a role in regulating RNAs during muscle formation. However, it is unknown which RNAs hnRNPA2B1 binds during skeletal muscle formation. Thus, we characterized the RNA-binding targets of hnRNPA2B1 in myoblasts and multinucleated myotubes using enhanced CLIP (eCLIP) (Figure 4.2a) (Van Nostrand et al., 2016). hnRNPA2B1 eCLIP peaks were highly correlated between biological replicates and identified known hnRNPA2B1 mRNA targets including hnRNPA2B1's own 3' UTR (Figure 4.2b-d). Similar to reports in neurons (Martinez et al., 2016), hnRNPA2B1 peaks were enriched in the 3' UTR of RNAs in both myoblasts and myotubes (Figure 4.2e).

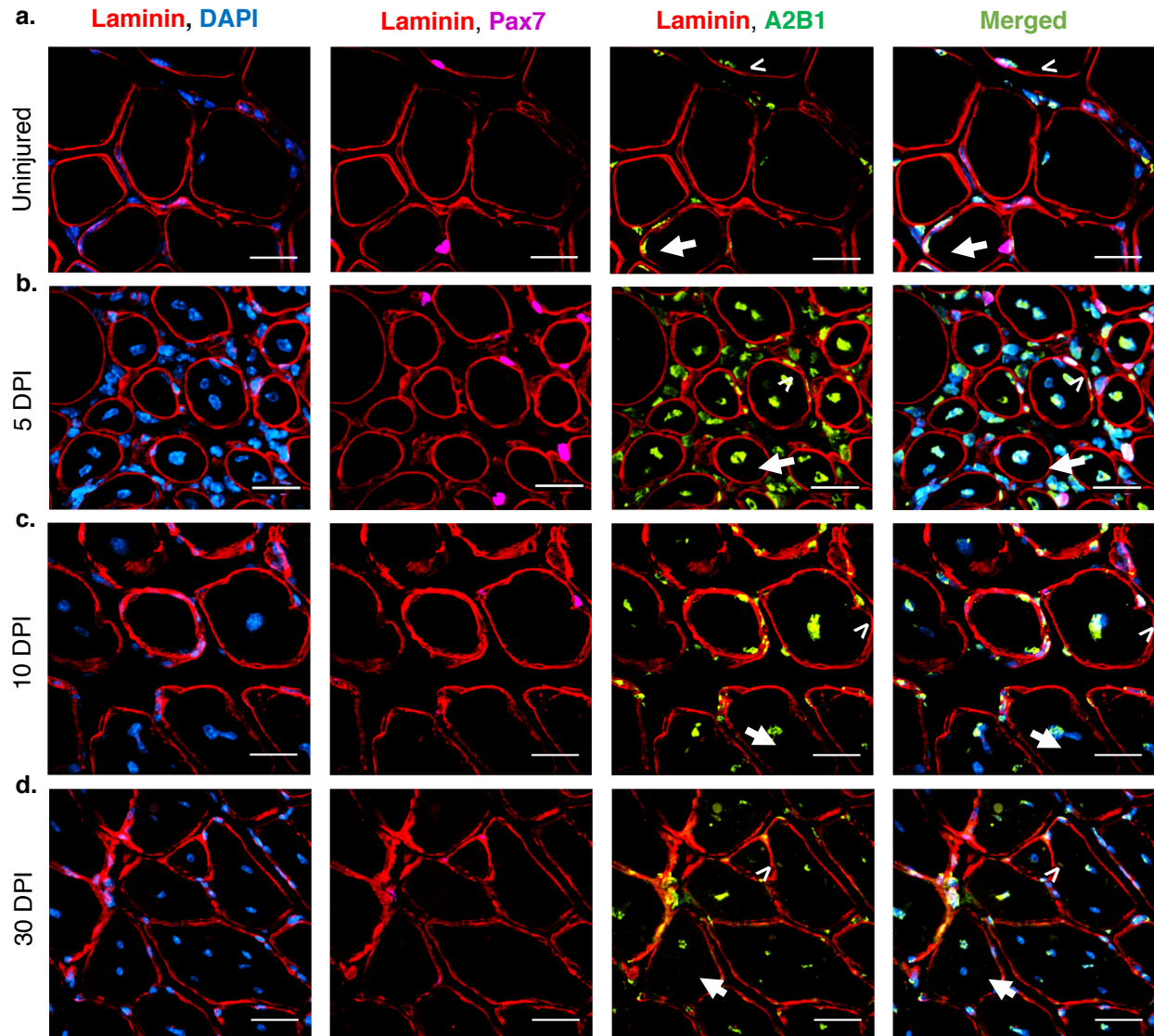


Figure 4.1. Localization of hnRNPA2B1 during skeletal muscle regeneration.

(a-d) Immunoreactivity for hnRNPA2B1 during in skeletal muscle in vivo. **(a)** hnRNPA2B1 localization in the myonucleus (arrow) and MuSC (arrowhead) in uninjured muscle. **(b)** hnRNPA2B1 localization in the myonucleus (arrow) and MuSC (arrowhead) in 5 days post injury (DPI) muscle. **(c)** hnRNPA2B1 localization in the myonucleus (arrow) and MuSC (arrowhead) in 10 DPI muscle. **(d)** hnRNPA2B1 localization in the myonucleus (arrow) and MuSC (arrowhead) in 30 DPI muscle. All images were scaled above background. Nuclei counterstained with DAPI. Scale bars are 25 μm .

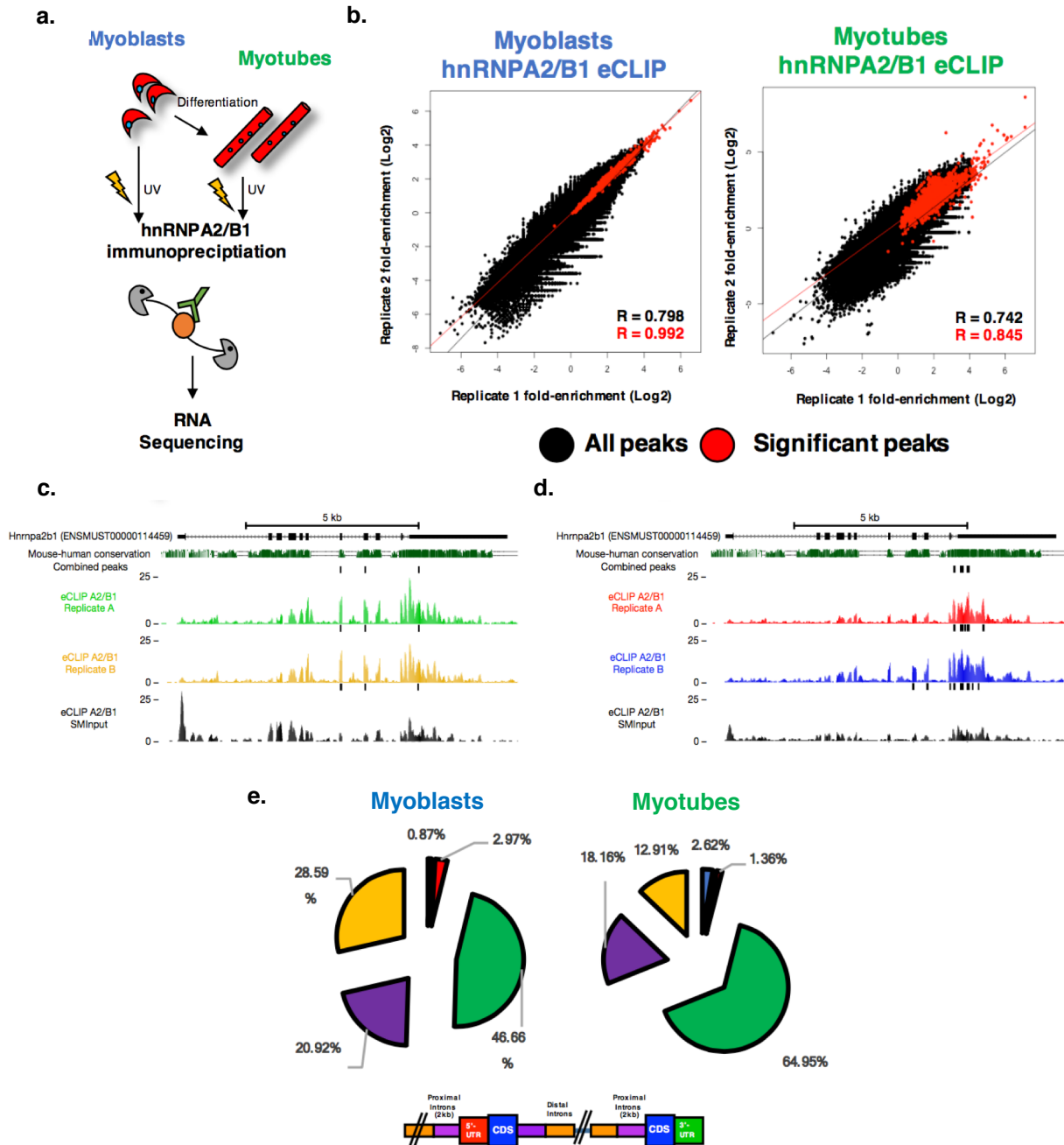


Figure 4.2. Enhanced CLIP reveals hnRNP A2/B1 interacts primarily with the 3' UTR of RNA in skeletal muscle.

(a) Schematic for hnRNP A2/B1 enhanced CLIP in during skeletal muscle differentiation. (b) Myoblast and myotube eCLIP are highly correlated for significant peaks (defined as significantly enriched over size matched input, $p < 10^{-8}$). (c) and (d) Representative gene tracks in both myoblasts and myotubes for hnRNP A2/B1 reveals hnRNP A2/B1 interacts with its own RNA transcript through binding to its own 3'UTR. (e) Location of peaks in hnRNP A2/B1 RNA targets reveals a strong bias towards 3'UTR interactions

TDP-43 and hnRNPA2B1 are similar RNA-binding proteins that are both associated with skeletal muscle diseases, but seem to have different localizations during skeletal muscle formation. These differences led us to ask whether TDP-43 and hnRNPA2B1 bind to the same or different RNA transcripts during muscle formation. While several RNA targets are shared between hnRNPA2B1 and TDP-43, the majority of target transcripts are distinct between these two RBPs suggesting they may be regulating distinct classes of RNAs during myogenesis (Figure 4.3a, b). TDP-43 interacts with transcripts that encode sarcomeric proteins (Vogler et al., 2018), whereas hnRNPA2B1 interacts with RNAs related to alternative splicing and splice site selection (Table 4.1). Together, the localization and RNA interaction of hnRNPA2B1 suggests it regulates splicing in the nucleus of myogenic cells during muscle formation.

To further examine the effects of hnRNPA2B1 in skeletal muscle formation we created an hnRNPA2B1 knockout (KO) C2C12 muscle cell line using CRISPR-Cas9. Three C2C12 myoblast clones were stably transfected with one or two hnRNPA2B1 specific guide RNAs (Figure 4.4a). Control cells were stably transfected with scrambled guide RNA (Figure 4.4a). Knockout efficiency was highly variable between hnRNPA2B1 sgRNAs; however, hnRNPA2B1sgRNA #1 effectively reduced hnRNPA2B1 protein levels to nearly undetectable levels compared to cells transfected with a scrambled control (Figure 4.4b). Three separate clones were isolated from cells transfected with hnRNPA2B1sgRNA #1 and were immunostained using a monoclonal and a polyclonal antibody against hnRNPA2B1 protein. Although both antibodies clearly showed reduced protein levels by Western blot, only the monoclonal hnRNPA2B1 antibody detected a

GO biological process complete	Fold Enrichment	P value
alternative mRNA splicing, via spliceosome	55.62	8.36E-03
mRNA splicing, via spliceosome	11.53	4.72E-03
mRNA processing	6.84	5.79E-03
mRNA metabolic process	6.23	1.50E-03
RNA splicing, via transesterification reactions with bulged adenosine as nucleophile	11.53	4.72E-03
RNA splicing, via transesterification reactions	11.46	4.93E-03
RNA splicing	8.53	6.68E-04
mRNA splice site selection	41.11	2.75E-02
cellular component organization	2.2	4.49E-04
cellular component organization or biogenesis	2.12	1.34E-03
cellular component assembly	2.81	3.76E-02
regulation of alternative mRNA splicing, via spliceosome	33.77	4.01E-03
regulation of mRNA splicing, via spliceosome	19.17	7.31E-03
regulation of RNA splicing	17.35	2.17E-04
muscle cell differentiation	7.79	2.24E-02
muscle structure development	5.64	3.67E-02
supramolecular fiber organization	6.99	4.71E-03
actin cytoskeleton organization	6.99	1.39E-03
cytoskeleton organization	4.33	6.83E-03
actin filament-based process	6.18	5.07E-03

Table 4.1. GO term analysis of RNAs that interact with hnRNPA2B1 in myotubes

Analysis of RNA transcripts identified by eCLIP on hnRNPA2B1 from n = 2 biological replicates.

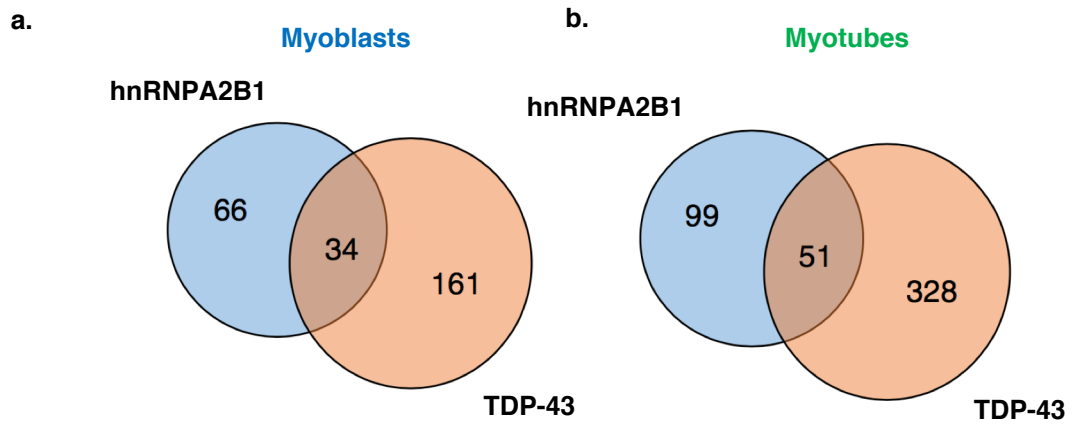


Figure 4.3. Enhanced CLIP reveals hnRNPA2B1 and TDP-43 mainly interact with distinct RNAs in muscle.

(a) Overlap of RNA targets in myoblasts between TDP-43 and hnRNPA2B1. **(b)** Overlap of RNA targets in myotubes between TDP-43 and hnRNPA2B1.

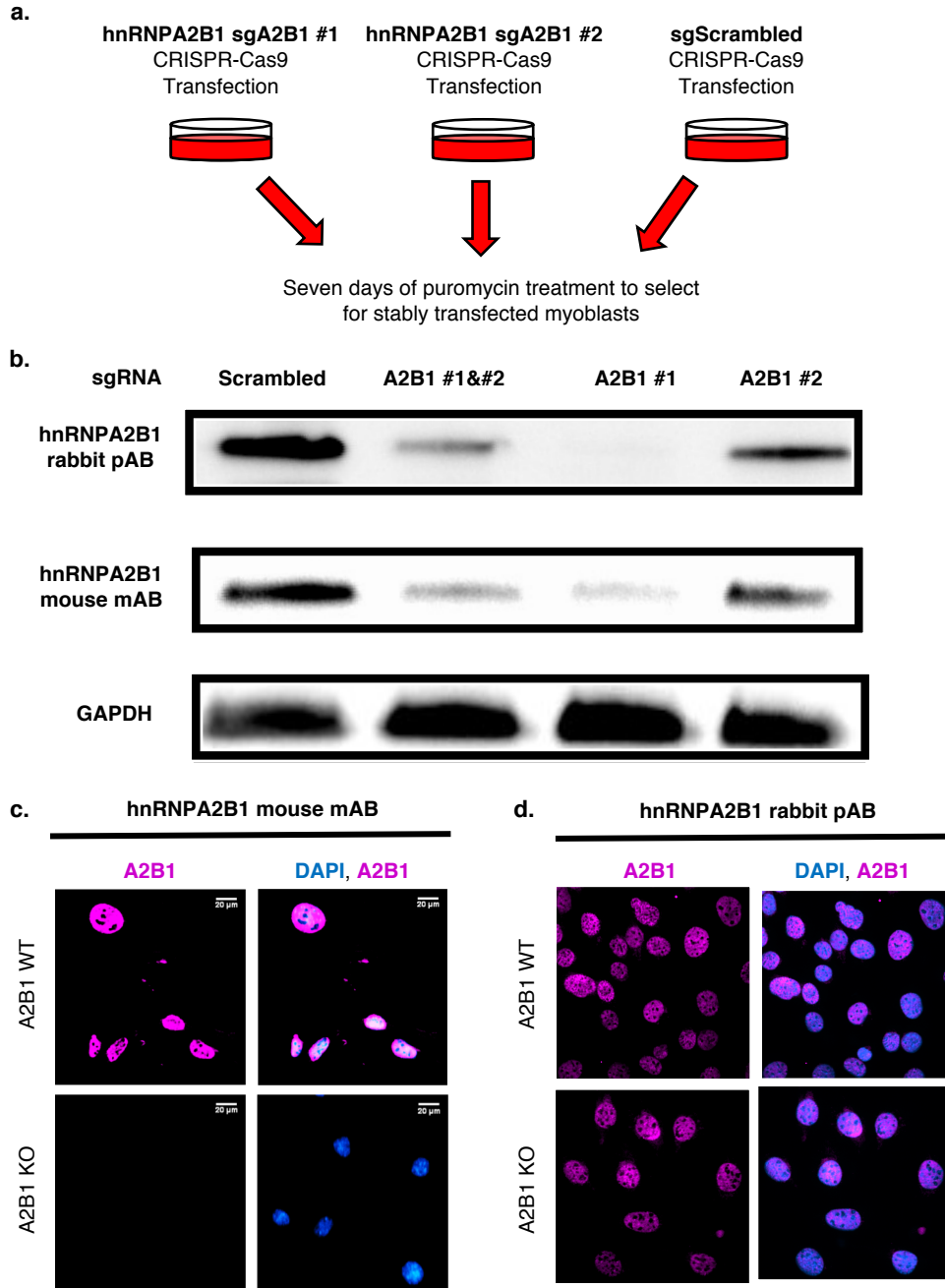


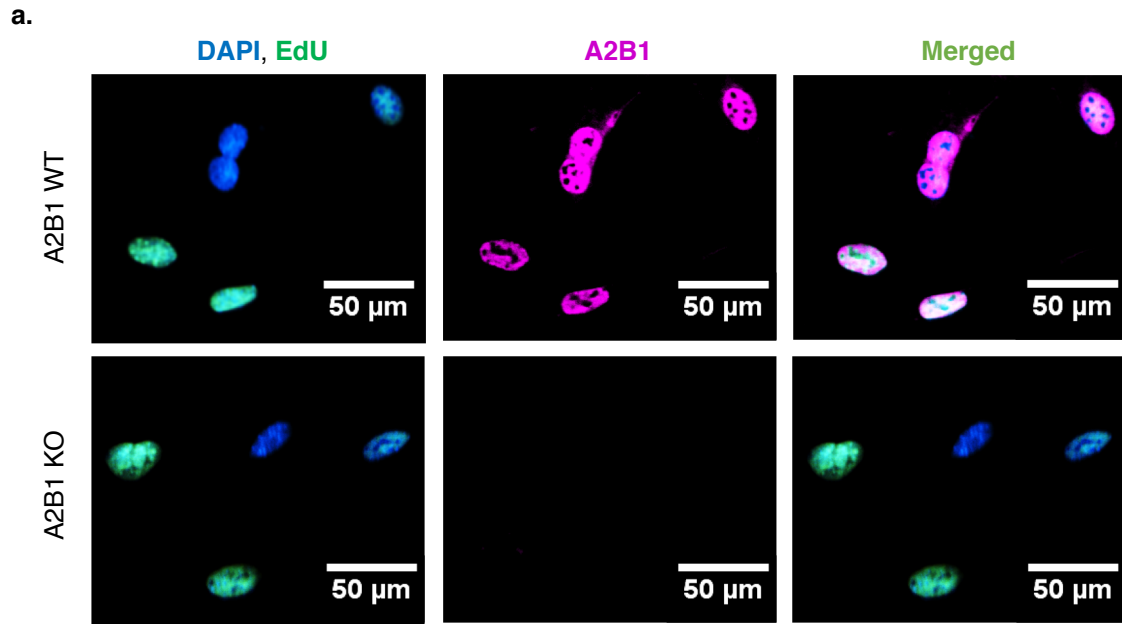
Figure 4.4. Knockout of hnRNPA2B1 in C2C12 myoblasts.

(a) Schematic for hnRNPA2B1 knockout in C2C12 myoblasts using CRISPR-Cas9. Two distinct guides targeting the hnRNPA2B1 locus were used. A scrambled guide RNA was used as a control. **(b)** Western blot analysis of hnRNPA2B1 protein in KO and scrambled control myoblasts. Two separate antibodies were used to probe for hnRNPA2B1: a rabbit polyclonal antibody (pAB) and a mouse monoclonal antibody (mAB). GAPDH served as a loading control **c.** hnRNPA2B1 immunoreactivity using the rabbit polyclonal antibody in KO and control cells **d.** hnRNPA2B1 immunoreactivity using the mouse monoclonal antibody in KO and control cells. Nuclei counterstained with DAPI. Scale bars are 20 μm .

knockout of protein by immunofluorescence (Figure 4.4c). The polyclonal hnRNPA2B1 antibody recognized a nuclear antigen regardless of hnRNPA2B1 knockout (Figure 4.4d). Thus, the specificity of the polyclonal antibody used in the current (Figure 4.2), and previously published (Nguyen et al., 2018), eCLIP data sets, is low.

We next asked, what is the functional effect of hnRNPA2B1 knockout in skeletal muscle cells? As hnRNPA2B1 knockdown is linked to decreased proliferation in cancer cells (Barceló et al., 2014; Golan-Gerstl et al., 2011), we assessed proliferation in hnRNPA2B1 knockout and control myoblasts. We treated cells with 5-ethynyl-2'-deoxyuridine (EdU) to mark dividing cells (Figure 4.5a). Surprisingly, the absence of hnRNPA2B1 had no significant effect on myoblast proliferation (Figure 4.5b). Thus, in muscle progenitor cells, hnRNPA2B1 is dispensable for cell proliferation.

Because hnRNPA2B1 is highly expressed during the early phase of muscle regeneration we next examined how loss of hnRNPA2B1 affects myoblast differentiation and muscle formation. After differentiation for 48 hours, hnRNPA2B1 knockout cells failed to make large multinucleated myotubes (Figure 4.6a). The hnRNPA2B1 knockout cells formed smaller myotubes containing fewer nuclei than control myotubes (Figure 4.6b, c). This appeared to be a defect in differentiation rather than fusion as hnRNPA2B1 knockout cells had delayed expression of the myosin heavy chain (MyHC) and the myogenic transcription factor myogenin (MyoG) (Figure 4.6d, e). Therefore, absence of hnRNPA2B1 impairs myoblast differentiation resulting in impaired skeletal muscle formation.



b. **Proliferation of C2C12 Myoblasts**

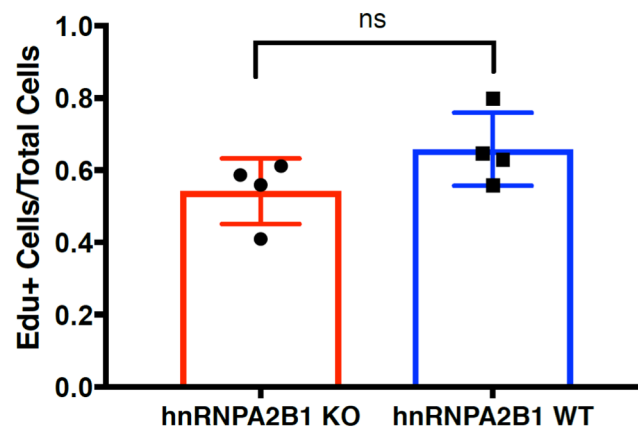


Figure 4.5. Knockout of hnRNPA2B1 in C2C12 myoblasts does not affect proliferation.

(a) Representative images of hnRNPA2B1 knockout (KO) and control (WT) myoblasts treated with EdU for 3 hours before cells were fixed. (b) Quantification of C2C12 myoblasts in (a) reveals non-significance (n.s.) between hnRNPA2B1 KO and scrambled control myoblasts. Scale bars are 50 μm.

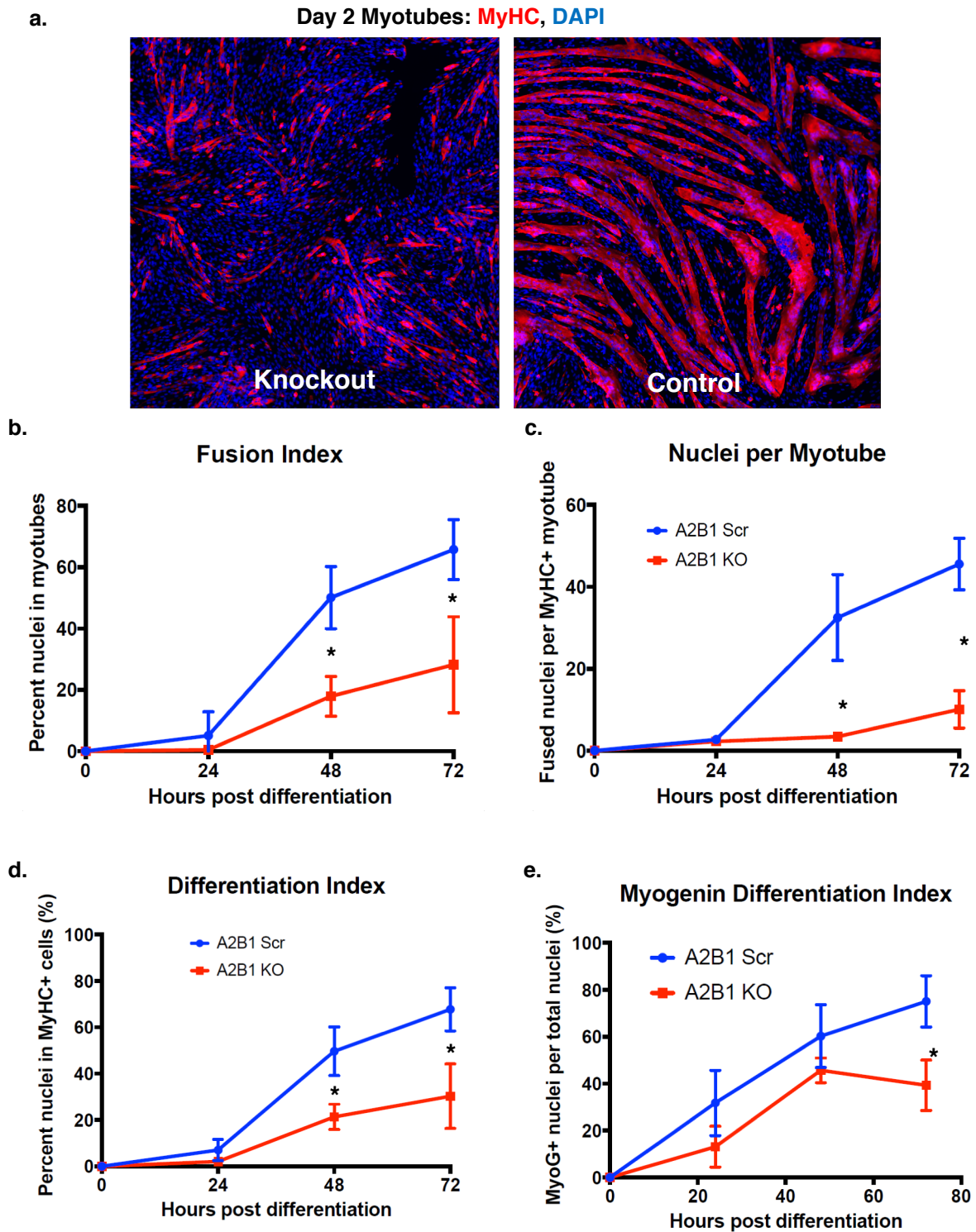


Figure 4.6. See next page for caption.

Figure 4.6. Knockout of hnRNPA2B1 inhibits myogenic differentiation.

(a) Representative images of hnRNPA2B1 knockout and control cells after 48 hours of differentiation. Myotubes stained with myosin heavy chain (MyHC) and nuclei counterstained with DAPI. **(b)** 72 hour time-course shows a delay in the fusion index in hnRNPA2B1 KO cells. **(c)** 72 hour time-course shows a delay in the number of nuclei in myosin heavy chain (MHC)-expressing cells in hnRNPA2B1 KO cells. **(d)** 72 hour time-course shows a delay in the number of cells expressing MyHC in hnRNPA2B1 KO cells. **(e)** 72 hour time-course shows a delay in the number of cells expressing myogenin (MyoG) in hnRNPA2B1 KO cells. Controls are sgScrambled C2C12 cells.

Discussion

The role of hnRNPA2B1 in regulating skeletal muscle differentiation

Here we show, hnRNPA2B1 is upregulated during normal skeletal muscle regeneration and binds primarily to the 3' UTR of a distinct class of RNAs that regulate splicing in skeletal muscle. Knockout of hnRNPA2B1 does not alter the proliferation of muscle progenitor cells (myoblasts) but delays skeletal muscle differentiation and muscle formation. While this study unveils a function of hnRNPA2B1 in normal skeletal muscle, many questions still remain. Chiefly, how the interaction between hnRNPA2B1 and RNAs that encode splicing factors, alters muscle differentiation and formation. It will be important to understand if the failure of hnRNPA2B1 to bind these RNA targets will reduce expression levels or protein levels. If knockout of hnRNPA2B1 reduces the expression or translation of key splicing regulators during muscle differentiation, this could explain how hnRNPA2B1 knockout impairs muscle differentiation and formation.

Many myogenic genes are alternatively spliced during skeletal muscle differentiation and formation (Bland et al., 2010). In fact, the MEF2 family of transcription factors are known to be alternatively spliced during muscle differentiation which drives the expression specific myogenic transcripts important for differentiation (Nakka et al., 2018). Interestingly, our data shows that hnRNPA2B1 interacts with the MEF2a transcript in myotubes. However, hnRNPA2B1 may work more globally by regulating the transcripts of proteins such as DDX5 (another myotube transcript with a hnRNPA2B1 peak in our data), which functions as a splicing-enhancer during terminal differentiation (Dardenne et al., 2014). Continued efforts to explore and validate how

hnRNPA2B1 regulates RNA targets of splicing will engender a higher degree of understanding for this mechanism.

Divergent roles of hnRNPA2B1 and TDP-43 in skeletal muscle

TDP-43 and hnRNPA2B1 appear to be related RNA-binding proteins in that they have similar structures, function as regulators of RNA splicing and they both aggregate in degenerative diseases (Bengoechea et al., 2015; Kim et al., 2013; Kuo et al., 2009; Martinez et al., 2016; Neumann et al., 2006; Wu et al., 2018). However, in skeletal muscle formation, these two RNA-binding proteins appear to have distinct roles. TDP-43 interreacts with large transcripts that encode sarcomeric proteins, where hnRNPA2B1 interreacts with transcripts implicated in splicing. TDP-43 moves into the cytoplasm during muscle regeneration and forms myo-granules with large RNAs, whereas hnRNPA2B1 remains in the nucleus during muscle regeneration and is not associated with myo-granules (Vogler et al., 2018). The knockout of TDP-43 causes cell-cycle and cell death of myoblasts, whereas the knockout of hnRNPA2B1 has no effect on the proliferation of myoblasts. In the future, it will be important to understand how these two seemingly similar RNA-binding proteins exact such differences on skeletal muscle cells.

The role of hnRNPA2B1 function in disease

Our experiments on hnRNPA2B1 underscore several broader principles relating to skeletal muscle formation, maintenance, and neuromuscular disease. First, cytosolic

localization and aggregation is believed to be a key driver of disease in several degenerative diseases plaguing the central nervous system and skeletal muscle (Bengoechea et al., 2015; Kim et al., 2013; Neumann et al., 2006; Wehl et al., 2008). While classically this localization is defined as pathogenic, our recent observations with TDP-43 suggest that the redistribution of this protein in disease is likely a consequence of a heightened requirement for normal cellular repair (Vogler et al., 2018). As such, we suggested additional RNA-binding proteins, which have been classically described as mislocalized, may in fact be reflecting a normal cellular repair program upregulated in disease by the increased need for regeneration and repair. However, this study shows that not all RNA-binding proteins follow this cytosolic localization pattern in normal regeneration. hnRNPA2B1 remains in the nucleus and interacts with the transcripts of nuclear proteins in muscle formation. Thus, the localization and function of other RNA-binding proteins associated with cytoplasmic localization in degenerative disease (e.g. TIA1, Martin-3, hnRNPA1, hnRNPD) warrant case-by-case examinations during skeletal muscle regeneration.

Since hnRNPA2B1 remains localized to the nucleus in healthy skeletal muscle, then its cytoplasmic localization in disease is likely altering its normal functions in skeletal muscle (Kim et al., 2013). Therefore, cytoplasmic localization of hnRNPA2B1 in disease could be disrupting skeletal muscle differentiation and splicing of myogenic transcripts. Over time, this could have degenerative effects on skeletal muscle. It will be important to examine the differentiation potential and RNA splicing in skeletal muscle cells from patients with MSP as well as other disease where cytoplasmic hnRNPA2B1 is

observed. Together, this may uncover a new therapeutic strategy for treating skeletal muscle conditions with cytoplasmic hnRNPA2B1.

Methods

Mice

Mice were bred and housed according to National Institutes of Health (NIH) guidelines for the ethical treatment of animals in a pathogen-free facility at the University of Colorado at Boulder. The University of Colorado Institutional Animal Care and Use Committee (IACUC) approved all animal protocols and procedures. Wild-type mice were C57Bl/6 (Jackson Labs, ME, USA). Tibialis anterior (TA) muscles were isolated from 3-6-month-old male and female wild-type mice. Control mice were age and sex matched from the mice and crosses described above.

Mouse Injuries

Mice at 3-6 months old were anesthetized with isoflurane and the left TA muscle was injected with 50 μ L of 1.2% BaCl₂ and then the injured and contralateral TA muscles were harvested at the indicated time points.

Immunofluorescence staining of tissue sections

TA muscles were dissected, fixed on ice for 2hrs with 4% paraformaldehyde, and then transferred to PBS with 30% sucrose at 4°C overnight. Muscle was mounted in O.C.T. (Tissue-Tek®) and cryo-sectioning was performed on a Leica cryostat to

generate 10µm thick sections. Tissues and sections were stored at -80°C until staining. Tissue sections were post-fixed in 4% paraformaldehyde for 10 minutes at room temperature (RT) and washed three times for 5 min in PBS. Immunostaining with anti-Pax7, anti-Laminin and anti-hnRNPA2B1 antibodies required heat-induced epitope retrieval where post-fixed slides were placed in citrate buffer, pH 6.0, and subjected to 6 min of high pressure-cooking in a Cuisinart model CPC-600 pressure cooker. For immunostaining, tissue sections were permeabilized with 0.25% Triton-X100 (Sigma) in PBS containing 2% bovine serum albumin (Sigma) for 60 min at RT. Incubation with primary antibody occurred at 4°C overnight followed by incubation with secondary antibody at room temperature (RT) for 1hr. Primary antibodies included mouse anti-Pax7 (Developmental Studies Hybridoma Bank, University of Iowa, USA) at 1:750, rabbit anti-laminin (Sigma-Aldrich) at 1:200, rabbit anti- hnRNPA2B1 (Abcam) at 1:200 and mouse anti-hnRNPA2B1 (Abcam) at 1:200. Alexa secondary antibodies (Molecular Probes) were used at a 1:1000 dilution. Sections were incubated with 1 µg/mL DAPI for 10 min at room temperature then mounted in Mowiol supplemented with DABCO (Sigma-Aldrich) or ProLong Gold (Thermo) as an anti-fade agent.

Microscopy and image analyses

Images were captured on a Nikon inverted spinning disk confocal microscope. Objectives used on the Nikon were: 10x/0.45NA Plan Apo, 20x/0.75NA Plan Apo and 40x/0.95 Plan Apo. Confocal stacks were projected as maximum intensity images for

each channel and merged into a single image. Brightness and contrast were adjusted for the entire image as necessary. Images were processed using Fiji ImageJ.

hnRNPA2B1 eCLIP-seq

C2C12 myoblasts were seeded at 6×10^6 cells per 15 cm plate, grown 24hrs at 37°C, 5% CO₂ and either harvested (undifferentiated myoblasts) or differentiated in differentiation media for 2 days. hnRNPA2B1 enhanced CLIP (eCLIP) was performed according to established protocols (Van Nostrand et al., 2016). In brief, hnRNPA2B1-RNA interactions were stabilized with UV crosslinking (254 nm, 150mJ/cm²). Cell pellets were collected and snap frozen in liquid N₂. Cells were thawed, lysed in eCLIP lysis buffer (50 mM Tris-HCl pH 7.4, 100 mM NaCl, 1% NP-40, 0.1% SDS, 0.5% sodium deoxycholate, and 1x protease inhibitor) and sonicated (Bioruptor). Lysate was RNase I (Ambion, 1:25) treated to fragment RNA. Protein-RNA complexes were immunoprecipitated using indicated antibody. One size-matched input (SMInput) library was generated per biological replicate using an identical procedure without immunoprecipitation. Stringent washes were performed as described, RNA was dephosphylated (FastAP, Fermentas), T4 PNK (NEB), and a 3' end RNA adaptor was ligated with T4 RNA ligase (NEB). Protein-RNA complexes were resolved on an SDS-PAGE gel, transferred to nitrocellulose membranes, and RNA was extracted from membrane. After RNA precipitation, RNA was reverse transcribed using SuperScript IV (Thermo Fisher Scientific), free primer was removed, and a 3' DNA adaptor was ligated onto cDNA products with T4 RNA ligase (NEB). Libraries were PCR amplified and dual-

indexed (Illumina TruSeq HT). Pair-end sequencing was performed on Illumina NextSeq sequencer.

Cell culture.

C2C12 cells: Immortalized murine myoblasts (American Type Culture Collection) were maintained on uncoated standard tissue culture plastic or gelatin-coated coverslips at 37°C with 5% CO₂ in DMEM with 20% fetal bovine serum and 1% penicillin/streptavidin. To promote myoblast fusion when the C2C12 cells reached confluence, they were switched to 5% horse serum, 1% penicillin/streptavidin and 1% Insulin-Transferrin-Selenium in DMEM.

hnRNPA2B1 CRISPR-Cas9 knockout and EdU incorporation

CRISPR-Cas9 knockout was performed in C2C12 myoblasts. Single guide RNA (sgRNA) against hnRNPA2B1 were designed using (crispr.mit.edu) and cloned into pSpCas9(BB)-2A-Puro (PX459). C2C12 myoblasts were transfected with JetPrime using standard protocols. Myoblasts were selected with puromycin (1 µg/mL) for one week. C2C12 myoblasts were incubated with 10µM 5-ethynyl-2'-deoxyuridine (EdU – Life Technologies) for two hours. Cells were washed, fixed and stained. For analysis that included EdU detection, EdU staining was completed prior to antibody staining using the Click-iT EdU Alexa fluor 488 detection kit (Molecular Probes) following manufacturer protocols.

Biochemical characterization of hnRNPA2B1 during myogenesis

In brief, C2C12 myoblasts and myotubes were lysed with RIPA buffer (50 mM Tris pH 7.5, 1% NP-40, 0.5% sodium deoxycholate, 0.05% SDS, 1 mM EDTA, 150 mM NaCl). Protein concentrations were determined using BCA assay (Thermo Scientific) according to standard procedures. Lysates were centrifuged at 18,000 x g for 20 minutes at 4°C. Western blotting was performed following resolution of protein lysates on SDS-PAGE.

Immunofluorescence Staining of Cultured Cells

C2C12 cells were washed with PBS in a laminar flow hood and fixed with 4% Paraformaldehyde for 10 min at room temperature in a chemical hood. Immunostaining for hnRNPA2B1 requires heat-induced epitope retrieval where post-fixed cells were placed in citrate buffer, pH 6.0, and subjected to 6 min of steaming. Cells were then permeabilized with 0.25% Triton-X100 in PBS containing 2% bovine serum albumin (Sigma) for 1 hour at RT. Incubation with primary antibody occurred at 4°C overnight followed by incubation with secondary antibody at room temperature for 1hr. Primary antibodies included mouse anti-hnRNPA2B1 (Abcam) at 1:200, rabbit anti-hnRNPA2B1 (Abcam) at 1:200, mouse anti-MyoG (Developmental Studies Hybridoma Bank, University of Iowa, USA) at 1:270, and a mouse anti-MHC (MF-20, Developmental Studies Hybridoma Bank, University of Iowa, USA) at 1:1. Alexa secondary antibodies (Molecular Probes) were used at a 1:1000 dilution. All antibodies were diluted in with 0.125% Triton-X100 in PBS containing 2% bovine serum albumin. Cells were incubated

with 1 $\mu\text{g}/\text{mL}$ DAPI for 10 min at room temperature then mounted in Mowiol supplemented with DABCO (Sigma-Aldrich) as an anti-fade agent.

Chapter 5:

Discussion

Although the basic cellular framework of muscle regeneration is known (summarized in Chapter 1), many of the molecular mechanisms that drive this process are not well understood. The principal theme of my thesis work was to explore molecular mechanisms that control normal muscle regeneration. I then applied what I learned in normal regeneration to understand pathophysiology in disease. I first examined how FGF signaling controls MuSCs numbers during normal muscle regeneration and then showed how increasing FGF signaling in MuSCs in aged mice affects age-related muscle degeneration. Next, I examined how the RNA-binding proteins TDP-43 and hnRNPA2B1 regulate RNAs during normal muscle regeneration. Since these two RNA-binding proteins are implicated or mutated in degenerative neuromuscular diseases, I then studied the links between their role in normal regeneration and how they contribute to disease. Together, this work underscores the importance of studying the mechanisms of normal physiology to understand disease pathophysiology; however, many questions about the mechanisms of normal muscle regeneration still remain.

Understanding RNA regulation in skeletal muscle is an active area of research (Anderson et al., 2016; Apponi et al., 2011; Chenette et al., 2016; Pedrotti et al., 2015); however, much of this work does not examine RNA regulation during muscle regeneration. The few studies that examine RNA regulation during muscle regeneration have focused on RNAs in MuSCs (Hausburg et al., 2015; Morrée et al., 2017). These studies examine how RNA-binding proteins regulate the MyoD transcript during MuSC activation. As this is a very early event in muscle regeneration, many questions still

remain regarding RNA regulation in skeletal muscle regeneration. Chiefly, when a new myofiber is constructed during regeneration, many large RNA must be transcribed, processed, transported and translated. These RNAs are some of the largest in the human body and encode structural proteins, such as those in the sarcomere and dystroglycan complex, that are critical for the integrity and functionality of skeletal muscle. Without a highly organized means of RNA regulation, these RNAs cannot be made into proteins to rebuild functional muscle during regeneration.

During muscle regeneration there is an increase in the translation of large RNAs that encode sarcomeric proteins, like titin, nebulin and myosin heavy chain. Many RNA-binding proteins interact with these RNA transcripts as they are being transcribed. The RNA-binding proteins help process the RNA by regulating splicing, polyadenylation and 5' capping (Apponi et al., 2011; Pedrotti et al., 2015). The failure of RNA-binding proteins to regulate these processes results in global RNA misregulation and poor muscle formation. Here we show, hnRNPA2B1 is upregulated during normal skeletal muscle regeneration and binds primarily to the 3' UTR of a distinct class of RNAs that regulate splicing in skeletal muscle. Knockout of hnRNPA2B1 does not alter the proliferation of myoblasts but delays skeletal muscle differentiation and muscle formation. We do not know the mechanisms for how hnRNPA2B1 knockout causes impaired muscle formation, but global splicing changes likely contribute. Profiling the transcriptome of hnRNPA2B1 knockout muscle cells will be an important next step. It will also be important to examine how similar RNA-binding proteins, such as hnRNPA1

(Liu et al., 2017b), affect splicing or compensate for the loss of hnRNPA2B1 in skeletal muscle.

After RNAs are transcribed and processed into an mRNA, they must be transported from the nucleus to the cytoplasm, where the mRNA is translated into a protein. These mRNAs form ribonucleoprotein (RNPs) assemblies with RNA-binding proteins as they are transported out of the nucleus. RNP assemblies are important for mRNA stability and for the prevention of aberrant RNA-RNA interactions. During muscle regeneration, many large mRNAs encoding sarcomeric proteins must be packaged and transported to the cytoplasm. How skeletal muscle cells regulate these large mRNAs during regeneration is not well studied. In Chapter 3, I discuss our discovery that the RNA-binding protein TDP-43 and RNAs that encode sarcomeric proteins, come together to form amyloid-like, RNP assemblies, called myo-granules, during muscle regeneration (Vogler et al., 2018). There is still much to be learned about myo-granules but how they regulate the stability and transport of large mRNAs is a particularly open area of research.

Myo-granules range in size from 50-250nm in diameter and are predominantly located in the cytoplasm of regenerating myofibers. It is unknown if myo-granules only form in the cytoplasm or if they form in the nucleus and are then transported into the cytoplasm. We have super-resolution microscopy evidence that suggests myo-granules are present in the nucleus during regeneration; however, electron microscopy validation is needed. If myo-granules form in the nucleus, it is likely they are not transported to the cytoplasm via the nuclear pore as the maximum export size is around 50nm (Solmaz et

al., 2011, 2013). However, large RNP assemblies have been shown to bud from the nuclear envelope in drosophila muscle (Jokhi et al., 2013). The budding mechanism is similar to how a virus particle exits the nucleus and may be used by large myo-granules to exit myonuclei during regeneration (Fradkin and Budnik, 2016). Once myo-granules are in the cytoplasm, it is unknown how they are transported. Myo-granules could freely diffuse around the cytoplasm or they could be actively transported on microtubules like neuronal RNA granules (Alami et al., 2014). Live-cell myo-granule tracking will be important in the future to understand the dynamics and transport of these RNPs during skeletal muscle regeneration.

Understanding the RNA composition of myo-granules is another important future direction. Although we know many mRNAs that encode sarcomereic proteins are incorporated within myo-granules, we do not have a comprehensive list of myo-granule mRNAs. By deep sequencing isolated myo-granules, we can determine the individual mRNAs within myo-granules. We can then study how these mRNAs are sorted and incorporated into myo-granules. Are there multiple mRNAs in a myo-granule or just one? Interestingly, many genes that encode contractile proteins are clustered on the same region of a chromosome in mice and humans (Weiss et al., 1999). This could be a conserved method to increase the efficiency of coordinated expression and packaging so that many of the sarcomere components end up in similar myo-granules. Alternatively, there are examples of RNPs that contain one, large mRNA that is formed in the nucleus and transported to the cytoplasm (Skoglund et al., 1983). Either way,

determining the specific mRNA components of myo-granules will be a helpful tool for understanding the regulation of sarcomeric mRNAs during muscle regeneration.

The protein composition of myo-granules may also serve as a mechanism to regulate RNA transcription, transport and translation during muscle regeneration. TDP-43 is a known component of myo-granules and has specific binding sites on mRNAs that encode sarcomeric proteins. However, it is possible that there are other classes of myo-granules that do not contain TDP-43. To test this, it will be important to knockout TDP-43 from muscle cells and examine myo-granule formation. Preliminary knockout experiments reveal that TDP-43 is an essential protein for skeletal muscle regeneration (Vogler et al., 2018), and no myofibers form without TDP-43. However, almost nothing is known about the role of TDP-43 in skeletal muscle formation, so it is unclear if the regeneration defect is due to the role of TDP-43 in myo-granules or another role of TDP-43 in muscle. Since TDP-43 has both nuclear and cytoplasmic functions in other cell types (Sephton et al., 2012), it will be important to decouple these two roles during skeletal muscle regeneration. Further, understanding the function of TDP-43 in other post-mitotic tissues, such as cardiomyocytes, and if myo-granules form in these tissues, will be an important next step.

TDP-43 containing myo-granules adopt a specific amyloid-like conformation during muscle regeneration. Amyloids are assemblies of proteins arranged in a highly organized manner (Eisenberg and Jucker, 2012) and are usually associated with degenerative diseases, where they form large irreversible aggregates. Although not all amyloids are found in disease (Boke et al., 2016; Maji et al., 2009), myo-granules

represent the first amyloid that is composed of a protein that also forms an amyloid in disease (Becker and Gitler, 2018; Vogler et al., 2018). Thus, it is important to understand the biophysical similarities and differences between myo-granules and amyloids that form in disease. Cryoelectron tomography of regenerating skeletal muscle will be useful to probe the in-situ biophysical structure of myo-granules. Gaining a better understanding of the myo-granule structure could shed light on how myo-granules can aggregate together to form larger amyloid fibrils *in vitro* (Vogler et al., 2018). Designing small molecules that prevent myo-granules aggregation would provide a unique therapeutic approach for diseases of protein aggregation. Further, structural studies could also identify how RNA interacts with myo-granules. For example, determining if RNA is buried within a myo-granule or is located on the outside of a myo-granule could link myo-granule structure to function.

Although myo-granules are similar in many ways to amyloid aggregates found in disease, a major difference is that they are cleared. We propose a model whereby the mechanisms that clear myo-granules are impaired in disease. Alternatively, there may be an increase in the formation of myo-granules in disease. Increasing the abundance of myo-granules enhances the possibility of amyloid fiber formation and/or aggregation of TDP-43 in disease (Chapter 3). This model may explain why TDP-43 aggregates occur in genetically diverse diseases including IBM (Salajegheh et al., 2009), which can be caused by mutations in the ubiquitin segregase VCP (Custer et al., 2010), OPMD, caused by Ala expansions in PABPN1 (Küsters et al., 2009), and DMRV, caused by mutations in the UDP-N-acetylglucosamine 2-epimerase gene (GNE) (Nishino et al.,

2002). Moreover, the seeding of TDP-43 aggregates by TDP-43 oligomers may also occur in neurons since reversible cytoplasmic TDP-43 accumulation occurs in models of acute neuronal injury *in vivo* (e.g. axotomy or traumatic brain injury) (Moisse et al., 2009; Wiesner et al., 2018). TDP-43 aggregates are also frequently observed on autopsy in neurologically normal elderly individuals (Nascimento et al., 2018). The age-dependent accumulation of TDP-43 aggregates may be caused by a failure to clear TDP-43, or other amyloid-like assemblies that formed during tissue repair. Over a lifetime, failures in proteostatic control mechanisms, including autophagy or endocytosis (Elobeid et al., 2016; Liu et al., 2017a; Wilson et al., 2013), could increase the likelihood that functional, amyloid-like assemblies transition into pathological aggregates. The accumulation of pathological aggregates in muscle could cause the insidious degeneration of skeletal muscle function during aging.

Skeletal muscle function and mass decline with age and can lead to increased morbidity and mortality (Landi et al., 2013). While the mechanisms for age-related muscle loss are multifactorial, reduction in the regenerative capacity of muscle is a clear contributor (Brooks and Faulkner, 1990; Day et al., 2010). Previous work has demonstrated that altered FGF signaling in MuSCs from aged muscle may drive the depletion of MuSCs in aged muscle, and thus, reduce the regenerative capacity of aged muscle (Bernet et al., 2014; Chakkalakal et al., 2012; Rozo et al., 2016). In Chapter 2, I discuss the manipulation of FGFR1 signaling in MuSC from young and aged mice. Increasing FGFR1 signaling in MuSCs has distinct effects on MuSC numbers in young and aged muscle. In MuSCs from young uninjured muscle, increasing FGFR1 signaling

has no effect on MuSC numbers. However, in young, regenerating skeletal muscle, constitutive FGFR1 signaling increases MuSC numbers. In contrast, in MuSCs from aged uninjured skeletal muscle, constitutive FGFR1 signaling increases MuSCs numbers. Thus, increasing endogenous MuSC numbers by FGFR1 activation identifies a potential new therapeutic opportunity to treat age-related muscle decline.

To unlock the therapeutic potential of FGFR1 activation in MuSC, we must identify the FGFR1-dependent pathways responsible for increasing MuSC in aged mice. A number of possible intracellular signaling pathways could be activated upon engagement of an FGFR with an FGF in aged muscle, including p38 α / β MAPK, ERK MAPK, PI3 kinase, Akt, activation of STAT, and stimulation of Phospholipase C gamma/Protein Kinase C signaling (Brewer et al., 2016; Ornitz and Itoh, 2015; Pawlikowski et al., 2017). Because of its role in promoting asymmetric MuSC division in aged mice FGFR activation of p38 α / β MAPK is a top candidate (Bernet et al., 2014; Jones et al., 2005). However, the connection between FGFR1 activation and p38 α / β MAPK signaling is still unclear. Analyzing the phospho-proteome of MuSC expressing caFGFR1 will help identify potential FGFR1 downstream pathways responsible for increasing MuSC numbers in aged muscle. Independent activation of downstream pathways, genetically or by small molecules, will help validate that therapeutically targeting FGFR1 signaling will be a beneficial treatment for increasing MuSC numbers in aged muscle.

The primary effect of increasing FGFR1 signaling in MuSCs in aged muscle was an increase in MuSC numbers. A secondary effect was an increase in myofiber size of

aged muscle. With the increase in myofiber size came a decrease in fatigue resistance of the muscle. Together, these changes made the aged muscle resemble a more youthful state. It is unclear how increasing FGFR1 signaling in MuSCs can change the skeletal muscle size and function. Increasing FGFR1 signaling in MuSC in aged mice may increase both MuSC numbers and fusion. Increasing fusion may increase the size and function of myofibers in aged muscle. Tracking fusion events in MuSCs that express caFGFR1 in aged muscle will be useful when examining this potential. Alternatively, increasing MuSC numbers or rescuing impaired MuSCs in aged muscle may provide a pro-hypertrophy signal to myofibers. Increasing MuSC numbers in aged animals through a non-FGFR1 pathway, for example by Wnt7a (Le Grand et al., 2009), will help identify if the increase in muscle size is dependent of FGFR1 signaling in MuSCs or only MuSC numbers.

Collectively, the data presented in this thesis identify two distinct mechanisms within skeletal muscle regeneration. Although distinct, FGF signaling in MuSCs and RNA regulation in myofibers cooperate to rebuild skeletal muscle after an injury or during disease. Elucidating the molecular pathways that drive these mechanisms will further our understanding of muscle regeneration and help us design 21st century therapies to treat skeletal muscle diseases.

References

- Abmayr, S.M., and Pavlath, G.K. (2012). Myoblast fusion: lessons from flies and mice. *Dev. Camb. Engl.* *139*, 641–656.
- Afroz, T., Hock, E.-M., Ernst, P., Foglieni, C., Jambeau, M., Gilhespy, L.A.B., Laferriere, F., Maniecka, Z., Plückthun, A., Mittl, P., et al. (2017). Functional and dynamic polymerization of the ALS-linked protein TDP-43 antagonizes its pathologic aggregation. *Nat. Commun.* *8*, 45.
- Akasaki, Y., Ouchi, N., Izumiya, Y., Bernardo, B.L., Lebrasseur, N.K., and Walsh, K. (2014). Glycolytic fast-twitch muscle fiber restoration counters adverse age-related changes in body composition and metabolism. *Aging Cell* *13*, 80–91.
- Alami, N.H., Smith, R.B., Carrasco, M.A., Williams, L.A., Winborn, C.S., Han, S.S.W., Kiskinis, E., Winborn, B., Freibaum, B.D., Kanagaraj, A., et al. (2014). Axonal transport of TDP-43 mRNA granules in neurons is impaired by ALS-causing mutations. *Neuron* *81*, 536–543.
- Allbrook, D.B., Han, M.F., and Hellmuth, A.E. (1971). Population of muscle satellite cells in relation to age and mitotic activity. *Pathology (Phila.)* *3*, 223–243.
- Almada, A.E., and Wagers, A.J. (2016). Molecular circuitry of stem cell fate in skeletal muscle regeneration, ageing and disease. *Nat Rev Mol Cell Biol* *17*, 267–279.
- Anderson, D.M., Cannavino, J., Li, H., Anderson, K.M., Nelson, B.R., McAnally, J., Bezprozvannaya, S., Liu, Y., Lin, W., Liu, N., et al. (2016). Severe muscle wasting and denervation in mice lacking the RNA-binding protein ZFP106. *Proc. Natl. Acad. Sci. U. S. A.* *113*, E4494-4503.
- Anderson, J.E., Mitchell, C.M., McGeachie, J.K., and Grounds, M.D. (1995). The time course of basic fibroblast growth factor expression in crush-injured skeletal muscles of SJL/J and BALB/c mice. *Exp Cell Res* *216*, 325–334.
- Apponi, L.H., Corbett, A.H., and Pavlath, G.K. (2011). RNA-binding proteins and gene regulation in myogenesis. *Trends Pharmacol. Sci.* *32*, 652–658.
- Asakura, A., Seale, P., Girgis-Gabardo, A., and Rudnicki, M.A. (2002). Myogenic specification of side population cells in skeletal muscle. *J Cell Biol* *159*, 123–134.
- Ayala, Y.M., Zago, P., D'Ambrogio, A., Xu, Y.-F., Petrucelli, L., Buratti, E., and Baralle, F.E. (2008). Structural determinants of the cellular localization and shuttling of TDP-43. *J. Cell Sci.* *121*, 3778–3785.

Ayala, Y.M., Conti, L.D., Avendaño-Vázquez, S.E., Dhir, A., Romano, M., D'Ambrogio, A., Tollervey, J., Ule, J., Baralle, M., Buratti, E., et al. (2011). TDP-43 regulates its mRNA levels through a negative feedback loop. *EMBO J.* 30, 277–288.

Barceló, C., Etchin, J., Mansour, M.R., Sanda, T., Ginesta, M.M., Sanchez-Arévalo Lobo, V.J., Real, F.X., Capellà, G., Estanyol, J.M., Jaumot, M., et al. (2014). Ribonucleoprotein HNRNPA2B1 Interacts With and Regulates Oncogenic KRAS in Pancreatic Ductal Adenocarcinoma Cells. *Gastroenterology* 147, 882-892.e8.

Beaudart, C., Rizzoli, R., Bruyère, O., Reginster, J.-Y., and Biver, E. (2014). Sarcopenia: burden and challenges for public health. *Arch. Public Health* 72.

Becker, L.A., and Gitler, A.D. (2018). A neurodegenerative-disease protein forms beneficial aggregates in healthy muscle. *Nature* 563, 477.

Bengoechea, R., Pittman, S.K., Tuck, E.P., True, H.L., and Weihl, C.C. (2015). Myofibrillar disruption and RNA-binding protein aggregation in a mouse model of limb-girdle muscular dystrophy 1D. *Hum. Mol. Genet.* 24, 6588–6602.

Bernet, J.D., Doles, J.D., Hall, J.K., Kelly Tanaka, K., Carter, T.A., and Olwin, B.B. (2014). p38 MAPK signaling underlies a cell-autonomous loss of stem cell self-renewal in skeletal muscle of aged mice. *Nat Med* 20, 265–271.

Bi, P., Ramirez-Martinez, A., Li, H., Cannavino, J., McAnally, J.R., Shelton, J.M., Sánchez-Ortiz, E., Bassel-Duby, R., and Olson, E.N. (2017). Control of muscle formation by the fusogenic micropeptide myomixer. *Science* 356, 323–327.

Birnkrant, D.J., Bushby, K., Bann, C.M., Apkon, S.D., Blackwell, A., Brumbaugh, D., Case, L.E., Clemens, P.R., Hadjiyannakis, S., Pandya, S., et al. (2018). Diagnosis and management of Duchenne muscular dystrophy, part 1: diagnosis, and neuromuscular, rehabilitation, endocrine, and gastrointestinal and nutritional management. *Lancet Neurol.* 17, 251–267.

Bland, C.S., Wang, E.T., Vu, A., David, M.P., Castle, J.C., Johnson, J.M., Burge, C.B., and Cooper, T.A. (2010). Global regulation of alternative splicing during myogenic differentiation. *Nucleic Acids Res.* 38, 7651–7664.

Blau, H.M., Cosgrove, B.D., and Ho, A.T.V. (2015). The central role of muscle stem cells in regenerative failure with aging. *Nat. Med.* 21, 854–862.

Bodine-Fowler, S. (1994). Skeletal muscle regeneration after injury: An overview. *J. Voice* 8, 53–62.

Boke, E., Ruer, M., Wühr, M., Coughlin, M., Lemaitre, R., Gygi, S.P., Alberti, S., Drechsel, D., Hyman, A.A., and Mitchison, T.J. (2016). Amyloid-like Self-assembly of a Cellular Compartment. *Cell* 166, 637–650.

- Brack, A.S., Conboy, M.J., Roy, S., Lee, M., Kuo, C.J., Keller, C., and Rando, T.A. (2007). Increased Wnt signaling during aging alters muscle stem cell fate and increases fibrosis. *Science* *317*, 807–810.
- Brewer, J.R., Mazot, P., and Soriano, P. (2016). Genetic insights into the mechanisms of Fgf signaling. *Genes Dev* *30*, 751–771.
- Brooks, S.V., and Faulkner, J.A. (1990). Contraction-induced injury: recovery of skeletal muscles in young and old mice. *Am. J. Physiol.-Cell Physiol.* *258*, C436–C442.
- Buratti, E., and Baralle, F.E. (2008). Multiple roles of TDP-43 in gene expression, splicing regulation, and human disease. *Front. Biosci. J. Virtual Libr.* *13*, 867–878.
- Buratti, E., Brindisi, A., Giombi, M., Tisminetzky, S., Ayala, Y.M., and Baralle, F.E. (2005). TDP-43 Binds Heterogeneous Nuclear Ribonucleoprotein A/B through Its C-terminal Tail AN IMPORTANT REGION FOR THE INHIBITION OF CYSTIC FIBROSIS TRANSMEMBRANE CONDUCTANCE REGULATOR EXON 9 SPLICING. *J. Biol. Chem.* *280*, 37572–37584.
- Burke, J.M., and Sullivan, C.S. (2017). DUSP11 – An RNA phosphatase that regulates host and viral non-coding RNAs in mammalian cells. *RNA Biol.* *14*, 1457–1465.
- Caldwell, C.J., Matthey, D.L., and Weller, R.O. (1990). Role of the basement membrane in the regeneration of skeletal muscle. *Neuropathol. Appl. Neurobiol.* *16*, 225–238.
- Carlson, B.M. (1973). The regeneration of skeletal muscle. A review. *Am. J. Anat.* *137*, 119–149.
- Chakkalakal, J.V., Jones, K.M., Basson, M.A., and Brack, A.S. (2012). The aged niche disrupts muscle stem cell quiescence. *Nature*.
- Chakkalakal, J.V., Christensen, J., Xiang, W., Tierney, M.T., Boscolo, F.S., Sacco, A., and Brack, A.S. (2014). Early forming label-retaining muscle stem cells require p27kip1 for maintenance of the primitive state. *Dev. Camb. Engl.* *141*, 1649–1659.
- Chen, A.K.-H., Lin, R.Y.-Y., Hsieh, E.Z.-J., Tu, P.-H., Chen, R.P.-Y., Liao, T.-Y., Chen, W., Wang, C.-H., and Huang, J.J.-T. (2010). Induction of Amyloid Fibrils by the C-Terminal Fragments of TDP-43 in Amyotrophic Lateral Sclerosis.
- Chenette, D.M., Cadwallader, A.B., Antwine, T.L., Larkin, L.C., Wang, J., Olwin, B.B., and Schneider, R.J. (2016). Targeted mRNA Decay by RNA Binding Protein AUF1 Regulates Adult Muscle Stem Cell Fate, Promoting Skeletal Muscle Integrity. *Cell Rep.* *16*, 1379–1390.

- Chiang, P.-M., Ling, J., Jeong, Y.H., Price, D.L., Aja, S.M., and Wong, P.C. (2010). Deletion of TDP-43 down-regulates Tbc1d1, a gene linked to obesity, and alters body fat metabolism. *Proc. Natl. Acad. Sci.* *107*, 16320–16324.
- Church, J.C.T., Noronha, R.F.X., and Allbrook, D.B. (1966). Satellite cells and skeletal muscle regeneration. *BJS* *53*, 638–642.
- Cilvik, S.N., Wang, J.I., Lavine, K.J., Uchida, K., Castro, A., Gierasch, C.M., Weinheimer, C.J., House, S.L., Kovacs, A., Nichols, C.G., et al. (2013). Fibroblast growth factor receptor 1 signaling in adult cardiomyocytes increases contractility and results in a hypertrophic cardiomyopathy. *PLoS One* *8*, e82979.
- Clegg, C.H., Linkhart, T.A., Olwin, B.B., and Hauschka, S.D. (1987). Growth factor control of skeletal muscle differentiation: commitment to terminal differentiation occurs in G1 phase and is repressed by fibroblast growth factor. *J Cell Biol* *105*, 949–956.
- Cohn, R.D., and Campbell, K.P. (2000). Molecular basis of muscular dystrophies. *Muscle Nerve* *23*, 1456–1471.
- Collins, C.A., Olsen, I., Zammit, P.S., Heslop, L., Petrie, A., Partridge, T.A., and Morgan, J.E. (2005). Stem cell function, self-renewal, and behavioral heterogeneity of cells from the adult muscle satellite cell niche. *Cell* *122*, 289–301.
- Collins, C.A., Zammit, P.S., Ruiz, A.P., Morgan, J.E., and Partridge, T.A. (2007). A population of myogenic stem cells that survives skeletal muscle aging. *Stem Cells* *25*, 885–894.
- Conboy, I.M., Conboy, M.J., Smythe, G.M., and Rando, T.A. (2003). Notch-mediated restoration of regenerative potential to aged muscle. *Science* *302*, 1575–1577.
- Conboy, I.M., Conboy, M.J., Wagers, A.J., Girma, E.R., Weissman, I.L., and Rando, T.A. (2005). Rejuvenation of aged progenitor cells by exposure to a young systemic environment. *Nature* *433*, 760–764.
- Cooper, R.N., Tajbakhsh, S., Mouly, V., Cossu, G., Buckingham, M., and Butler-Browne, G.S. (1999). In vivo satellite cell activation via Myf5 and MyoD in regenerating mouse skeletal muscle. *J Cell Sci* *112* (Pt 17), 2895–2901.
- Cornelison, D.D., and Wold, B.J. (1997). Single-cell analysis of regulatory gene expression in quiescent and activated mouse skeletal muscle satellite cells. *Dev Biol* *191*, 270–283.
- Cornelison, D.D., Filla, M.S., Stanley, H.M., Rapraeger, A.C., and Olwin, B.B. (2001). Syndecan-3 and syndecan-4 specifically mark skeletal muscle satellite cells and are implicated in satellite cell maintenance and muscle regeneration. *Dev Biol* *239*, 79–94.

Cosgrove, B.D., Gilbert, P.M., Porpiglia, E., Mourkioti, F., Lee, S.P., Corbel, S.Y., Llewellyn, M.E., Delp, S.L., and Blau, H.M. (2014). Rejuvenation of the muscle stem cell population restores strength to injured aged muscles. *Nat. Med.* *20*, 255–264.

Cox, J., and Mann, M. (2008). MaxQuant enables high peptide identification rates, individualized p.p.b.-range mass accuracies and proteome-wide protein quantification. *Nat. Biotechnol.* *26*, 1367–1372.

Cox, J., Neuhauser, N., Michalski, A., Scheltema, R.A., Olsen, J.V., and Mann, M. (2011). Andromeda: A Peptide Search Engine Integrated into the MaxQuant Environment.

Custer, S.K., Neumann, M., Lu, H., Wright, A.C., and Taylor, J.P. (2010). Transgenic mice expressing mutant forms VCP/p97 recapitulate the full spectrum of IBMPFD including degeneration in muscle, brain and bone. *Hum. Mol. Genet.* *19*, 1741–1755.

D'Ambrogio, A., Buratti, E., Stuani, C., Guarnaccia, C., Romano, M., Ayala, Y.M., and Baralle, F.E. (2009). Functional mapping of the interaction between TDP-43 and hnRNP A2 in vivo. *Nucleic Acids Res.* *37*, 4116–4126.

Dardenne, E., Polay Espinoza, M., Fattet, L., Germann, S., Lambert, M.-P., Neil, H., Zonta, E., Mortada, H., Gratadou, L., Deygas, M., et al. (2014). RNA Helicases DDX5 and DDX17 Dynamically Orchestrate Transcription, miRNA, and Splicing Programs in Cell Differentiation. *Cell Rep.* *7*, 1900–1913.

Day, K., Shefer, G., Shearer, A., and Yablonka-Reuveni, Z. (2010). The depletion of skeletal muscle satellite cells with age is concomitant with reduced capacity of single progenitors to produce reserve progeny. *Dev Biol* *340*, 330–343.

Diaper, D.C., Adachi, Y., Lazarou, L., Greenstein, M., Simoes, F.A., Di Domenico, A., Solomon, D.A., Lowe, S., Alsubaie, R., Cheng, D., et al. (2013). Drosophila TDP-43 dysfunction in glia and muscle cells cause cytological and behavioural phenotypes that characterize ALS and FTL. *Hum. Mol. Genet.* *22*, 3883–3893.

Dumont, N.A., Wang, Y.X., von Maltzahn, J., Pasut, A., Bentzinger, C.F., Brun, C.E., and Rudnicki, M.A. (2015). Dystrophin expression in muscle stem cells regulates their polarity and asymmetric division. *Nat. Med.* *21*, 1455–1463.

Eisenberg, D., and Jucker, M. (2012). The amyloid state of proteins in human diseases. *Cell* *148*, 1188–1203.

Elden, A.C., Kim, H.-J., Hart, M.P., Chen-Plotkin, A.S., Johnson, B.S., Fang, X., Armakola, M., Geser, F., Greene, R., Lu, M.M., et al. (2010). Ataxin-2 intermediate-length polyglutamine expansions are associated with increased risk for ALS. *Nature* *466*, 1069–1075.

- Elobeid, A., Libard, S., Leino, M., Popova, S.N., and Alafuzoff, I. (2016). Altered Proteins in the Aging Brain. *J. Neuropathol. Exp. Neurol.* *75*, 316–325.
- Eswarakumar, V.P., Lax, I., and Schlessinger, J. (2005). Cellular signaling by fibroblast growth factor receptors. *Cytokine Growth Factor Rev.* *16*, 139–149.
- Evans, W.J., and Campbell, W.W. (1993). Sarcopenia and age-related changes in body composition and functional capacity. *J. Nutr.* *123*, 465–468.
- Fallini, C., Bassell, G.J., and Rossoll, W. (2012). The ALS disease protein TDP-43 is actively transported in motor neuron axons and regulates axon outgrowth. *Hum. Mol. Genet.* *21*, 3703–3718.
- Fan, X., and Rouleau, G.A. (2003). Progress in understanding the pathogenesis of oculopharyngeal muscular dystrophy. *Can. J. Neurol. Sci. J. Can. Sci. Neurol.* *30*, 8–14.
- Fang, Y.-S., Tsai, K.-J., Chang, Y.-J., Kao, P., Woods, R., Kuo, P.-H., Wu, C.-C., Liao, J.-Y., Chou, S.-C., Lin, V., et al. (2014). Full-length TDP-43 forms toxic amyloid oligomers that are present in frontotemporal lobar dementia-TDP patients. *Nat. Commun.* *5*, 4824.
- Fatimy, R.E., Davidovic, L., Tremblay, S., Jaglin, X., Dury, A., Robert, C., Koninck, P.D., and Khandjian, E.W. (2016). Tracking the Fragile X Mental Retardation Protein in a Highly Ordered Neuronal RiboNucleoParticles Population: A Link between Stalled Polyribosomes and RNA Granules. *PLOS Genet.* *12*, e1006192.
- Feige, P., Brun, C.E., Ritso, M., and Rudnicki, M.A. (2018). Orienting Muscle Stem Cells for Regeneration in Homeostasis, Aging, and Disease. *Cell Stem Cell* *23*, 653–664.
- Fielding, R.A., Manfredi, T.J., Ding, W., Fiatarone, M.A., Evans, W.J., and Cannon, J.G. (1993). Acute phase response in exercise. III. Neutrophil and IL-1 beta accumulation in skeletal muscle. *Am. J. Physiol.-Regul. Integr. Comp. Physiol.* *265*, R166–R172.
- Flanagan-Steet, H., Hannon, K., McAvoy, M.J., Hullinger, R., and Olwin, B.B. (2000). Loss of FGF receptor 1 signaling reduces skeletal muscle mass and disrupts myofiber organization in the developing limb. *Dev Biol* *218*, 21–37.
- Floss, T., Arnold, H.H., and Braun, T. (1997). A role for FGF-6 in skeletal muscle regeneration. *Genes Dev* *11*, 2040–2051.
- Fradkin, L.G., and Budnik, V. (2016). This Bud's For You: Mechanisms of Cellular Nucleocytoplasmic Trafficking via Nuclear Envelope Budding. *Curr. Opin. Cell Biol.* *41*, 125–131.

Freibaum, B.D., Chitta, R., High, A.A., and Taylor, J.P. (2010). Global analysis of TDP-43 interacting proteins reveals strong association with RNA splicing and translation machinery. *J. Proteome Res.* *9*, 1104–1120.

Fry, C.S., Lee, J.D., Mula, J., Kirby, T.J., Jackson, J.R., Liu, F., Yang, L., Mendias, C.L., Dupont-Versteegden, E.E., McCarthy, J.J., et al. (2014). Inducible depletion of satellite cells in adult, sedentary mice impairs muscle regenerative capacity without affecting sarcopenia. *Nat Med* *21*, 76–80.

Fukuzawa, A., Idowu, S., and Gautel, M. (2005). Complete human gene structure of obscurin: implications for isoform generation by differential splicing. *J. Muscle Res. Cell Motil.* *26*, 427–434.

Ganassi, M., Badodi, S., Quiroga, H.P.O., Zammit, P.S., Hinitz, Y., and Hughes, S.M. (2018). Myogenin promotes myocyte fusion to balance fibre number and size. *Nat. Commun.* *9*, 4232.

Garber, K. (2016). No longer going to waste. *Nat Biotechnol* *34*, 458–461.

Garrett, K.L., and Anderson, J.E. (1995). Colocalization of bFGF and the myogenic regulatory gene myogenin in dystrophic mdx muscle precursors and young myotubes in vivo. *Dev Biol* *169*, 596–608.

Glisovic, T., Bachorik, J.L., Yong, J., and Dreyfuss, G. (2008). RNA-binding proteins and post-transcriptional gene regulation. *FEBS Lett.* *582*, 1977–1986.

Goh, Q., and Millay, D.P. (2017). Requirement of myomaker-mediated stem cell fusion for skeletal muscle hypertrophy. *ELife* *6*.

Golan-Gerstl, R., Cohen, M., Shilo, A., Suh, S.-S., Bakács, A., Coppola, L., and Karni, R. (2011). Splicing Factor hnRNP A2/B1 Regulates Tumor Suppressor Gene Splicing and Is an Oncogenic Driver in Glioblastoma. *Cancer Res.* *71*, 4464–4472.

Grahame Bulfield, W. G. Siller, P. A. L. Wight, and Karen J. Moore (1984). X chromosome-linked muscular dystrophy (mdx) in the mouse. *PNAS USA* *81*, 1189–1192.

Grimm, J.B., English, B.P., Chen, J., Slaughter, J.P., Zhang, Z., Revyakin, A., Patel, R., Macklin, J.J., Normanno, D., Singer, R.H., et al. (2015). A general method to improve fluorophores for live-cell and single-molecule microscopy. *Nat. Methods* *12*, 244–250.

Halfmann, R., and Lindquist, S. (2008). Screening for Amyloid Aggregation by Semi-Denaturing Detergent-Agarose Gel Electrophoresis. *J. Vis. Exp. JoVE*.

- Hannon, K., Kudla, A.J., McAvoy, M.J., Clase, K.L., and Olwin, B.B. (1996). Differentially expressed fibroblast growth factors regulate skeletal muscle development through autocrine and paracrine mechanisms. *J Cell Biol* *132*, 1151–1159.
- Hardy, D., Besnard, A., Latil, M., Jouvion, G., Briand, D., Thépenier, C., Pascal, Q., Guguin, A., Gayraud-Morel, B., Cavaillon, J.-M., et al. (2016). Comparative Study of Injury Models for Studying Muscle Regeneration in Mice. *PLoS One* *11*, e0147198.
- Hasty, P., Bradley, A., Morris, J.H., Edmondson, D.G., Venuti, J.M., Olson, E.N., and Klein, W.H. (1993). Muscle deficiency and neonatal death in mice with a targeted mutation in the myogenin gene. *Nature* *364*, 501–506.
- Hausburg, M.A., Doles, J.D., Clement, S.L., Cadwallader, A.B., Hall, M.N., Blackshear, P.J., Lykke-Andersen, J., and Olwin, B.B. (2015). Post-transcriptional regulation of satellite cell quiescence by TTP-mediated mRNA decay. *Elife* *4*, e03390.
- He, W.A., Berardi, E., Cardillo, V.M., Acharyya, S., Aulino, P., Thomas-Ahner, J., Wang, J., Bloomston, M., Muscarella, P., Nau, P., et al. (2013). NF- κ B-mediated Pax7 dysregulation in the muscle microenvironment promotes cancer cachexia. *J Clin Invest* *123*, 4821–4835.
- Hindi, S.M., Tajrishi, M.M., and Kumar, A. (2013). Signaling Mechanisms in Mammalian Myoblast Fusion. *Sci Signal* *6*, re2–re2.
- Hoffman, E.P., Brown, R.H.J., and Kunkkel, L.M. (1987). Dystrophin: the protein product of the duchenne muscular dystrophy locus. *Cell* *51*, 919–928.
- Holtzer, H., Hijikata, T., Lin, Z.X., Zhang, Z.Q., Holtzer, S., Protasi, F., Franzini-Armstrong, C., and Sweeney, H.L. (1997). Independent Assembly of 1.6 μ m Long Bipolar MHC Filaments and I-Z-I Bodies. *Cell Struct. Funct.* *22*, 83–93.
- Hwang, A.B., and Brack, A.S. (2018). Chapter Ten - Muscle Stem Cells and Aging. In *Current Topics in Developmental Biology*, D. Sassoon, ed. (Academic Press), pp. 299–322.
- Igaz, L.M., Kwong, L.K., Chen-Plotkin, A., Winton, M.J., Unger, T.L., Xu, Y., Neumann, M., Trojanowski, J.Q., and Lee, V.M.-Y. (2009). Expression of TDP-43 C-terminal Fragments in Vitro Recapitulates Pathological Features of TDP-43 Proteinopathies. *J. Biol. Chem.* *284*, 8516–8524.
- J. DiMario, N. Buffinger, S. Yamada, and R.C. Strohman (1989). Fibroblast growth factor in the extracellular matrix of dystrophic (mdx) mouse muscle. *Science* *244*, 688–690.

- Jain, S., Wheeler, J.R., Walters, R.W., Agrawal, A., Barsic, A., and Parker, R. (2016). ATPase-Modulated Stress Granules Contain a Diverse Proteome and Substructure. *Cell* *164*, 487–498.
- Johnson, B.S., Snead, D., Lee, J.J., McCaffery, J.M., Shorter, J., and Gitler, A.D. (2009). TDP-43 Is Intrinsically Aggregation-prone, and Amyotrophic Lateral Sclerosis-linked Mutations Accelerate Aggregation and Increase Toxicity. *J. Biol. Chem.* *284*, 20329–20339.
- Jokhi, V., Ashley, J., Noma, A., Ito, N., Wakabayashi-Ito, N., Moore, M.J., and Budnik, V. (2013). Torsin mediates primary envelopment of large ribonucleoprotein granules at the nuclear envelope. *Cell Rep.* *3*, 988–995.
- Jones, N.C., Tyner, K.J., Nibarger, L., Stanley, H.M., Cornelison, D.D., Fedorov, Y.V., and Olwin, B.B. (2005). The p38alpha/beta MAPK functions as a molecular switch to activate the quiescent satellite cell. *J Cell Biol* *169*, 105–116.
- Karalaki, M., Fili, S., Philippou, A., and Koutsilieris, M. (2009). Muscle Regeneration: Cellular and Molecular Events. *In Vivo* *23*, 779–796.
- Karsch-Mizrachi, I., Travis, M., Blau, H., and Leinwand, L.A. (1989). Expression and DNA sequence analysis of a human embryonic skeletal muscle myosin heavy chain gene. *Nucleic Acids Res.* *17*, 6167–6179.
- Kastner, S., Elias, M.C., Rivera, A.J., and Yablonka-Reuveni, Z. (2000). Gene expression patterns of the fibroblast growth factors and their receptors during myogenesis of rat satellite cells. *J Histochem Cytochem* *48*, 1079–1096.
- Kawahara, Y., and Mieda-Sato, A. (2012). TDP-43 promotes microRNA biogenesis as a component of the Drosha and Dicer complexes. *Proc. Natl. Acad. Sci. U. S. A.* *109*, 3347–3352.
- Kayed, R., Head, E., Thompson, J.L., McIntire, T.M., Milton, S.C., Cotman, C.W., and Glabe, C.G. (2003). Common structure of soluble amyloid oligomers implies common mechanism of pathogenesis. *Science* *300*, 486–489.
- Keefe, A.C., Lawson, J.A., Flygare, S.D., Fox, Z.D., Colasanto, M.P., Mathew, S.J., Yandell, M., and Kardon, G. (2015). Muscle stem cells contribute to myofibres in sedentary adult mice. *Nat Commun* *6*, 7087.
- Keene, J.D. (2007). RNA regulons: coordination of post-transcriptional events. *Nat. Rev. Genet.* *8*, 533–543.
- Khong, A., Jain, S., Matheny, T., Wheeler, J.R., and Parker, R. (2018). Isolation of mammalian stress granule cores for RNA-Seq analysis. *Methods* *137*, 49–54.

- Kim, H.J., Kim, N.C., Wang, Y.-D., Scarborough, E.A., Moore, J., Diaz, Z., MacLea, K.S., Freibaum, B., Li, S., Molliex, A., et al. (2013). Mutations in prion-like domains in hnRNPA2B1 and hnRNPA1 cause multisystem proteinopathy and ALS. *Nature* *495*, 467–473.
- Kim, S.H., Shanware, N.P., Bowler, M.J., and Tibbetts, R.S. (2010). Amyotrophic Lateral Sclerosis-associated Proteins TDP-43 and FUS/TLS Function in a Common Biochemical Complex to Co-regulate HDAC6 mRNA. *J. Biol. Chem.* *285*, 34097–34105.
- Knoblich, J.A. (2008). Mechanisms of asymmetric stem cell division. *Cell* *132*, 583–597.
- Kraemer, B.C., Schuck, T., Wheeler, J.M., Robinson, L.C., Trojanowski, J.Q., Lee, V.M.Y., and Schellenberg, G.D. (2010). Loss of murine TDP-43 disrupts motor function and plays an essential role in embryogenesis. *Acta Neuropathol. (Berl.)* *119*, 409–419.
- Kuang, S., Kuroda, K., Le Grand, F., and Rudnicki, M.A. (2007). Asymmetric self-renewal and commitment of satellite stem cells in muscle. *Cell* *129*, 999–1010.
- Kudla, A.J., Jones, N.C., Rosenthal, R.S., Arthur, K., Clase, K.L., and Olwin, B.B. (1998). The FGF receptor-1 tyrosine kinase domain regulates myogenesis but is not sufficient to stimulate proliferation. *J Cell Biol* *142*, 241–250.
- Kuo, P.-H., Doudeva, L.G., Wang, Y.-T., Shen, C.-K.J., and Yuan, H.S. (2009). Structural insights into TDP-43 in nucleic-acid binding and domain interactions. *Nucleic Acids Res.* *37*, 1799–1808.
- Küstters, B., Hoeve, B.J.A. van, Schelhaas, H.J., Laak, H. ter, Engelen, B.G.M. van, and Lammens, M. (2009). TDP-43 accumulation is common in myopathies with rimmed vacuoles. *Acta Neuropathol. (Berl.)* *117*, 209–211.
- Kwiatkowski, B.A., Kirillova, I., Richard, R.E., Israeli, D., and Yablonka-Reuveni, Z. (2008). FGFR4 and its novel splice form in myogenic cells: Interplay of glycosylation and tyrosine phosphorylation. *J Cell Physiol* *215*, 803–817.
- Labeit, S., Lahmers, S., Burkart, C., Fong, C., McNabb, M., Witt, S., Witt, C., Labeit, D., and Granzier, H. (2006). Expression of distinct classes of titin isoforms in striated and smooth muscles by alternative splicing, and their conserved interaction with filamins. *J. Mol. Biol.* *362*, 664–681.
- Landi, F., Cruz-Jentoft, A.J., Liperoti, R., Russo, A., Giovannini, S., Tosato, M., Capoluongo, E., Bernabei, R., and Onder, G. (2013). Sarcopenia and mortality risk in frail older persons aged 80 years and older: results from the SIRENTE study. *Age Ageing* *42*, 203–209.

- Le Grand, F., Jones, A.E., Seale, V., Scimè, A., and Rudnicki, M.A. (2009). Wnt7a activates the planar cell polarity pathway to drive the symmetric expansion of satellite stem cells. *Cell Stem Cell* 4, 535–547.
- Lehtokari, V.-L., Pelin, K., Sandbacka, M., Ranta, S., Donner, K., Muntoni, F., Sewry, C., Angelini, C., Bushby, K., Van den Bergh, P., et al. (2006). Identification of 45 novel mutations in the nebulin gene associated with autosomal recessive nemaline myopathy. *Hum. Mutat.* 27, 946–956.
- Lepper, C., Partridge, T.A., and Fan, C.-M. (2011). An absolute requirement for Pax7-positive satellite cells in acute injury-induced skeletal muscle regeneration. *Development* 138, 3639–3646.
- Li, J., Han, S., Cousin, W., and Conboy, I.M. (2015). Age-specific functional epigenetic changes in p21 and p16 in injury-activated satellite cells. *Stem Cells* 33, 951–961.
- Li, S., Zhang, P., Freibaum, B.D., Kim, N.C., Kolaitis, R.-M., Molliex, A., Kanagaraj, A.P., Yabe, I., Tanino, M., Tanaka, S., et al. (2016). Genetic interaction of hnRNPA2B1 and DNAJB6 in a Drosophila model of multisystem proteinopathy. *Hum. Mol. Genet.* 25, 936–950.
- Lim, R.W., and Hauschka, S.D. (1984). EGF responsiveness and receptor regulation in normal and differentiation-defective mouse myoblasts. *Dev Biol* 105, 48–58.
- Liu, G., Coyne, A.N., Pei, F., Vaughan, S., Chaung, M., Zarnescu, D.C., and Buchan, J.R. (2017a). Endocytosis regulates TDP-43 toxicity and turnover. *Nat. Commun.* 8, 2092.
- Liu, T.-Y., Chen, Y.-C., Jong, Y.-J., Tsai, H.-J., Lee, C.-C., Chang, Y.-S., Chang, J.-G., and Chang, Y.-F. (2017b). Muscle developmental defects in heterogeneous nuclear Ribonucleoprotein A1 knockout mice. *Open Biol.* 7.
- Liu, W., Klose, A., Forman, S., Paris, N.D., Wei-LaPierre, L., Cortés-Lopéz, M., Tan, A., Flaherty, M., Miura, P., Dirksen, R.T., et al. (2017c). Loss of adult skeletal muscle stem cells drives age-related neuromuscular junction degeneration. *ELife* 6, e26464.
- Llamusi, B., Bargiela, A., Fernandez-Costa, J.M., Garcia-Lopez, A., Klima, R., Feiguin, F., and Artero, R. (2013). Muscleblind, BSF and TBPH are mislocalized in the muscle sarcomere of a Drosophila myotonic dystrophy model. *Dis. Model. Mech.* 6, 184–196.
- Lovci, M.T., Ghanem, D., Marr, H., Arnold, J., Gee, S., Parra, M., Liang, T.Y., Stark, T.J., Gehman, L.T., Hoon, S., et al. (2013). Rbfox proteins regulate alternative mRNA splicing through evolutionarily conserved RNA bridges. *Nat. Struct. Mol. Biol.* 20, 1434–1442.

Lu, H., Huang, D., Ransohoff, R.M., and Zhou, L. (2011). Acute skeletal muscle injury: CCL2 expression by both monocytes and injured muscle is required for repair. *FASEB J.* *25*, 3344–3355.

Lukjanenko, L., Jung, M.J., Hegde, N., Perruisseau-Carrier, C., Migliavacca, E., Rozo, M., Karaz, S., Jacot, G., Schmidt, M., Li, L., et al. (2016). Loss of fibronectin from the aged stem cell niche affects the regenerative capacity of skeletal muscle in mice. *Nat Med* *22*, 897–905.

Mackenzie, I.R., Nicholson, A.M., Sarkar, M., Messing, J., Purice, M.D., Pottier, C., Annu, K., Baker, M., Perkerson, R.B., Kurti, A., et al. (2017). TIA1 Mutations in Amyotrophic Lateral Sclerosis and Frontotemporal Dementia Promote Phase Separation and Alter Stress Granule Dynamics. *Neuron* *95*, 808-816.e9.

Maji, S.K., Perrin, M.H., Sawaya, M.R., Jessberger, S., Vadodaria, K., Rissman, R.A., Singru, P.S., Nilsson, K.P.R., Simon, R., Schubert, D., et al. (2009). Functional Amyloids as Natural Storage of Peptide Hormones in Pituitary Secretory Granules. *Science* *325*, 328–332.

Martinez, F.J., Pratt, G.A., Van Nostrand, E.L., Batra, R., Huelga, S.C., Kapeli, K., Freese, P., Chun, S.J., Ling, K., Gelboin-Burkhart, C., et al. (2016). Protein-RNA networks regulated by normal and ALS-associated mutant HNRNPA2B1 in the nervous system. *Neuron* *92*, 780–795.

Mauro, A. (1961). Satellite cell of skeletal muscle fibers. *J Biophys Biochem Cytol* *9*, 493–495.

Meriglioli, M.N., and Roubenoff, R. (2015). Prospect for Pharmacological Therapies to Treat Skeletal Muscle Dysfunction. *Calcif. Tissue Int.* *96*, 234–242.

Miljkovic, N., Lim, J.-Y., Miljkovic, I., and Frontera, W.R. (2015). Aging of Skeletal Muscle Fibers. *Ann. Rehabil. Med.* *39*, 155–162.

Millay, D.P., O'Rourke, J.R., Sutherland, L.B., Bezprozvannaya, S., Shelton, J.M., Bassel-Duby, R., and Olson, E.N. (2013). Myomaker is a membrane activator of myoblast fusion and muscle formation. *Nature* *499*, 301–305.

Millay, D.P., Sutherland, L.B., Bassel-Duby, R., and Olson, E.N. (2014). Myomaker is essential for muscle regeneration. *Genes Dev.* *28*, 1641–1646.

Mitchell, K.J., Pannérec, A., Cadot, B., Parlakian, A., Besson, V., Gomes, E.R., Marazzi, G., and Sassoon, D.A. (2010). Identification and characterization of a non-satellite cell muscle resident progenitor during postnatal development. *Nat Cell Biol* *12*, 257–266.

Moisse, K., Volkening, K., Leystra-Lantz, C., Welch, I., Hill, T., and Strong, M.J. (2009). Divergent patterns of cytosolic TDP-43 and neuronal progranulin expression following

axotomy: Implications for TDP-43 in the physiological response to neuronal injury. *Brain Res.* 1249, 202–211.

Mompeán, M., Hervás, R., Xu, Y., Tran, T.H., Guarnaccia, C., Buratti, E., Baralle, F., Tong, L., Carrión-Vázquez, M., McDermott, A.E., et al. (2015). Structural Evidence of Amyloid Fibril Formation in the Putative Aggregation Domain of TDP-43.

Morrée, A. de, Velthoven, C.T.J. van, Gan, Q., Salvi, J.S., Klein, J.D.D., Akimenko, I., Quarta, M., Biressi, S., and Rando, T.A. (2017). Stauf1 inhibits MyoD translation to actively maintain muscle stem cell quiescence. *Proc. Natl. Acad. Sci.* 114, E8996–E9005.

Moss, F.P., and Leblond, C.P. (1970a). Nature of dividing nuclei in skeletal muscle of growing rats. *J Cell Biol* 44, 459–462.

Moss, F.P., and Leblond, C.P. (1970b). Satellite cells as the source of nuclei in muscles of growing rats. *Anat Rec* 170, 421–436.

Murphy, M.M., Lawson, J.A., Mathew, S.J., Hutcheson, D.A., and Kardon, G. (2011). Satellite cells, connective tissue fibroblasts and their interactions are crucial for muscle regeneration. *Development* 138, 3625–3637.

Nakka, K., Ghigna, C., Gabellini, D., and Dilworth, F.J. (2018). Diversification of the muscle proteome through alternative splicing. *Skelet. Muscle* 8, 8.

Narici, M.V., and Maffulli, N. (2010). Sarcopenia: characteristics, mechanisms and functional significance. *Br. Med. Bull.* 95, 139–159.

Nascimento, C., Di Lorenzo Alho, A.T., Bazan Conceição Amaral, C., Leite, R.E.P., Nitrini, R., Jacob-Filho, W., Pasqualucci, C.A., Hokkanen, S.R.K., Hunter, S., Keage, H., et al. (2018). Prevalence of transactive response DNA-binding protein 43 (TDP-43) proteinopathy in cognitively normal older adults: systematic review and meta-analysis. *Neuropathol. Appl. Neurobiol.* 44, 286–297.

Naski, M.C., Wang, Q., Xu, J., and Ornitz, D.M. (1996). Graded activation of fibroblast growth factor receptor 3 by mutations causing achondroplasia and thanatophoric dysplasia. *Nat Genet* 13, 233–237.

Neumann, M., Sampathu, D.M., Kwong, L.K., Truax, A.C., Micsenyi, M.C., Chou, T.T., Bruce, J., Schuck, T., Grossman, M., Clark, C.M., et al. (2006). Ubiquitinated TDP-43 in frontotemporal lobar degeneration and amyotrophic lateral sclerosis. *Science* 314, 130–133.

Nguyen, E.D., Balas, M.M., Griffin, A.M., Roberts, J.T., and Johnson, A.M. (2018). Global profiling of hnRNP A2/B1-RNA binding on chromatin highlights LncRNA interactions. *RNA Biol.* 15, 901–913.

Nishino, I., Noguchi, S., Murayama, K., Driss, A., Sugie, K., Oya, Y., Nagata, T., Chida, K., Takahashi, T., Takusa, Y., et al. (2002). Distal myopathy with rimmed vacuoles is allelic to hereditary inclusion body myopathy. *Neurology* *59*, 1689–1693.

Olguin, H.C., and Olwin, B.B. (2004). Pax-7 up-regulation inhibits myogenesis and cell cycle progression in satellite cells: a potential mechanism for self-renewal. *Dev Biol* *275*, 375–388.

Olguin, H.C., Yang, Z., Tapscott, S.J., and Olwin, B.B. (2007). Reciprocal inhibition between Pax7 and muscle regulatory factors modulates myogenic cell fate determination. *J Cell Biol* *177*, 769–779.

Olwin, B.B., and Hauschka, S.D. (1986). Identification of the fibroblast growth factor receptor of Swiss 3T3 cells and mouse skeletal muscle myoblasts. *Biochemistry* *25*, 3487–3492.

Ornitz, D.M., and Itoh, N. (2015). The Fibroblast Growth Factor signaling pathway. *Wiley Interdiscip Rev Dev Biol* *4*, 215–266.

Pawlikowski, B., Pulliam, C., Betta, N.D., Kardon, G., and Olwin, B.B. (2015). Pervasive satellite cell contribution to uninjured adult muscle fibers. *Skelet. Muscle* *5*, 42.

Pawlikowski, B., Vogler, T.O., Gadek, K., and Olwin, B.B. (2017). Regulation of skeletal muscle stem cells by fibroblast growth factors. *Dev. Dyn.* *246*, 359–367.

Pedrotti, S., Giudice, J., Dagnino-Acosta, A., Knoblauch, M., Singh, R.K., Hanna, A., Mo, Q., Hicks, J., Hamilton, S., and Cooper, T.A. (2015). The RNA-binding protein Rbfox1 regulates splicing required for skeletal muscle structure and function. *Hum. Mol. Genet.* *24*, 2360–2374.

Piccirillo, R., Demontis, F., Perrimon, N., and Goldberg, A.L. (2014). Mechanisms of muscle growth and atrophy in mammals and *Drosophila*. *Dev Dyn* *243*, 201–215.

Piovesan, A., Caracausi, M., Antonaros, F., Pelleri, M.C., and Vitale, L. (2016). GeneBase 1.1: a tool to summarize data from NCBI Gene datasets and its application to an update of human gene statistics. *Database* *2016*.

Platt, R.J., Chen, S., Zhou, Y., Yim, M.J., Swiech, L., Kempton, H.R., Dahlman, J.E., Parnas, O., Eisenhaure, T.M., Jovanovic, M., et al. (2014). CRISPR-Cas9 Knockin Mice for Genome Editing and Cancer Modeling. *Cell* *159*, 440–455.

Polymenidou, M., Lagier-Tourenne, C., Hutt, K.R., Huelga, S.C., Moran, J., Liang, T.Y., Ling, S.-C., Sun, E., Wancewicz, E., Mazur, C., et al. (2011). Long pre-mRNA depletion and RNA missplicing contribute to neuronal vulnerability from loss of TDP-43. *Nat. Neurosci.* *14*, 459–468.

- Price, F.D., von Maltzahn, J., Bentzinger, C.F., Dumont, N.A., Yin, H., Chang, N.C., Wilson, D.H., Frenette, J., and Rudnicki, M.A. (2014). Inhibition of JAK-STAT signaling stimulates adult satellite cell function. *Nat Med* 20, 1174–1181.
- Quiat, D., Voelker, K.A., Pei, J., Grishin, N.V., Grange, R.W., Bassel-Duby, R., and Olson, E.N. (2011). Concerted regulation of myofiber-specific gene expression and muscle performance by the transcriptional repressor Sox6. *Proc. Natl. Acad. Sci. U. S. A.* 108, 10196–10201.
- Quinlan, J.G., Michaels, S.E., Denman, D.L., Lyden, S.P., Cambier, D.M., and Johnson, S.R. (1995). Radiation inhibition of mdx mouse muscle regeneration: Dose and age factors. *Muscle Nerve* 18, 201–206.
- Quinn, M.E., Goh, Q., Kurosaka, M., Gamage, D.G., Petrany, M.J., Prasad, V., and Millay, D.P. (2017). Myomerger induces fusion of non-fusogenic cells and is required for skeletal muscle development. *Nat Commun* 8, 15665.
- Rao, N., Evans, S., Stewart, D., Spencer, K.H., Sheikh, F., Hui, E.E., and Christman, K.L. (2013). Fibroblasts influence muscle progenitor differentiation and alignment in contact independent and dependent manners in organized co-culture devices. *Biomed Microdevices* 15, 161–169.
- Relaix, F., Montarras, D., Zaffran, S., Gayraud-Morel, B., Rocancourt, D., Tajbakhsh, S., Mansouri, A., Cumano, A., and Buckingham, M. (2006). Pax3 and Pax7 have distinct and overlapping functions in adult muscle progenitor cells. *J Cell Biol* 172, 91–102.
- Renton, A.E., Chiò, A., and Traynor, B.J. (2014). State of play in amyotrophic lateral sclerosis genetics. *Nat. Neurosci.* 17, 17–23.
- Reznik, M. (1969). Thymidine-3H uptake by satellite cells of regenerating skeletal muscle. *J Cell Biol* 40, 568–571.
- Rhee, D., Sanger, J.M., and Sanger, J.W. (1994). The premyofibril: evidence for its role in myofibrillogenesis. *Cell Motil. Cytoskeleton* 28, 1–24.
- Rodriguez-Ortiz, C.J., Hoshino, H., Cheng, D., Liu-Yescevitiz, L., Blurton-Jones, M., Wolozin, B., LaFerla, F.M., and Kitazawa, M. (2013). Neuronal-Specific Overexpression of a Mutant Valosin-Containing Protein Associated with IBMPFD Promotes Aberrant Ubiquitin and TDP-43 Accumulation and Cognitive Dysfunction in Transgenic Mice. *Am. J. Pathol.* 183, 504–515.
- Roman, W., Martins, J.P., Carvalho, F.A., Voituriez, R., Abella, J.V.G., Santos, N.C., Cadot, B., Way, M., and Gomes, E.R. (2017). Myofibril contraction and crosslinking drive nuclear movement to the periphery of skeletal muscle. *Nat Cell Biol.*

- Rozo, M., Li, L., and Fan, C.-M. (2016). Targeting β 1-integrin signaling enhances regeneration in aged and dystrophic muscle in mice. *Nat Med* 22, 889–896.
- Rui, Y., Bai, J., and Perrimon, N. (2010). Sarcomere Formation Occurs by the Assembly of Multiple Latent Protein Complexes. *PLoS Genet.* 6.
- Ryall, J.G., Schertzer, J.D., and Lynch, G.S. (2008). Cellular and molecular mechanisms underlying age-related skeletal muscle wasting and weakness. *Biogerontology* 9, 213–228.
- Sacco, A., Mourkioti, F., Tran, R., Choi, J., Llewellyn, M., Kraft, P., Shkreli, M., Delp, S., Pomerantz, J.H., Artandi, S.E., et al. (2010). Short Telomeres and Stem Cell Exhaustion Model Duchenne Muscular Dystrophy in mdx/mTR Mice. *Cell* 143, 1059–1071.
- Salajegheh, M., Pinkus, J.L., Taylor, J.P., Amato, A.A., Nazareno, R., Baloh, R.H., and Greenberg, S.A. (2009). Sarcoplasmic redistribution of nuclear TDP-43 in inclusion body myositis. *Muscle Nerve* 40, 19–31.
- Sambasivan, R., Yao, R., Kissenpfennig, A., Van Wittenberghe, L., Paldi, A., Gayraud-Morel, B., Guenou, H., Malissen, B., Tajbakhsh, S., and Galy, A. (2011). Pax7-expressing satellite cells are indispensable for adult skeletal muscle regeneration. *Development* 138, 3647–3656.
- Sanes, J.R., Marshall, L.M., and McMahan, U.J. (1978). Reinnervation of muscle fiber basal lamina after removal of myofibers. Differentiation of regenerating axons at original synaptic sites. *J. Cell Biol.* 78, 176–198.
- Sangwan, S., Zhao, A., Adams, K.L., Jayson, C.K., Sawaya, M.R., Guenther, E.L., Pan, A.C., Ngo, J., Moore, D.M., Soriaga, A.B., et al. (2017). Atomic structure of a toxic, oligomeric segment of SOD1 linked to amyotrophic lateral sclerosis (ALS). *Proc. Natl. Acad. Sci.* 114, 8770–8775.
- Sato, K., Li, Y., Foster, W., Fukushima, K., Badlani, N., Adachi, N., Usas, A., Fu, F.H., and Huard, J. (2003). Improvement of muscle healing through enhancement of muscle regeneration and prevention of fibrosis. *Muscle Nerve* 28, 365–372.
- Schmid, B., Hruscha, A., Hogl, S., Banzhaf-Strathmann, J., Strecker, K., van der Zee, J., Teucke, M., Eimer, S., Hegermann, J., Kittelmann, M., et al. (2013). Loss of ALS-associated TDP-43 in zebrafish causes muscle degeneration, vascular dysfunction, and reduced motor neuron axon outgrowth. *Proc. Natl. Acad. Sci. U. S. A.* 110, 4986–4991.
- Seale, P., Sabourin, L.A., Girgis-Gabardo, A., Mansouri, A., Gruss, P., and Rudnicki, M.A. (2000). Pax7 is required for the specification of myogenic satellite cells. *Cell* 102, 777–786.

Seed, J., Olwin, B.B., and Hauschka, S.D. (1988). Fibroblast growth factor levels in the whole embryo and limb bud during chick development. *Dev Biol* 128, 50–57.

Sephton, C.F., Cenik, B., Cenik, B.K., Herz, J., and Yu, G. (2012). TDP-43 in CNS development and function: clues to TDP-43-associated neurodegeneration. *Biol. Chem.* 393, 589–594.

Shafiq, S.A., Gorycki, M.A., and Milhorat, A.T. (1967). An electron microscopic study of regeneration and satellite cells in human muscle. *Neurology* 17, 567-74 passim.

Sheehan, S.M., and Allen, R.E. (1999). Skeletal muscle satellite cell proliferation in response to members of the fibroblast growth factor family and hepatocyte growth factor. *J Cell Physiol* 181, 499–506.

Shefer, G., Van de Mark, D.P., Richardson, J.B., and Yablonka-Reuveni, Z. (2006). Satellite-cell pool size does matter: defining the myogenic potency of aging skeletal muscle. *Dev Biol* 294, 50–66.

Shi, X., and Garry, D.J. (2006). Muscle stem cells in development, regeneration, and disease. *Genes Dev* 20, 1692–1708.

Skoglund, U., Andersson, K., Björkroth, B., Lamb, M.M., and Daneholt, B. (1983). Visualization of the formation and transport of a specific hnRNP particle. *Cell* 34, 847–855.

Smith, B.A., and Jackman, J.E. (2011). Kinetic Analysis of 3′–5′ Nucleotide Addition Catalyzed by Eukaryotic tRNA^{His} Guanylyltransferase.

Smith, C., Kruger, M.J., Smith, R.M., and Myburgh, K.H. (2008). The Inflammatory Response to Skeletal Muscle Injury. *Sports Med.* 38, 947–969.

Snow, M.H. (1978). An autoradiographic study of satellite cell differentiation into regenerating myotubes following transplantation of muscles in young rats. *Cell Tissue Res* 186, 535–540.

Solmaz, S.R., Chauhan, R., Blobel, G., and Melčák, I. (2011). Molecular Architecture of the Transport Channel of the Nuclear Pore Complex. *Cell* 147, 590–602.

Solmaz, S.R., Blobel, G., and Melčák, I. (2013). Ring cycle for dilating and constricting the nuclear pore. *Proc. Natl. Acad. Sci. U. S. A.* 110, 5858–5863.

Sorichter, S., Mair, J., Koller, A., Gebert, W., Rama, D., Calzolari, C., Artner-Dworzak, E., and Puschendorf, B. (1997). Skeletal troponin I as a marker of exercise-induced muscle damage. *J. Appl. Physiol.* 83, 1076–1082.

Sparrow, J.C., and Schöck, F. (2009). The initial steps of myofibril assembly: integrins pave the way. *Nat. Rev. Mol. Cell Biol.* 10, 293–298.

- Spudich, J.A., and Watt, S. (1971). The Regulation of Rabbit Skeletal Muscle Contraction I. BIOCHEMICAL STUDIES OF THE INTERACTION OF THE TROPOMYOSIN-TROPONIN COMPLEX WITH ACTIN AND THE PROTEOLYTIC FRAGMENTS OF MYOSIN. *J. Biol. Chem.* *246*, 4866–4871.
- Taylor, J.P. (2015). Multisystem proteinopathy: Intersecting genetics in muscle, bone, and brain degeneration. *Neurology* *10.1212/WNL.0000000000001862*.
- Tedesco, F.S., Dellavalle, A., Diaz-Manera, J., Messina, G., and Cossu, G. (2010). Repairing skeletal muscle: regenerative potential of skeletal muscle stem cells. *J Clin Invest* *120*, 11–19.
- Tidball, J.G. (2005). Inflammatory processes in muscle injury and repair. *Am J Physiol Regul Integr Comp Physiol* *288*, R345-53.
- Tidball, J.G. (2017). Regulation of muscle growth and regeneration by the immune system. *Nat. Rev. Immunol.* *17*, 165–178.
- Tierney, M.T., Aydogdu, T., Sala, D., Malecova, B., Gatto, S., Puri, P.L., Latella, L., and Sacco, A. (2014). STAT3 signaling controls satellite cell expansion and skeletal muscle repair. *Nat. Med.* *20*, 1182–1186.
- Tokunaga, M., Imamoto, N., and Sakata-Sogawa, K. (2008). Highly inclined thin illumination enables clear single-molecule imaging in cells. *Nat. Methods* *5*, 159–161.
- Tollervey, J.R., Curk, T., Rogelj, B., Briese, M., Cereda, M., Kayikci, M., König, J., Hortobágyi, T., Nishimura, A.L., Župunski, V., et al. (2011). Characterizing the RNA targets and position-dependent splicing regulation by TDP-43. *Nat. Neurosci.* *14*, 452–458.
- Troy, A., Cadwallader, A.B., Fedorov, Y., Tyner, K., Tanaka, K.K., and Olwin, B.B. (2012). Coordination of satellite cell activation and self-renewal by Par-complex-dependent asymmetric activation of p38alpha/beta MAPK. *Cell Stem Cell* *11*, 541–553.
- Van Nostrand, E.L., Pratt, G.A., Shishkin, A.A., Gelboin-Burkhart, C., Fang, M.Y., Sundararaman, B., Blue, S.M., Nguyen, T.B., Surka, C., Elkins, K., et al. (2016). Robust transcriptome-wide discovery of RNA-binding protein binding sites with enhanced CLIP (eCLIP). *Nat Methods* *13*, 508–514.
- Van Treeck, B., and Parker, R. (2018). Emerging Roles for Intermolecular RNA-RNA Interactions in RNP Assemblies. *Cell* *174*, 791–802.
- Vogler, T.O., Gadek, K.E., Cadwallader, A.B., Elston, T.L., and Olwin, B.B. (2016). Isolation, Culture, Functional Assays, and Immunofluorescence of Myofiber-Associated Satellite Cells. *Methods Mol. Biol. Clifton NJ* *1460*, 141–162.

Vogler, T.O., Wheeler, J.R., Nguyen, E.D., Hughes, M.P., Britson, K.A., Lester, E., Rao, B., Betta, N.D., Whitney, O.N., Ewachiw, T.E., et al. (2018). TDP-43 and RNA form amyloid-like myo-granules in regenerating muscle. *Nature*.

Volkening, K., Leystra-Lantz, C., Yang, W., Jaffee, H., and Strong, M.J. (2009). Tar DNA binding protein of 43 kDa (TDP-43), 14-3-3 proteins and copper/zinc superoxide dismutase (SOD1) interact to modulate NFL mRNA stability. Implications for altered RNA processing in amyotrophic lateral sclerosis (ALS). *Brain Res.* *1305*, 168–182.

Wang, J.K., Gao, G., and Goldfarb, M. (1994). Fibroblast growth factor receptors have different signaling and mitogenic potentials. *Mol Cell Biol* *14*, 181–188.

Wang, Y.X., Feige, P., Brun, C.E., Hekmatnejad, B., Dumont, N.A., Renaud, J.-M., Faulkes, S., Guindon, D.E., and Rudnicki, M.A. (2019). EGFR-Aurka Signaling Rescues Polarity and Regeneration Defects in Dystrophin-Deficient Muscle Stem Cells by Increasing Asymmetric Divisions. *Cell Stem Cell* *0*.

Webster, C., Silberstein, L., Hays, A.P., and Blau, H.M. (1988). Fast muscle fibers are preferentially affected in Duchenne muscular dystrophy. *Cell* *52*, 503–513.

Webster, M.T., Manor, U., Lippincott-Schwartz, J., and Fan, C.-M. (2016). Intravital Imaging Reveals Ghost Fibers as Architectural Units Guiding Myogenic Progenitors during Regeneration. *Cell Stem Cell* *18*, 243–252.

Weihl, C.C., Temiz, P., Miller, S.E., Watts, G., Smith, C., Forman, M., Hanson, P.I., Kimonis, V., and Pestronk, A. (2008). TDP-43 accumulation in IBM muscle suggests a common pathogenic mechanism with Frontotemporal dementia. *J. Neurol. Neurosurg. Psychiatry* *79*, 1186–1189.

Weinstein, M., Xu, X., Ohyama, K., and Deng, C.X. (1998). FGFR-3 and FGFR-4 function cooperatively to direct alveogenesis in the murine lung. *Development* *125*, 3615–3623.

Weiss, A., McDonough, D., Wertman, B., Acakpo-Satchivi, L., Montgomery, K., Kucherlapati, R., Leinwand, L., and Krauter, K. (1999). Organization of human and mouse skeletal myosin heavy chain gene clusters is highly conserved. *Proc. Natl. Acad. Sci.* *96*, 2958–2963.

Wheeler, J.R., Matheny, T., Jain, S., Abrisch, R., and Parker, R. (2016). Distinct stages in stress granule assembly and disassembly. *ELife* *5*, e18413.

Wheeler, J.R., Jain, S., Khong, A., and Parker, R. (2017). Isolation of yeast and mammalian stress granule cores. *Methods* *126*, 12–17.

Wiesner, D., Tar, L., Linkus, B., Chandrasekar, A., olde Heuvel, F., Dupuis, L., Tsao, W., Wong, P.C., Ludolph, A., and Roselli, F. (2018). Reversible induction of TDP-43 granules in cortical neurons after traumatic injury. *Exp. Neurol.* *299*, 15–25.

Wilson, R.S., Yu, L., Trojanowski, J.Q., Chen, E.-Y., Boyle, P.A., Bennett, D.A., and Schneider, J.A. (2013). TDP-43 Pathology, Cognitive Decline, and Dementia in Old Age. *JAMA Neurol.* *70*, 1418–1424.

Winey, M., Meehl, J.B., O'Toole, E.T., and Giddings, T.H. (2014). Conventional transmission electron microscopy. *Mol. Biol. Cell* *25*, 319–323.

Wu, B., Su, S., Patil, D.P., Liu, H., Gan, J., Jaffrey, S.R., and Ma, J. (2018). Molecular basis for the specific and multivariant recognitions of RNA substrates by human hnRNP A2/B1. *Nat. Commun.* *9*.

Yablonka-Reuveni, Z., Seger, R., and Rivera, A.J. (1999). Fibroblast growth factor promotes recruitment of skeletal muscle satellite cells in young and old rats. *J Histochem Cytochem* *47*, 23–42.

Yablonka-Reuveni, Z., Danoviz, M.E., Phelps, M., and Stuelsatz, P. (2015). Myogenic-specific ablation of *Fgfr1* impairs FGF2-mediated proliferation of satellite cells at the myofiber niche but does not abolish the capacity for muscle regeneration. *Front. Aging Neurosci.* *7*, 85.

Yeung, Y.-G., and Stanley, E.R. (2010). Rapid Detergent Removal From Peptide Samples With Ethyl Acetate For Mass Spectrometry Analysis. *Curr. Protoc. Protein Sci.* Editor. Board John E Coligan AI *CHAPTER*, Unit-16.12.

Yin, H., Price, F., and Rudnicki, M.A. (2013). Satellite cells and the muscle stem cell niche. *Physiol. Rev.* *93*, 23–67.

Yucel, N., Chang, A.C., Day, J.W., Rosenthal, N., and Blau, H.M. (2018). Humanizing the mdx mouse model of DMD: the long and the short of it. *NPJ Regen. Med.* *3*.

Zatz, M., Rapaport, D., Vainzof, M., Passos-Bueno, M.R., Bortolini, E.R., Pavanello, R. de C., and Peres, C.A. (1991). Serum creatine-kinase (CK) and pyruvate-kinase (PK) activities in Duchenne (DMD) as compared with Becker (BMD) muscular dystrophy. *J. Neurol. Sci.* *102*, 190–196.

Zenker, F.A. von (1864). Über die veränderungen der willkührlichen Muskeln im Typhus abdominalis nebst einem Excurs über die pathologische Neubildung quergestreiften Muskelgewebes: Eine pathologische Untersuchung (F.C.W. Vogel).

Zhang, Q., Vashisht, A.A., O'Rourke, J., Corbel, S.Y., Moran, R., Romero, A., Miraglia, L., Zhang, J., Durrant, E., Schmedt, C., et al. (2017). The microprotein Minion controls cell fusion and muscle formation. *Nat Commun* *8*, 15664.

Zhao, P., Caretti, G., Mitchell, S., McKeegan, W.L., Boskey, A.L., Pachman, L.M., Sartorelli, V., and Hoffman, E.P. (2006). Fgfr4 is required for effective muscle regeneration in vivo. Delineation of a MyoD-Tead2-Fgfr4 transcriptional pathway. *J Biol Chem* 281, 429–438.